DEVELOPMENT OF A PHYSIOLOGICALLY BASED PHARMACOKINETIC (PBPK) MODEL OF MITRAGYNINE

YA KIMHEANG

A Thesis Submitted to the Graduate School of Naresuan University
in Partial Fulfillment of the Requirements
for the Master of Science Degree in Pharmacology and Biomolecular Sciences
August 2019

Thesis entitled "Development of a Physiologically Based Pharmacokinetic (PBPK) Model of Mitragynine"

by Ms. Ya Kimheang

has been approved by the Graduate School as partial fulfillment of the requirements for the Master of Science Program in Pharmacology and Biomolecular Sciences of Naresuan University

Oral Defense Committee

..... Chair

(Chairat Uthaipibull, Ph.D.)

..... Advisor

(Associate Professor Manupat Lohitnavy, Ph.D.)

..... Co-Advisor

(Assistant Professor Janthima Methaneethorn, Ph.D.)

..... Internal Examiner

(Assistant Professor Dumrongsak Pekthong, Ph.D.)

..... External Examiner

(Wimonchat Tangamornsuksan, Ph.D.)

Approved

.....

(Professor Paisarn Muneesawang, Ph.D.)

Dean of the Graduate School

15 AUG 2019

ACKNOWLEDGEMENT

Firstly, I would like to express my deepest gratitude to Royal Scholarship under Her Royal Highness Princess Maha Chakri Sirindhorn for providing me a great opportunity to pursue my Master Degree in Faculty of Pharmaceutical Sciences, Naresuan University.

I would like to express the deepest appreciation to my advisor, Associate Professor Dr. Manupat Lohitnavy and also my co-advisor Assistant Professor Dr. Janthima Methaneethorn for their continually and convincingly advice, outstanding guidance, and insightful encouragement for both academically and personally. Without their assistance and guidance, I could not have completed this thesis successfully and taken on the journey to be a researcher.

I would like to give special thanks to the committee members: Dr. Chairat Uthaipibull, Assistant Professor Dr. Dumrongsak Pekthong for their valuable comments and constructive suggestions; and Dr. Wimonchat Tangamornsuksan for her intellectual contributions, patient guidance, valuable suggestions, and encouragement. I really appreciate their willingness to give their time so generously to be committee members of my thesis examination.

I would like to express my appreciation to Professor C.Norman Scholfield who provided assistance and generously supported with constructive suggestions. My special thanks would be given to my seniors: Miss Pajaree Mongkhon who gave me valuable advice, moral support, kindness, and insightful encouragement; and also Dr.Quoc Ba Tran who trained me about computer coding.

I would like to acknowledge all lecturers and staffs in Faculty of Pharmaceutical Sciences, Naresuan University, for their guidance and support in academic throughout the length of my study.

Last but not least, I would like to deeply appreciations to my parents for their unconditional love, insightful encouragement, support, and understand in every circumstance throughout my life. I also greatly give my special thanks to my best friends for their emotional support and trust.

Ya Kimheang

Title	DEVELOPMENT OF A PHYSIOLOGICALLY BASED PHARMACOKINETIC (PBPK) MODEL OF MITRAGYNINE
Author	Ya Kimheang
Advisor	Associate Professor Manupat Lohitnavy, Ph.D.
Co-Advisor	Assistant Professor Janthima Methaneethorn, Ph.D.
Academic Paper	Thesis M.S. in Pharmacology and Biomolecular Sciences Program, Naresuan University, 2019
Keywords	Mitragynine, kratom, physiologically based pharmacokinetic (PBPK) model, rats, humans

ABSTRACT

Introduction: Mitragynine is a major psychoactive alkaloid in leaves of kratom (*Mitragyna speciosa* Korth.). Kratom is a tropical tree found in southern Thailand and northern states of the Malay Peninsula. Kratom is commercially available and primarily used as an alternative to treat opioid withdrawal. Mitragynine is responsible for most of the pharmacological properties in kratom leaves. The pharmacological effects of mitragynine are established but its pharmacokinetic properties are not fully characterized. The aim of this study was to develop a physiologically based pharmacokinetic (PBPK) model of mitragynine using systematic review to collect available pharmacokinetic studies as well as relevant properties of mitragynine. The primary goal of the developed PBPK model is used to predict mitragynine concentration levels in plasma, brain, and other tissues in both rats and humans.

Method: From our systematic review focusing on the available pharmacokinetic properties of mitragynine, 3 pharmacokinetic studies were retrieved to develop a PBPK model of mitragynine. Those included 1 study in rats receiving a single intravenous administration of mitragynine, 1 study in rats receiving a single oral administration of mitragynine, and 1 study in humans receiving repeated oral dosing of mitragynine in the form of kratom tea. The developed PBPK model comprised of 6 tissue compartments including lung, brain, fat, slowly perfused tissues, kidney, and

liver. Features of this current PBPK model of mitragynine included 1) involvement of breast cancer resistant protein (BCRP)-mediated transport in the brain; 2) integrating of hepatic CYP3A4-mediated metabolism in the liver; and 3) a diffusion-limited transport in the fat compartment. The PBPK model was developed using Berkeley Madonna Software (version 8.3.1) for a model simulation tool.

Results and discussion: The simulation results of the developed PBPK model of mitragynine could properly predict the kinetic behaviors of mitragynine from the selected pharmacokinetic studies in rats following a single intravenous administration and oral administration, and in humans with orally repeated dosage of mitragynine in the form of kratom tea. This model can describe mitragynine concentration-time courses in plasma and other tissue compartments particularly in the brain of both in rats and in humans. For human study, simulated results of 5 individual plasma mitragynine concentration-time courses were comparable to those of the observed datasets, subsequently individual mitragynine concentration levels in the brain were predicted. From simulating results in humans, prediction mitragynine concentration levels in the brain was about 2-folds higher as compared to those of the simulation results in rats, indicating by the developed PBPK model of mitragynine was conducted with different dosing scenario following a single dose in rats and multiple dosing in humans (kratom chronic users). The relative sensitivity analysis of input parameter values and model outputs was performed. The most sensitive parameters is tissue-to-plasma partition coefficient of mitragynine particularly in the slowly perfused tissues followed by in the liver. In addition, parameters related to protein transporter kinetics; i.e. maximum velocity (Vmax), had moderate sensitive effect particularly protein-mediated transport in the brain and hepatic metabolism of mitragynine in the liver.

Conclusion: PBPK models of mitragynine both in rats and in humans were developed based on published information of pharmacokinetic studies. The developed PBPK model could successfully describe the datasets from 3 selected pharmacokinetic studies. This modeling with biologically relevant features of the psychoactive alkaloid in the body also provided an important basis for further improvement in clinical applications. All information in this model can help to define the appropriate dosing regimen of mitragynine and apply to predict the drug disposition in target patients leading to achieving therapeutic effects.

LIST OF CONTENTS

Chapter **Page**

LIST OF CONTENTS

Chapter **Page**

LIST OF TABLE

Table **Page**

LIST OF FIGURES

Figure **Page**

LIST OF FIGURES (CONT.)

Figure **Page**

LIST OF FIGURES (CONT.)

Figure **Page**

LIST OF FIGURES (CONT.)

Figure **Page**

LIST OF FIGURES (CONT.)

Figure **Page**

ABBREVIATIONS

PBPK	=	Physiologically based pharmacokinetic
Caco-2 cells	=	Human epithelial colorectal adenocarcinoma cells
MDCK cells	=	Madin-darby canine kidney cells
NADPH	=	Nicotinamide adenine dinucleotide phosphate
UDPGA	=	Uridine 5'-diphospho-glucuronic acid
CYP	=	Cytochrome P450
P-gp	=	P-glycoprotein
PXR	=	Pregnane X receptor
UGT	=	Uridine 5'-diphospho-glucuronosyltransferase
BCRP	=	Breast cancer resistance protein
C_{max}	=	Maximum plasma concentration
T_{max}	=	Time to reach maximum concentration
AUC	=	Area under the curve
V_d	=	Volume distribution
CL	=	Clearance
$t_{1/2}$	=	Half-life
F	=	Bioavilability
ka	=	Absorption rate constant
ke	=	Elimination rate constant

CHAPTER I

INTRODUCTION

Statement of purpose

Mitragyna speciosa Korth. (kratom) is a tropical plant that belongs to Rubiaceae family. This plant is primarily grown in Southeast Asia particularly in southern of Thailand and adjoining northern of Malaysia (1-3). In Southeast Asia, the majority of users consumed kratom leaves by chewing fresh leaves, smoking dried leaves, and brewing the leaves with hot water then drinking as tea (4). Kratom leaves showed an opioid-like effect in a dose-dependent fashion (5). Laborers consumed kratom leaves to promote physical endurance, to increase energy, to relieve fatigue, and to improve their tolerance or longer working under the sun (4, 6). Kratom is classified as an illicit narcotic plant in some countries such as Thailand, Malaysia, Myanmar, and Australia (4, 7). Recently, kratom is permitted for medical use and research only in Thailand (8). However, kratom is not controlled but under surveillance in the United States, the United Kingdom, and other countries (5). Kratom is commercially available on the internet as a dietary supplement for chronic pain management (9) and as an alternative for the treatment of opioid withdrawal (10). Remarkably, adverse effects of kratom are alarming due to some reported fatalities when used concurrently with other substances such as propylhexedrine (11), and O-desmethyltramadol (12).

More than 40 alkaloids have been isolated from kratom leaves (13). Among these, mitragynine is the principle indole alkaloid (66% of total alkaloids) when extracted by organic solvents (13, 14). Mitragynine possesses antinociceptive effects (15-17), ileum relaxant (18), reducing gastric acid secretion (19), antidepressant (20), and anti-inflammatory (21). Interestingly, mitragynine is a partial agonist of μ-opioid receptors and also competitive antagonist at the κ-and δ-opioid receptors. Moreover, mitragynine is G-protein-biased agonist of the μ-opioid receptors without recruiting β-arrestin; therefore, it can cause less respiratory depression while maintaining an analgesic activity (22).

There have been several reports on physicochemical properties and pharmacokinetic studies of mitragynine. Mitragynine is a weak base and is high lipophilic (23); thus, it can passively transport through the blood-brain barrier into the brain which is the major site of action (24). The contribution of various drug metabolizing enzymes in the elimination of mitragynine has indicated that mitragynine metabolism is mediated by hepatic metabolism. To date, information related to pharmacokinetic properties of mitragynine have been established both *in vitro* assay and *in vivo* experiments; however, the knowledge of mitragynine pharmacokinetic behaviors in animals and humans are still limited particularly information on tissue disposition both in animals and in humans.

Physiologically based pharmacokinetic (PBPK) model is a mathematical method that provided a mechanistic approach for predicting pharmacokinetic behavior of drugs or compounds of interest across different species particularly pharmacokinetic disposition in various tissues by employing physiological, biochemical, and physicochemical parameters. In addition, this approach can also be applied as a guide to determine appropriate dosage regimens in early drug development and also be applied in later stage drug development to predict drug disposition in target patients (25). Based on the limited information on mitragynine pharmacokinetics and several advantages of PBPK models, the primary goal of this study was to develop a PBPK model of mitragynine using published pharmacokinetic data. The developed PBPK model can be used for predicting mitragynine concentration-time profiles in plasma and other tissues in both animals and humans. The findings of this study can promote optimal therapeutic effect and appropriate doses of mitragynine in clinical contexts.

Research aims

1. To systematically review mitragynine pharmacokinetics conducted *in vitro*, *in vivo* and employ such information for physiologically based pharmacokinetic (PBPK) model development
2. To develop a PBPK model of mitragynine both in rats and in humans
3. To apply the developed PBPK model in predicting concentration-time courses of mitragynine in organs of interest such as lung, fat, brain, slowly perfused tissues, kidney, and liver

Research significance

Despite pharmacological effects of mitragynine have been established but clinical studies on the pharmacokinetics of mitragynine related to its potential uses in medicine are still under-investigated. In addition, information relevant to tissue dispositions of mitragynine is still limited. This study aimed to establish PBPK models of mitragynine for predicting tissue disposition of mitragynine in rats and in humans. The developed PBPK model is substantially important during the early stage of drug development and it can ultimately be used to determine appropriate dosing regimens during first in human studies leading to a better therapeutic outcome. This model can also be applied in the later stage of drug development to predict drug disposition in target patients.

Research scope

This was an *in silico* experimental study, fundamentally performed on a computer software. The Berkeley Madonna Software (developed by Robert Macey and George Oster of the University of California at Berkeley, version 8.3.18) was employed to develop a PBPK model of mitragynine for prediction of mitragynine disposition in rats and in humans.

CHAPTER II

LITERATURE REVIEW

Plant description of kratom

Mitragyna speciosa Korth. (Rubiaceae) is a tropical tree commonly found in southern Thailand and northern states of the Malay Peninsula. In Thailand, this plant is known variously as kratom, thom, ithang, kakuam, kraton, krathom and as biak-biak, ketum in Malaysia (2-4). This plant is a large tree which can reach up to 15 meters in height. Flowers are observed as dark yellow spherical clusters with 120 florets attached to the leaf axils on long stalks while leaves are dark glossy green color and an oval shape that grow up over 18 cm in lengths and 10 cm in widths (Figure 1). During the dry season, leaves fall abundantly then new growth is plentiful during the rainy season (2).

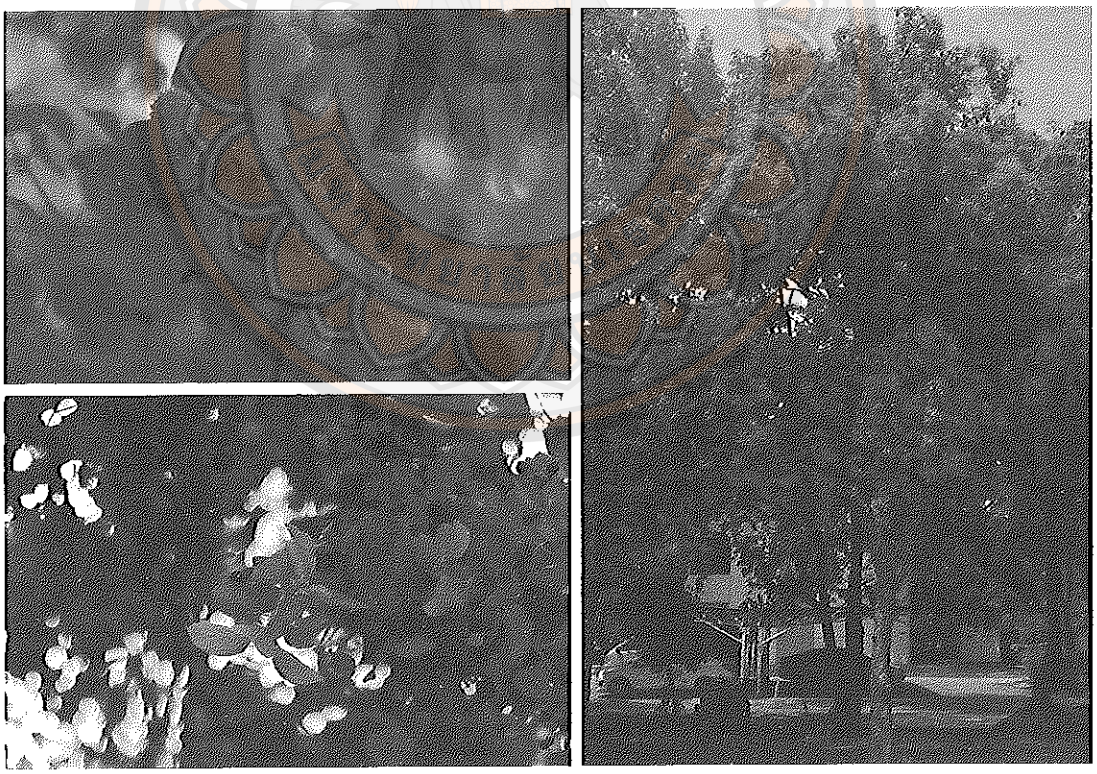

Figure 1 General description of kratom

Legal status of kratom

Kratom is classified as an illicit narcotic plant in some countries including Thailand, Malaysia, Myanmar, and Australia (7). In Thailand, kratom is classified under Thai Narcotics Act since 1979 and also banned under Poisons Act since 1952 in Malaysia (4, 6). Currently, Thai National Legislation Assembly permits kratom as a medical use only (8). Kratom is not currently an illegal substance in the United State and the United Kingdom (5, 26, 27) but it is placed into Schedule I of Controlled Substance Act by the United State Drug Enforcement Administration, and Food and Drug Administration to ensure a safe use (28, 29).

Preparations and consumptions of kratom

Majority of kratom users consumed fresh leaves by chewing and dried leaves by smoking or brewing as a tea (4). In addition, kratom fresh leaves can be chewed either alone or taken with betel nuts (Areca catechu) to remove veins before eating and mixed together with juice and salts (2).

In Southeast Asia, laborers eat its fresh leaves to promote physical endurance, to increase energy, to relieve fatigue, and to improve their tolerance to the sun (7, 30). Kratom has been used as a folk remedy to treat some illnesses including coughing, diarrhea, diabetes, and hypertension (6, 30, 31). Kratom leaves showed opiate-like effects in a dose-dependent fashion, as shown in Table 1 (5). In addition, it provides euphoric effects (i.e. improve mood and reduce stress) and enhances sexual performance (32).

In Malaysia (i.e. Penang and Kedah), kratom leaves are rinsed with water to remove all traces of dirt and are boiled for a few hours, resulting in a greenish brown solution but extremely bitter taste. Kratom users consumed an average of three medium-sized glasses (approximately 250 mL per glass) of kratom solution which contains approximately 68-75 mg of mitragynine in daily consumption (1). In addition, occasional kratom users are not associated with severe pain or sleep problems as opioid withdrawal symptoms. However, chronic users of kratom were moderately associated with pain and sleep problems (33).

Kratom is rapidly becoming a substance of abuse in southern Thailand. It is consumed as homemade ice cocktails called a "4x100 Cocktails" where kratom leaves are suspended "Coca-Cola" with codeine or diphenhydramine syrup (4, 34). Kratom is also consumed as an herbal blend called a "Krypton" which is a mixture of kratom leaves with O-desmethyltramadol and is sold widely on the internet (12, 35, 36). The regular consumption of kratom leaves can cause some side effects such as anorexia, dehydration, weight loss, hyperpigmentation (green/dark colored skin), constipation, and psychosis (1, 30, 31).

Kratom is not demanded only in Southeast Asia but also in Western countries. Recently, in Europe and the United States, kratom products (i.e. capsule, powder) are commercially available over the internet as a dietary supplement for management of chronic pain (9) and as an alternative for the treatment of opioid withdrawal (26). They were purchased in cheap price compared to other opioid substances leading to an increase in the prevalence of use.

Table 1 Dosing ranges of kratom as raw leaves producing different types of effects and psychological clinical manifestations

Kratom use	Dose (raw leaves)	Overall Effects	Clinical Manifestations
Low to moderate	1-5 grams	Mild-stimulant	Increased alertness, physical energy, talkativeness, sociable behavior
Moderate to high	5-15 grams	Opioid-like effects	Pain and opioid withdrawal relief, treatment of diarrhea, euphoria (less intense than opioid drugs)
Very high	>15 grams	Sedation	Induce stupor, sweating, dizziness, nausea, dysphoria followed by calmness and a dreamlike state

Source: Adapted from Prozialeck, et al. (5)

Phytochemistry of kratom

More than 40 alkaloids have been isolated and identified from kratom leaves. Among these, mitragynine is the most abundant alkaloids which are accounted for approximately 12% and 66% of total alkaloids in kratom leaves grown in Malaysia and Thailand, respectively (37). Other constituents in kratom leaves include paynantheine (9%), speciogynine (7%), 7-hydroxymitragynine (2%), and speciociliatine (1%) (34, 38). The alkaloids contributing pharmacological effects are mitragynine and 7-hydroxymitragynine (37, 39). Mitragynine exerts various pharmacological activity (as described below) while 7-hydroxymitragynine is the minor constituent but also demonstrates high potency on an opioid receptor, as an analgesic effect (22).

Pharmacological properties of mitragynine

Mitragynine possesses an antinociceptive effect involving on supraspinal opioid systems (15). In addition, mitragynine involves in both descending noradrenergic and serotonergic systems of the supraspinal opioid system in the brain (16) and mediates its effect via μ- and δ-opioid receptors (17).

Action on the gastrointestinal tract has been investigated. Studies have shown that mitragynine inhibits ileum contraction (18) and reduces gastric acid secretion via inhibition of 2-deoxy-D-glucose (19). Furthermore, it also possesses a stimulant activity by inhibiting neurotransmitter release from the nerve endings at the vas deferens via blocking of the neuronal Ca^{2+} channels (40).

Mitragynine also exerts antidepressant action in animals through the restoration of monoamine neurotransmitter levels, i.e. serotonin, noradrenaline, and dopamine, and reducing the corticosterone concentration, as indicated by forced swim test and tail suspension tests (20).

Mitragynine exhibits an anti-inflammatory effect by suppressing prostaglandin E2 production via the inhibition of cyclo-oxygenase 2 mRNA and protein expression (21). Furthermore, it can promote diabetic treatment by increasing the rate of glucose uptake through glucose transporter stimulation in muscle cells (41).

Interestingly, the molecular targets of mitragynine are able bind to μ-opioid receptors. The compound acts as a partial agonist at μ-opioid receptors but as a competitive antagonist at κ- and δ-opioid receptors. Mitragynine is a G-protein-biased agonist at μ-opioid receptor without recruiting the β-arrestin; thus, causing less respiratory depression while maintaining analgesia (22), as illustrated in Figure 2.

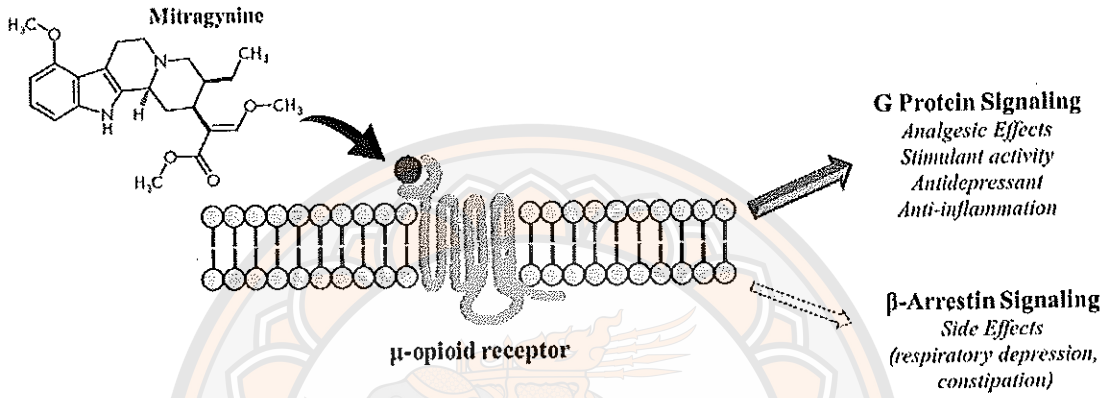

Figure 2 Mechanism of action of mitragynine

Source: Adapted from Kruegel, et al. (22)

Toxicity of mitragynine

The sub-chronic toxicity of mitragynine was also investigated. Orally administered mitragynine with a dose of 175 mg/kg in mice did not provide a toxic effect. However, when the dose of mitragynine was increased to 1,300 mg/kg, seizures in the tested animals were observed with mortality in less than 1 hr. The lethal dose of mitragynine was 477 mg/kg (42).

Another study has indicated on the effects of sub-chronic exposure to mitragynine. Following oral administration of mitragynine (1, 10, 100 mg/kg) in rats for 28 days, no mortality or toxic effects were observed as relatively safe at lower doses. Whereas mitragynine was orally administered in rats with sub-chronic high dose of 100 mg/kg for 28 days, resulted as histopathological, hematological, and biochemical alterations (43). For histopathological changes, there exposed on brain, liver, and kidney. Brain abnormalities were observed such as local vacuolation and necrosis of

neuronal cells. Liver was indicated by hepatocytes hypertrophy, dilation of sinusoids, and hemorrhage in hepatocytes but no necrosis or inflammatory cells filtration. Kidney was altered such as swollen glomerulus capsule. Therefore, at highest dose in rats for 28 days, there also induced alteration on neuronal cells, acute hepatoxicity, and mild nephrotoxicity.

Physicochemical properties of mitragynine

Mitragynine is the principle indole alkaloid in the extracts of kratom leaves (13, 14). The molecular formula of mitragynine is $C_{23}H_{30}N_2O_4$ and its molecular weight is 398.50 g/mole, as illustrated in Figure 3 (44). Mitragynine is a white amorphous powder with the melting point at approximately 102-106 ^{0}C (45). Mitragynine is a weak base (pKa = 8.1) with lipophilic properties (Log P = 1.70) (23).

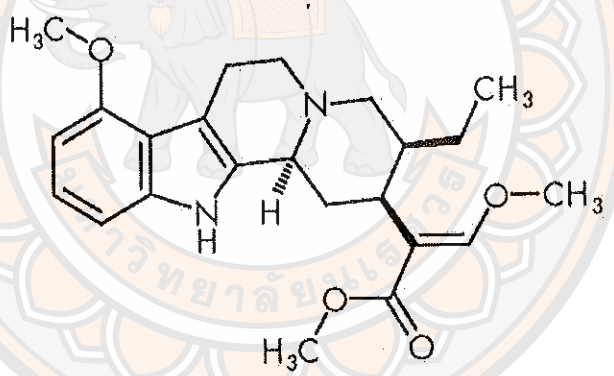

Figure 3 Chemical structure of mitragynine

Source: Adapted from Zacharias, et al. (44)

Pharmacokinetic properties of mitragynine

The information outlined in this section obtained from the systematic review that was performed in order to collect the published literature on the pharmacokinetics of mitragynine. The methodology and results from the systematical review were subsequently demonstrated in Appendix A.

The information on pharmacokinetic properties of mitragynine was divided into 6 main parts: 1) Absorption; 2) Distribution; 3) Elimination; 4) Intravenous administration in rats; 5) Oral administration in rats; and 6) Oral administration in humans.

Absorption

In vitro experimental: at 37 ^{0}C, mitragynine was moderately stable at neutral pH (~3.5% degradation after 3 hr) but approximately 26% degraded in acidic condition (pH = 1.2) after 1-2 hr, as presented in Table 2 (23, 24). Being a weak base, mitragynine was highly solubilized at pH 4.0 and moderately solubilized at pH 7.4 in aqueous solution, as described in Table 2 (46). Therefore, mitragynine is highly solubilized and ionized in the acidic condition, while unionized form can diffuse into the cytosol. Permeability was investigated either a phospholipid bilayer or coherent monolayers of Caco-2 cell monolayers (emulating the intestinal barrier) or MDCK (model of the blood-brain barrier) cells, which emulate the intestinal or the blood-brain barriers (47). For Caco-2 cell monolayers, forward fluxes and reverse fluxes were 25 x 10^{-6} cm/sec and 27 x 10^{-6} cm/sec, which were independent concentration and P-glycoprotein (P-gp) is an extrusion transporter (24). Corresponding mitragynine fluxes across MDCK cell monolayers were 15 x 10^{-6} cm/sec and 17 x 10^{-6} cm/sec, respectively (24). Flux ratio of mitragynine was approximately 1, as indicated by passive diffusion through membranes. Likewise, mitragynine flux through the phospholipid bilayer at pH 4 and pH 7.4 were 0.23 x 10^{-6} cm/sec and 11 x 10^{-6} cm/sec, respectively (46). The higher penetration in neutral media accords with the absorption of mitragynine as the unchanged molecular form. Mitragynine was rated as diffusible using atenolol, propranolol, caffeine, carbamazepine, furosemide, and metoprolol, as comparators. Those results are summarized in Table 3. Therefore, these bi-directional flux capabilities suggest that permeability of mitragynine through the membrane is passive diffusion. Furthermore, mitragynine can be classified as a class II of the Biopharmaceutical Classification System due to its highly permeable across membranes and lower water solubility (48).

In situ experimental: a single pass intestinal permeability technique was employed to assess the permeability of mitragynine across the gut epithelium (49). Flux rates of mitragynine was 1.11 x 10^{-4} cm/sec in the absorption direction which compared favorably with permeably propranolol (1.12 x 10^{-4} cm/sec) and atenolol (0.41 x 10^{-4}

cm/sec). Flux rates of mitragynine were unchanged in the presence of the inhibitors of P-gp (azithromycin) and cytochrome P450 3A4 (ciprofloxacin), suggesting that absorption of mitragynine is passive and rapid. Additionally, flux rate of mitragynine in rats was used to predict flux rate of human intestinal permeability. The result was approximately 4.03 x 10^{-4} cm/sec, indicating that mitragynine is completely absorbed into the intestinal membrane.

Table 2 Summary of studies investigating the solubility of mitragynine

Author (Year)	Compounds/ Assays	Results	
	Simulated biological fluids		
	Assays	Concentration (μM)	RD (%)
Manda, et al. (2014) (24)	SGF (120 min)	8.03 ± 0.5	26
	SIF (180 min)	10.79 ± 0.25	3.6
Ramanathan, et al. (2015) (23)	SGF (60 min)	35.13 ± 0.5	26
	SIF (180 min)	17.57 ± 2.01	3.5
	Aqueous solubility determination		
	Compounds	Concentration (μM) pH 4	Concentration (μM) pH 7.4
Kong, et al. (2017) (46)	Mitragynine	130.0 ± 0.1	82.7 ± 1.9
	DES	24.1 ± 4.2	19.3 ± 0.5
	Estriol	89.8 ± 8.17	86.5 ± 3.0
	Furosemide	187.8 ± 1.0	197.5 ± 3.1

Note: SGF = simulated gastric fluid; SIF = simulated intestinal fluid; DES = Diethylstilbestrol

Table 3 Summary of studies investigating the permeability of mitragynine

Author (Year)	Model	Compound	P_{app} (10^{-6} cm/sec)	
			Absorptive flux	Secretory flux
Manda, et al. (2014) (24)	Caco-2 cells	Mitragynine (5 μM)	24.2 ± 2.6	26.3 ± 2.7
		Mitragynine (10μM)	25.3 ± 2.2	29.1 ± 2.0
		Atenolol (200μM)	2.0 ± 0.6	2.1 ± 0.4
		Propranolol (200μM)	34.2 ± 2.6	35.4 ± 1.9
	MDCK cells	Mitragynine (5 μM)	15.3 ± 1.7	17.2 ± 1.6
		Mitragynine (10μM)	16.2 ± 1.8	18.1 ± 1.7
		Atenolol (200μM)	1.1 ± 0.2	1.2 ± 0.1
		Caffeine (100μM)	23.2 ± 2.8	24.3 ± 1.5
Kong, et al. (2017) (46)	PAMPA	Mitragynine	0.23 ± 0.0005	11.14 ± 0.06
		Carbamazepine	0.21 ± 0.005	0.13 ± 0.002
		Furosemide	0.72 ± 0.008	0.75 ± 0.003
		Metoprolol	4.55 ± 0.002	4.49 ± 0.007

Note: Caco-2 cells = human epithelial colorectal adenocarcinoma cells; MDCK cells = madin-darby canine kidney cells; PAMPA = parallel artificial membrane permeability assay; P_{app} = apparent permeability.

Distribution

By equilibrium dialysis, about 95% of mitragynine (5-15 μM) bound to plasma protein after 24 hr at 37 ^{0}C in human plasma (24). In addition, approximately 85% of mitragynine (10 μM) binds to plasma proteins after 1 hr at 37 ^{0}C in human plasma, determined by ultrafiltration (46). Those studies indicated that mitragynine can preferentially bind to plasma protein.

Elimination

Effect of mitragynine on drug metabolizing enzymes:

Incubation with liver microsomes or liver S9 fraction using nicotinamide adenine dinucleotide phosphate (NADPH) or uridine 5'-diphospho-glucuronic acid (UDPGA) as cofactors, mitragynine was extensively metabolized via phase I and moderately via phase II metabolism. Approximately 15-55% of mitragynine was

metabolized depending on incubation time and conditions (30-120 min), as summarized in Table 4 (24, 46).

On individual cytochrome P450 (CYP) enzymes, mitragynine enhanced expression of CYP1A2, CYP3A4, and CYP2D6, as shown in Table 4 (50-53). Mitragynine induced CYP1A2 and weakly induced CYP3A4, as measured by mRNA and protein expression (50). In order of potency, mitragynine inhibited CYP2D6 and weakly inhibited some CYP isoenzymes (51). Identification on pregnane x receptor (PXR), which is the transcription factor of P-gp and some CYPs, the results showed that PXR was also upregulated. A common enzyme inducer (aryl hydrocarbon receptor) was affected but mitragynine can induce only CYP1A2 (52). Notably, mitragynine is predominantly mediated by CYP3A4, as represented by fraction metabolized mitragynine of approximately 67% (53). Other drug metabolizing enzymes influenced by mitragynine includes aminopyrine N-demethylase, glutathione S-transferase (54), carboxylesterase (55), and uridine 5'-diphospho-glucuronosyltransferase (UGT) (56, 57), as shown in Table 4.

For phase II drug metabolizing enzymes, mitragynine weakly inhibited UGT, as evidence by using 4-methylumbelliferone glucuronidation in recombinant UGT isoforms (56). However, a study using zidovudine glucuronidation in rat liver microsome showed that mitragynine strongly inhibited UGT (57).

The activity of mitragynine on efflux transporters, P-gp (24, 52, 58, 59) and breast cancer resistance protein (BCRP) (60) was also investigated, as summarized in Table 4. Mitragynine can inhibit P-gp, as evidence by the accumulation of calcein-AM in intracellular (24), infective on the P-gp ATPase stimulation (58), and down-regulation of mRNA expression of P-gp in Caco-2 expression system (59). In addition, mitragynine can induce P-gp as shown by an increase in mRNA expression, leading to an increase in P-gp activity, and resulting in the reduction of the calcein-AM uptake (52). Those studies concluded that mitragynine can both induce and inhibit P-gp; thus, co-administration of mitragynine and drugs which are P-gp substrates may possibly lead to in drug-herbal interaction. In addition, mitragynine is indicated as BCRP-mediated transport because of potentially exhibited BCRP ATPase stimulation (60).

Metabolites of mitragynine:

Mitragynine metabolites were identified via urinary excretion by LC-MS/MS. After oral dosing of 40 mg/kg mitragynine into rats, urine samples were withdrawn after 24 hr (61). The metabolic pathway is indicated by hydrolysis of the methyl ester in position 16, O-demethylation of the methoxy group at positions 9 and 17, followed either by intermediate aldehydes, by oxidation to carboxylic acids, or reduction to alcohols. Mitragynine also undergoes phase II metabolism via glucuronidation and sulfate conjugation. The conjugated metabolites were identified in urines. Seven phases I mitragynine metabolites were identified. Five conjugated metabolites, i.e. 4 glucuronides and 1 sulphonate were presumed to be phase II metabolites (identified from urinary excretion of rats), 3 glucuronidates and 3 sulphonates were found from human urinary excretion, as shown in Table 5.

Table 4 Summary of studies investigating on action of mitragynine with drug metabolizing enzymes and protein-medicated transporters

Author	Year	Assay	Compound	Results
Metabolic stability of mitragynine (% metabolized)				
Manda, et al. (24)	2014	Human liver microsomes	Mitragynine	30 %
		Liver S9 fraction		55 %
Kong, et al. (46)	2017	Rat liver microsomes	Mitragynine	~ 15 %
			Propranolol	~ 80 %
			Verapamil	~ 30 %
Cytochrome P450 mediated metabolism of mitragynine				
Lim, et al. (50)	2013	CYP1A2	25 μM	Induction
		CYP2D6		No induction
		CYP3A4		Weak induction
Hanapi, et al. (51)	2013	CYP2D6	0.02-200 μM	Potent inhibitory (IC_{50} = 0.4 ± 0.3 μM)
				Noncompetitive inhibition (K_i = 12.9 μM)
		CYP3A4		Moderate inhibitory (IC_{50} = 41.3 ± 6.7 μM)
				Competitive inhibition (K_i = 379.2 μM)
		CYP2C9		Moderate inhibitory (IC_{50} = 9.7 ± 4.8 μM)
				Noncompetitive inhibition (K_i = 155.8 μM)
Manda, et al. (52)	2017	CYP1A2	1-10 μM	Induction
		CYP3A4		No induction
Kamble, et al. (53)	2018	CYP3A4	1 μM	Induction

Table 4 (cont.)

Author	Year	Assay	Compound	Results
Effect of mitragynine on the other drug metabolizing enzymes				
Anwar, et al. (54)	2012	N-demethylase	0.25-250 μM	Induction
		Glutathione-S-transferase		Inhibition (IC_{50} = 11.8-24.4 μM)
Meyer, et al. (55)	2015	Carboxylesterase	0.01-100 μM	Hydrolysis
Haron, et al. (56)	2015	UGT	100 μM	Inhibition 4-methylumbelliferone glucuronidation in RLM, HLM, UGT1A1 and UGT2B7 (IC_{50} > 100 μM)
Huda Abdullah, et al. (57)	2018		100 μM	Inhibition zidovudine glucuronidation in HLM (IC_{50} = 8.11 ± 4.48 μM)
Protein-mediated efflux transporters of mitragynine				
Manda, et al. (24)	2014	P-glycoprotein	5-10 μM	Inhibition
Meyer, et al. (58)	2015		5 μM	Inhibition
Manda, et al. (52)	2017		0.001-10 μM	Induction
Rusli, et al. (59)	2019		0.005-500 μM	Inhibition
Wagmann, et al. (60)	2018	Breast Cancer Resistance Protein	0.005-500 μM	Induction

Note: CYP450 = cytochrome P450; IC_{50} = half maximal inhibitory concentration; K_i = inhibitory constant; UGT = uridine 5'-diphospho-glucuronosyltransferase; RLM = rat liver microsomes; HLM = human liver microsomes

Table 5 Summary of phase I and phase II mitragynine metabolites

Metabolites of mitragynine	Abbreviation
Phase I metabolites	
9-O-demethyl mitragynine	9-O-DM-MG, 2
16-carboxy mitragynine	16-COOH-MG, 3
9-O-demethyl-16-carboxy mitragynine	9-O-DM-16-COOH-MG, 4
17-O-demethyl-16,17-dihydro mitragynine	17-O-DM-DH-MG, 5
9,17-O-bisdemethyl-16,17-dihyro mitragynine	9,17-O-BDM-DH-MG, 6
17-carboxy-16,17-dihydro mitragynine	17-COOH-DH-MG, 7
9-O-demethyl-17-carboxy-16,17-dihydro mitragynine	9-O-DM-17-COOH-DH-MG, 8
Phase II metabolites	
9-O-demethyl mitragynine glucuronide	9-O-DM-G-MG, 2G [a, b]
9-O-demethyl mitragynine sulfate	9-O-DM-S-MG, 2S [b]
16-carboxy mitragynine glucuronide	16-COOH-G-MG, 3G [a, b]
9-O-demethyl-16-carboxy mitragynine glucuronide	9-O-DM-16-COOH-G-MG, 4G [a]
9-O-demethyl-16-carboxy mitragynine sulfate	9-O-DM-16-COOH-S-MG, 4S [a, b]
17-O-demethyl-16,17-dihydro mitragynine glucuronide	17-O-DM-DH-G-MG, 5G [b]
9,17-O-bisdemethyl-16,17-dihyro mitragynine glucuronide	9,17-O-BDM-DH-G-MG, 6G [a]
9,17-O-bisdemethyl-16,17-dihyro mitragynine sulfate	9,17-O-BDM-DH-S-MG, 6S [b]

[a] Metabolites of mitragynine could be identified in urinary rats.

[b] Metabolites of mitragynine could be identified in urinary humans.

Source: Adapted from Phillip, et al. (61)

Intravenous administration of mitragynine in rats

Pharmacokinetics of intravenously administered mitragynine (1.5 and 5 mg/kg) into rats are summarized in Table 6 (62-64). The maximum plasma concentration (C_{max}) was 10 μM at time to reach maximal concentration (T_{max}) of 1 min (63). In contrast, the study by Parthasarathy, et al. reported the C_{max} of 6 μM at T_{max} of 70 min, suggesting the puzzling slow by using a robust cross-over design and tail vein for sampling (62). Volume of distribution (V_d) varied from 0.8 to 8 L/kg; while clearance (CL) rates varied from 0.3 to 1.3 L/hr/kg (62-64).

Kong, et al. used sampling plasma and brain by microdialysis with sampling periods of 30 min (65). The reported C_{max} in plasma was 3.8 μM which equated to 38 μM for whole plasma assuming 90% protein binding, V_d was 9.8 L/kg, and half-life ($t_{1/2}$) was 13 hr (longer than other intravenous studies). In the brain, extracellular fluid levels monitored by dialysis (presumably without protein), C_{max} was 2.3 μM; $t_{1/2}$ was longer (13 hr); V_d was higher (17 L/kg); and AUC_{brain}/AUC_{plasma} was 0.66, indicating substantial penetration of the blood-brain barrier and tissue loading.

Oral administration of mitragynine in rats

Absorption of mitragynine is classified as the first-order process as indicated by proportionally increased dose with increasing C_{max} varied from 1-1.8 μM (62, 64, 66, 67). The results of each study are summarized in Table 6. Mitragynine is rapidly absorbed with an approximate T_{max} of 1.5 hr (64, 66, 67). However, a delay time of 4.5 hr was noticed (62); which is caused by a variety of mitragynine formulations (i.e. 100% propylene glycol, pH 4.7 of acetate, 20% Tween 20, 1% Cremophor). This impacts an absorption process especially the dispersing agents. Apparent volume of distribution (V_d/F) varied from 33 to 90 L/kg, indicating extensive redistribution into tissues (62, 64, 66, 67). Apparent clearance (CL/F) of mitragynine was 1.6 L/hr (7.3 L/hr/kg for approximately 220 g of body weight) (66), and 6.35 to 7 L/hr/kg (62, 64, 67). In addition, mitragynine has prolonged and incomplete absorption with low absolute bioavailability (F = 3%) (62). Whereas, a study by Avery, et al. reported oral bioavailability of mitragynine (F = 17%) (64), as indicated on the variety formulations that likely impact on absorption process especially the dispersing agents. All of the studies assumed that absorption of mitragynine exhibited first-order kinetic behavior.

Table 6 Pharmacokinetics of mitragynine following intravenous administration and oral administration in animals

Author (Year)	Parthasarathy, et al. (2010) (62)	Vuppala, et al. (2011) (63)	Avery, et al. (2019) (64)	Kong, et al. (2017) (65)	
Species	male SD rats	male SD rats	male SD rats	female SD rats	
BW (g)	280-315	150-250	200-250	250-300	
Dose (mg/kg)	1.5	5	5	10	
Formulation	20% Tween 20	1% Cremophor	1% Cremophor	10% Tween 20	
Analytical method	HPLC-UV	UPLC-MS	UPLC-MS	UFLC-MS	
LOD (μM)**	0.063	0.0005	-	-	
LOQ (μM)**	0.125	0.0025	0.0025	0.025	
Route of sampling (i.v.)	tail vein	jugular vein	jugular vein	jugular vein	
Sampling	Plasma	Plasma	Plasma	Dialyzed plasma	Brain ECF
C_{max} (μM)**	5.77 ± 3.01	9.79 ± 1.76	-	(3.81 ± 0.38)	(2.31 ± 0.13)
T_{max} (hr)	1.2 ± 1.1	0.016	-	0.5	0.5
$AUC_{0-\infty}$ (μM/hr)**	23.09 ± 16.31	8.53 ± 2.26	10.66 ± 1.42	11.62 ± 1.1	6.73 ± 0.35
V_d (L/kg)	0.79 ± 0.42	8.2 ± 2.2	8 ± 1.5	9.84 ± 0.62	16.94 ± 1.11
CL (L/h kg)	0.29 ± 0.27	1.2 ± 0.2	1.3 ± 0.1	2.26 ± 0.21	3.78 ± 0.18
ke (1/hr)	0.24[a]	0.26[a]	0.12 ± 0.04	0.24 ± 0.03	0.23 ± 0.01
$t_{1/2}$ (hr)	2.9 ± 2.1	2.6 ± 0.4	6 ± 1.5	13.14 ± 1.42	13.22 ± 2.55

Table 6 (cont.)

Author (Year)	Janchawee, et al. (2007) (66)	de Moraes, et al. (1997) (67)	Parthasarathy, et al. (2010) (62)	Avery, et al. (2019) (64)
Species	male Wistar rats	male Wistar rats	male SD rats	male SD rats
BW (g)	220-290	200-250	280-315	200-250
Dose (mg/kg)	40	20	50	20
Formulation	Propylene glycol	1% Acetic acid	20% Tween 20	1% Cremophor
Analytical method	HPLC-UV	LC-MS	HPLC-UV	UPLC-MS
LOD (μM)**	0.075	-	0.063	-
LOQ (μM)**	0.25	0.0005	0.125	0.0025
Route of sampling (p.o)	retro-orbital sinus	decapitation	tail vein	jugular vein
Sample	Serum	Plasma	Plasma	Plasma
C_{max} (μM)**	1.58 ± 0.45	1.06	1.76 ± 0.53	1.15 ± 0.1
T_{max} (hr)	1.83 ± 1.25	1.26	4.5 ± 3.6	1.5 ± 0.3
k_a (1/hr)	1.43 ± 0.9	2.4	-	-
$AUC_{0-\infty}$ (μM/hr)**	17.54 ± 7.35	7.9	20.58 ± 7.53	7.25 ± 0.44
V_d/F (L/kg)	89.5 ± 30.3	37.9	64 ± 23	33.8 ± 3.1
CL/F (L/h kg)	7.3[b]	6.35	7 ± 3	7.1 ± 0.5
ke (1/h)	0.07 ± 0.01	0.18	0.105[a]	0.21 ± 0.01
$t_{1/2}$ (hr)	9.43 ± 1.74	3.85	6.6 ± 1.3	3.3 ± 0.2

** All reported values in ug/mL have been converted to μM

(x) These values are for unbound mitragynine, presumably excluding protein bound and each sample taken over 30 min.

[a] k_e value has been calculated from formulation ($k_e = 0.693/t_{1/2}$)

[b] CL/F value has been converted unit from L/h to L/h kg

Note: SD = Sprague-Dawley; BW = body weight; i.v. = intravenous administration; p.o. = per oral; LOD = limit of detection; LOQ = limit of quantification; HPLC-UV = high performance liquid chromatography coupled to ultra-violet; LC-MS = high performance liquid chromatography coupled to tandem mass spectrometry; UPLC-MS = ultra-performance liquid chromatography coupled with a mass spectrometer; UFLC-MS = ultra-fast liquid chromatography equipped with a mass spectrometer; ECF = extracellular fluid; C_{max} = maximum serum/plasma concentration; T_{max} = time to reach maximum concentration; $AUC_{0-\infty}$ = area under the curve from time equals zero to infinity; V_d = volume distribution; CL = clearance; k_e = elimination rate constant; $t_{1/2}$ = half-life; F = bioavailability

Oral administration in humans

Pharmacokinetics of mitragynine was assessed in ten healthy male subjects (kratom users) (68). These subjects were divided into five groups to receive different dosing regimens of mitragynine (6.25-11.5 mg) in kratom tea (60 mL) for 7 days. Prior to loading doses, participants were randomly administered a single oral dose of kratom tea (60 or 120 mL) containing mitragynine (6.25-23 mg) on the 8th day. For experimental design, dosing regimens of each human subject are summarized in Table 7. Blood samples were collected at 15, 30, and 45 minutes, 1, 1.25, 1.5, 1.75, 2, 2.5, 3, 4, 6, 9, 12, 19, and 24 hr. Urine samples were also collected during the study period. Mitragynine concentration levels were analyzed using liquid chromatography-tandem mass spectrometry (LC-MS). Mitragynine exerts two-compartment disposition kinetics, as evidenced by a biexponential decline in a semilog plot. A linear correlation between loading dose and C_{max} (R^2 = 0.6773) as well as area under the curve from time equals zero to infinity ($AUC_{0-\infty}$) (R^2 = 0.4873) was observed in this study, suggesting that mitragynine exhibits first-order kinetics. In plasma, C_{max} varied from 0.007 to 0.04 μM, as dose-dependent. T_{max} was reached at 0.8 hr. The terminal half-life was 23.24 ± 16.07 hr. The average apparent of volume distribution and clearance rates were 38.04 ± 24.32 L/kg and 98.1 ± 51.34 L/h/kg, respectively. About 0.14% of unchanged form was detected in urine, suggesting that it is not extensively excreted in the urine.

Table 7 Summary dosing regimens of mitragynine pharmacokinetic in humans

Dosing regimens	Subjects	Daily doses (day 1-7)	Loading dose (day 8)	Total doses
I	3	6.25 mg per day	12.5 mg	56.25 mg
II	2	6.25 mg per day	6.25 mg	50 mg
III	1	9.96 mg per day	19.92 mg	89.64 mg
IV	3	9.96 mg per day	9.96 mg	79.68 mg
V	1	11.50 mg per day	23 mg	103.5 mg

Source: Adapted from Trakulsrichai, et al. (68)

Physiologically based pharmacokinetic (PBPK) model

Definition of PBPK model

PBPK model is a computational tool that provides a mechanistic approach for predicting absorption, distribution, metabolism, and excretion of the interested substance (either synthetic or natural chemical substances) based on physiological, biochemical, and physicochemical parameters. PBPK models can predict concentration-time profiles of the interested substance in several tissues of interest. Apart from that, PBPK models are well-known for extrapolation across species. In addition, PBPK models can be employed to simulate pharmacokinetic profiles in various physiological conditions (25, 69).

Applications and limitation of the PBPK model

Classical pharmacokinetic models are used to describe the compound disposition by dividing the whole body into one or multiple compartments. Generally, the number of compartments depends on rate of compound distribution into tissues. For example, if the compound is rapidly distributed into all tissues, the pharmacokinetics of that compound is then characterized with a 1-compartment. However, the main limitation of this pharmacokinetic model is that it cannot be extrapolated across species because it is not based on physiological properties (70, 71).

Notably, PBPK modeling is widely used in the environmental toxicology and risk assessment as well as in pharmacology. It also involves in an early stage of drug development and clinical study (25). PBPK models differ from one or multiple compartment models in that it represents physiological, physicochemical, and also biochemical process in the species of interest (72). Especially, PBPK models correlate between substance-dependent and physiologically-dependent that are extensively used to estimate drug kinetics with different species or different routes of administration. The PBPK models; however, have some limitations in that they require comprehensive information such as physiological, biochemical and physiochemical data. These data are sometimes inconsistent among different sources. Occasionally, certain data are not available, and laboratory work needs to be conducted (73).

PBPK model development

Model representation and mathematical descriptions

Firstly, components of PBPK model consists of the pre-selected relevant tissues, generally include the target tissues, the eliminating tissues, as well as compound storage tissues. These tissues are linked together by the circulation blood system (71, 72).

Secondly, each compartment is described by a unique differential equation. The mathematical representations are derived from the law of mass action. The principle equation for the rate change of the substance in tissue compartment versus time (dC_T/dt) is performed. The differential equation of each tissue compartment is assumed as perfusion-limited or flow-limited model and/or permeability-limited or diffusion-limited model (73-75).

Flow-limited model is employed with an assumption that distribution of substance to the tissue compartments is achieved at equilibrium between tissue and blood and the distribution is limited by the blood flow rate to the tissues (76, 77). The equation of the flow-limited model is described as following:

$$\frac{dA_T}{dt} = Q_T * (C_A - C_{VT}) = Q_T * \left(C_A - \frac{C_T}{P_T}\right) \qquad \text{Equation 1}$$

where dA_T/dt is the rate of change of the substance in the tissue; Q_T is the blood flow rate to the tissue; C_A is the substance concentration in arterial blood entering the tissue; C_{VT} is the substance concentration in the venous blood leaving the tissue; C_T is the substance concentration in the tissue; and P_T is the partition coefficient of the compound in the tissue.

Diffusion-limited model is generally employed when the rate of substance distribution across membrane is limited by diffusion process. This model can be divided into two sub-compartments including the vascular and extravascular space (76-78). The equation of the diffusion-limited model is described as following:

$$\frac{dA_{T,V}}{dt} = Q_T * \left(C_A - C_{T,V}\right) + PA_T * \left(\frac{C_{T,E}}{P_T} - C_{T,V}\right) \qquad \text{Equation 2}$$

$$\frac{dA_{T,E}}{dt} = PA_T * \left(C_{T,V} - \frac{C_{T,E}}{P_T}\right) \qquad \text{Equation 3}$$

where $dA_{T,V}/dt$ and $dA_{T,E}/dt$ represents the rate of change of substance in the vascular and extravascular tissue; $V_{T,V}$ and $V_{T,E}$ are the volumes of the tissue vascular and extravascular space; $C_{T,V}$ and $C_{T,E}$ are the substance concentration in the tissue vascular and extravascular; and PA_T is the diffusion permeate constant of the tissue.

Model parameterizations

Components of PBPK model consist of the tissues which are represented by specific compartments. In PBPK model, input parameters are required to solve differential equation; thus, there are divided into three types including the physiological specific properties (organ volumes or mass, tissue compositions, blood flow rates), physicochemical specific properties (plasma protein binding, tissue-to-plasma distribution or partition coefficient) and biochemical properties (membrane transporter, enzymatic activity, rate of absorption) (25, 69, 71, 73).

1. Physiological parameters

Physiological parameter values are varied among species and depend on body weight which is set to standard reference values for the rat (0.25 kg) and human (70 kg). Physiological parameter values such as tissue volumes (V_T), blood flow to tissues (Q_T), and cardiac output (Q_C) are obtained from published literature by Brown, et al. (79).

Tissue mass balances are represented as percentage of average body weight, as shown in Table 8. These values require mass-to-volume conversion with the assumption of unity density, which approximately equals to 1 (79). Typically, tissue volumes are expressed as unit of liter (L) that is readily calculated by multiplying the body weight with the corresponding fractional volume of tissue.

Tissue blood flow rates are represented as percentage of cardiac output, as shown in Table 9. Cardiac output values in rats and humans are calculated using blood flow fraction constant (80) and are scaled up with body weight to the power function exponent of 0.75 (81).

Table 8 Fractional volumes of certain tissues in rats and humans

Tissue	Rats*	Humans*
Adipose	~7.0	21.4
Bone	7.3	14.3
Brain	0.6	2.0
Gastrointestinal tract	2.7	1.7
Heart	0.3	0.5
Kidneys	0.7	0.4
Liver	3.4	2.6
Lungs	0.5	0.8
Muscle	40.4	40.0
Skin	19.0	3.7
Gastrointestinal tract contents	~5.0	1.4
Blood	7.4	7.9
Rest of body	5.7	3.3
Total	100.0	100.0

* All values are expressed as percentage of average body weight.

Source: Adapted from Brown, et al. (79)

Table 9 Regional blood flow distribution for rats and humans

Tissue	Rats*	Humans*
Adipose	7.0	5.2
Adrenals	0.3	-
Bone	12.2	4.2
Brain	2.0	11.4
Heart	5.1	4.0
Kidneys	14.1	17.5
Liver (Total)	18.3	22.7
Hepatic artery	2.1	-
Portal vein	15.3	18.1
Lung	2.1	-
Muscle	27.8	19.1
Skin	5.8	5.8
Thyroid	-	1.6

* All values are represented as percentage of cardiac output.

Source: Adapted from Brown, et al. (79)

2. Physicochemical parameters

Tissue disposition varies depending on chemical properties. The primary physicochemical parameters refer to tissue-plasma partition coefficients, which represent the distribution of a substance between tissues and blood at equilibrium (82). Predicted values of tissue-plasma partition coefficients ($P_{t:p}$) can be calculated using a conceptual equation developed by Poulin, et al. (82). The estimation concept developed by Poulin, et al. is that at steady state condition, the drug is homogeneously distributed into tissue by a passive diffusion process. In this process, certain input parameters are required including substance-specific parameters (lipophilicity, fraction unbound of plasma protein) obtained from *in vitro* experiment and species-specific parameters referred to as the fractional composition of the wet tissues obtained from the literature, as shown in Table 10. Values of fraction unbound (f_u) are quantified using specific

reversible binding to plasma proteins obtained from *in vitro* experimental technique. Values of $P_{t:p}$ for both non-adipose and adipose tissues are described as followed:

$$P_{t:p\ non-adipose} = \frac{[P_{o:w} \times (V_{nlt} + 0.3V_{pht})] + [1 \times (V_{wt} + 0.7V_{pht})]}{[P_{o:w} \times (V_{nlp} + 0.3V_{php})] + [1 \times (V_{wp} + 0.7V_{php})]} \times \frac{fu_p}{fu_t} \quad \text{Equation 4}$$

$$P_{t:p\ adipose} = \frac{[D_{o:w} \times (V_{nlt} + 0.3V_{pht})] + [1 \times (V_{wt} + 0.7V_{pht})]}{[D_{o:w} \times (V_{nlp} + 0.3V_{php})] + [1 \times (V_{wp} + 0.7V_{php})]} \times \frac{fu_p}{1} \quad \text{Equation 5}$$

where $P_{o:w}$, $D_{o:w}$ is the antilog of the log n-octanol:water partition coefficient and oil:buffer partition coefficient, V is the fractional tissue volume content of neutral lipids (nl), phospholipids (ph), and water (w), t is the tissue, p is the plasma, fu_p is the unbound fraction in the plasma, fu_t is the unbound fraction in the tissue that calculated using the equation: $fu_t = 1 / (1 + (((1\text{-}fu_p)/ fu_p*0.5)$.

Table 10 Fractional compositions of certain tissues in rats and in humans

Tissue	Volume fraction of wet tissue weight					
	Water (V_w)		Neutral Lipids (V_{nl})		Phospholipids (V_{ph})	
	Rats	Humans	Rats	Humans	Rats	Humans
Adipose	0.12	0.18	0.853	0.79	0.002	0.002
Bone	0.446	0.439	0.0273	0.074	0.0027	0.0011
Brain	0.788	0.77	0.0392	0.051	0.0533	0.0565
Gut	0.749	0.718	0.0292	0.0487	0.0138	0.0163
Heart	0.779	0.758	0.014	0.0115	0.0118	0.0166
Kidney	0.771	0.783	0.0123	0.0207	0.0284	0.0162
Liver	0.705	0.751	0.0138	0.0348	0.0303	0.0252
Lung	0.79	0.811	0.0279	0.003	0.014	0.009
Muscle	0.756	0.76	0.01	0.0238	0.009	0.0072
Skin	0.651	0.718	0.0239	0.0284	0.018	0.0111
Spleen	0.771	0.788	0.0077	0.0201	0.0136	0.0198
Plasma	0.960	0.945	0.00147	0.0035	0.00083	0.00225

Source: Adapted from Poulin, et al. (82)

3. Biochemical parameters

For biochemical parameter, it consists of absorption rate constants, metabolic parameters (i.e, first-order or second-order kinetics, Michaelis-Menten kinetic), and transporter activity (69, 74). These values are obtained from the published literature and are optimized from appropriate studies by visually comparing simulations with the selected dataset. These parameters can be estimated from *in vivo* studies or can be used an appropriate *in vitro-in vivo* extrapolation to scale up from *in vitro* studies to *in vivo* (81).

The metabolism rate is generally described by Michaelis-Menten kinetics. The reported rate of maximum velocity of metabolism (V_{max}) are varied depending on the experimental system. Data from *in vitro* experiments are required to be scaled up to whole tissue with scaling factors such as either microsomes, hepatocytes, or liver weight in gram of body weight, depending on species. Michaelis-Menten constant (K_m) value is used directly with conversion to appropriate units for running the model because it is expressed as concentration in venous at equilibrium with liver (83).

Model evaluation

PBPK models are developed using several differential equations performed by programming language (coding). Model evaluation is considered the ability of the model to predict the pharmacokinetic behaviors of the compounds. The adequacy of model parameters are evaluated based on comparison the results of model simulation with experimental data. Evaluating of the PBPK model has involved by visually inspection of the plots of model simulations compared to experimental values against a variance analysis. Optimization is offered using computer software leading to estimate unknown parameters from experimental data.

Regardless, sensitivity analysis is assessed to quantify how input parameters influence the output or to describe the relative importance of each input parameter that actual impact of changes in individual parameters on the output of model simulation. Model validation is defined as the process that assesses the adequacy and consistency of a model in predicting the kinetic behavior of the chemicals (84).

CHAPTER III

RESEARCH METHODOLOGY

This chapter represents the methodology employed in this study. The PBPK model development of mitragynine is divided into 6 main parts: 1) Characteristics of selected pharmacokinetic studies, 2) Conceptual PBPK model structure, 3) Mathematical representations, 4) Model parameterizations, 5) Computer software, and 6) Sensitivity analysis. The detail on each step is described below.

Characteristics of selected pharmacokinetic studies

In order to develop a PBPK model of mitragynine, a systematic review was performed to collect pharmacokinetic data of mitragynine from the published literature, as described in Chapter 2 (literature review). From literature searching, two pharmacokinetic studies in rats (64, 65) and one pharmacokinetic study in humans (68) were retrieved. The related studies are described below.

In the study by Kong, et al. (2017), six female Sprague-Dawley rats were intravenously administrated with a single dose of 10 mg/kg of mitragynine. Serial concentration levels of mitragynine were determined in plasma and in the brain every 30 min up to 7.5 hr. Mitragynine concentrations were determined using a microdialysis technique and an ultra-fast liquid chromatography-mass spectrometry (UFLC-MS) (65).

In another study by Avery, et al. (2019), six male Sprague-Dawley rats were orally administered with a single dose of 20 mg/kg mitragynine. Subsequently, serial blood samples were collected at the following time points: 0.083, 0.167, 0.25, 0.33, 0.5, 1, 2, 4, 6, 8, 12, and 24 hr. Samples were determined using an ultra-performance liquid chromatography-tandem mass spectrometry (UPLC-MS) (64).

To date, only one study concerning mitragynine pharmacokinetic in ten human subjects (kratom users) was identified (68), as shown in Table 7. Through personal communication, only five concentration-time profiles of mitragynine in plasma were obtained from the authors. Dosing schedule of five human subjects is summarized in Table 11. In brief, serial plasma samples were collected at 15, 30, and 45 minutes, 1, 1.25, 1.5, 1.75, 2, 2.5, 3, 4, 6, 9, 12, 19, and 24 hr post-kratom tea administration.

Individual plasma mitragynine concentrations were withdrawn by microdialysis technique and analyzed the mitragynine concentration levels using liquid chromatography-tandem mass spectrometry (LC-MS).

Table 11 Summary dosing regimens of mitragynine in five human subjects

Regimen	Subject	Daily doses (day 1-7)	Loading dose (day 8)	Total doses
I	1	9.96 mg per day	9.96 mg	79.68 mg
I	2	9.96 mg per day	9.96 mg	79.68 mg
I	3	9.96 mg per day	9.96 mg	79.68 mg
II	4	9.96 mg per day	19.92 mg	89.64 mg
III	5	11.50 mg per day	23 mg	103.5 mg

Source: Adapted from Trakulsrichai, et al. (68)

Conceptual PBPK model structure of mitragynine

A schematic representation of the conceptual PBPK model structure of mitragynine is illustrated in Figure 4. The whole-body PBPK model is described as a set of tissue compartments corresponding to tissues such as lung, fat, brain, slowly perfused tissues, kidney, and liver, which linked together by the circulatory blood system. A list of tissue compartments and their assumptions in the current PBPK model of mitragynine are described below:

1. Lung compartment represented as an interchange of the arterial and venous blood in the series with all other compartments.
2. Fat compartment represented as a storage tissue.
3. Brain compartment represented as a target tissue.
4. Slowly perfused tissues compartment represented as a slow rate of distribution (muscle).
5. Kidney compartment represented as rapidly perfused tissues.
6. Liver compartment function as a metabolizing organ.

Features of the PBPK model of mitragynine included: 1) protein-mediated transport in the brain; 2) enzyme-mediated metabolism in the liver; and 3) a diffusion-limited transport in the fat compartment. In the brain, protein-mediated transport was characterized by BCRP-mediated efflux transporter, which plays an important role in the disposition of mitragynine in the brain (60). In the liver, metabolism of mitragynine was assumed to solely occur in the liver. The hepatic CYP3A4 is an enzyme responsible for the metabolism of mitragynine which accounted for approximately 67% (51, 53). Initially, the flow-limited model was assumed for all tissue compartments. However, it was not adequately captured the plasma concentration-time course of mitragynine. Subsequently, the disposition of mitragynine in the fat compartment was assumed to be diffusion-limited model, which was divided into two sub-compartments (vascular and extravascular). Following this model structure, intravenous administration was developed first, while an oral administration was employed model structure as same intravenous model.

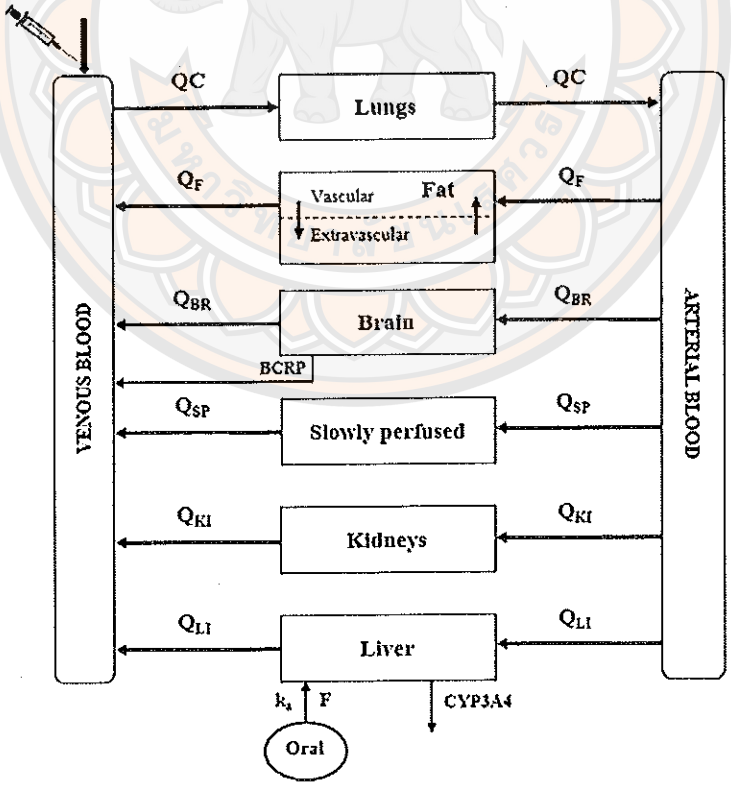

Figure 4 A schematic representation of the physiologically based pharmacokinetic (PBPK) model structure for mitragynine

Mathematical representations of the PBPK model for mitragynine

1. Route of administrations

The amount of mitragynine in the circulation system following an intravenous administration ($Input_{IV}$) was described as follow:

$$Input_{IV} = \frac{Dose * BW}{Time_{IV}} \quad \text{Equation 6}$$

The amount of mitragynine in the circulation system following an oral administration ($Input_{oral}$) was calculated as follows:

$$Input_{oral} = k_a * A_{GU} \quad \text{Equation 7}$$

$$A_{GU} = Dose * BW * F \quad \text{Equation 8}$$

where Dose is the mg per kg of body weight; BW is the body weight (kg); $Time_{IV}$ is the duration period of the injection (hr); A_{GU} is the amount of mitragynine in the gut lumen after oral administration (μg); k_a is the absorption rate constant (1/hr); and F is the bioavailability (%).

2. Venous and arterial blood

The rate of change of mitragynine in the venous blood (dA_V/dt) was calculated as follows:

$$\frac{dA_V}{dt} = Q_F * C_{VF} + Q_{BR} * C_{VBR} + Q_{SP} * C_{VSP} + Q_{KI} * C_{VKI} + Q_{LI} * C_{VLI} - QC * C_V$$

Equation 9

The rate of change of mitragynine in the arterial blood (dA_A/dt) was calculated as follows:

$$\frac{dA_A}{dt} = QC * C_{ALU} - C_A * (Q_F + Q_{BR} + Q_{SP} + Q_K + Q_{LI}) \quad \text{Equation 10}$$

where QC is the cardiac output (L/hr); C_V and C_A are the concentration of mitragynine in the venous blood (μg/L) and arterial blood (μg/L); C_{ALU} is the concentration of mitragynine in the arterial blood leaving the lung (μg/L); Q_F, Q_{BR}, Q_{SP}, Q_{KI}, Q_{LI} are the blood flow rate into the fat, brain, slowly perfused tissues, kidney, and liver (L/hr); and C_{VF}, C_{VBR}, C_{VSP}, C_{VKI}, C_{VLI} are the concentration of mitragynine in the venous blood leaving the fat, brain, slowly perfused tissues, kidney, and liver (μg/L).

3. Lung

The rate of change of mitragynine in the lung (dA_{LU}/dt) was calculated as follows:

$$\frac{dA_{LU}}{dt} = QC * (C_V - C_{ALU}) \qquad \text{Equation 11}$$

$$C_{ALU} = \frac{C_{LU}}{P_{LU}} = \frac{A_{LU}}{V_{LU} * P_{LU}}$$

where A_{LU} is the mass of mitragynine in the lung (μg); C_{LU} is the concentration of mitragynine in the lung (μg/L); V_{LU} is the volume of the lung (L); and P_{LU} is the partition coefficient of mitragynine in the lung.

4. Fat

The rate of change of mitragynine in the fat (dA_F/dt) was calculated as follows:

Vascular space

$$\frac{dA_{F,V}}{dt} = Q_F * (C_A - C_{F,V}) + PA_F * \left(\frac{C_{F,E}}{P_F} - C_{F,V}\right) \qquad \text{Equation 12}$$

$$C_{F,V} = \frac{A_{F,V}}{V_F * V_{F,V}}$$

Extravascular space

$$\frac{dA_{F,E}}{dt} = PA_F * \left(C_{F,V} - \frac{C_{F,E}}{P_F}\right) \qquad \text{Equation 13}$$

$$C_{F,E} = \frac{A_{F,E}}{V_F * (1 - V_{F,V})}$$

where $dA_{F,V}/dt$ and $dA_{F,E}/dt$ are the rates of change of mitragynine in the fat vascular space and extravascular space (µg); $C_{F,V}$ and $C_{F,E}$ are the concentration of mitragynine in the fat vascular space and extravascular space (µg/L); $V_{F,V}$ is the fraction of vascular space in fat (L); PA_F is the fat diffusion permeate constant; and P_F is the partition coefficient of mitragynine in the fat compartment.

5. Brain

The rate of change of mitragynine in the brain (dA_{BR}/dt) was calculated as follows:

$$\frac{dA_{BR}}{dt} = Q_{BR} * (C_A - C_{VBR}) - \frac{dA_{BCRP}}{dt} \qquad \text{Equation 14}$$

$$C_{VBR} = \frac{C_{BR}}{P_{BR}} = \frac{A_{BR}}{V_{BR} * P_{BR}}$$

where A_{BR} is the mass of mitragynine in the brain (µg); C_{BR} is the concentration of mitragynine in the brain (µg/L); V_{BR} is the volume of the brain (L); and P_{BR} is the partition coefficient of mitragynine in the brain.

In the brain, involvement of BCRP-mediated transport of mitragynine was incorporated. A Michaelis-Menten kinetic behavior was described as follow:

$$\frac{dA_{BCRP}}{dt} = (V_{max\_BCRP} * C_{VBR})/(K_{m\_BCRP} + C_{VBR}) \qquad \text{Equation 15}$$

where dA_{BCRP}/dt is the rate of change of mitragynine efflux transport; V_{max_BCRP} is the maximum velocity of BCRP (µmole/hr); and K_{m_BCRP} is the Michaelis-Menten constant of BCRP (µmole/L).

6. Slowly perfused tissues

The rate of change of mitragynine in the slowly perfused tissues (dA_{SP}/dt) was calculated as follows:

$$\frac{dA_{SP}}{dt} = Q_{SP} * (C_A - C_{VSP}) \qquad \text{Equation 16}$$

$$C_{VSP} = \frac{C_{SP}}{P_{SP}} = \frac{A_{SP}}{V_{SP} * P_{SP}}$$

where A_{SP} is the mass of mitragynine in the slowly perfused tissues (μg); C_{SP} is the concentration of mitragynine in the slowly perfused tissues (μg/L); V_{SP} is the volume of the slowly perfused tissues (L); and P_{SP} is the partition coefficient of mitragynine in the slowly perfused tissues.

7. Kidney

The change in the mass of mitragynine over time in the kidney (dA_{KI}/dt) was calculated as follows:

$$\frac{dA_{KI}}{dt} = Q_{KI} * (C_A - C_{VKI}) \qquad \text{Equation 17}$$

$$C_{VKI} = \frac{C_{KI}}{P_{KI}} = \frac{A_{KI}}{V_{KI} * P_{KI}}$$

where A_{KI} is the mass of mitragynine in the kidney (μg); C_{KI} is the concentration of mitragynine in the kidney (μg/L); V_{KI} is the volume of the kidney (L); and P_{KI} is the partition coefficient of mitragynine in the kidney.

8. Liver

The rate of change of mitragynine in the liver (dA_{LI}/dt) was calculated as follows:

$$\frac{dA_{LI}}{dt} = Q_{LI} * (C_A - C_{VLI}) - Met_H \qquad \text{Equation 18}$$

$$C_{VLI} = \frac{C_{LI}}{P_{LI}} = \frac{A_{LI}}{V_{LI} * P_{LI}}$$

where A_{LI} is the mass of mitragynine in the liver (μg); C_{LI} is the concentration of mitragynine in the liver (μg/L); V_{LI} is the volume of the liver (L); and P_{LI} is the partition coefficient of mitragyning in the liver.

In the liver, hepatic enzyme-mediated metabolism of mitragynine was assumed by CYP3A4. To describe the hepatic CYP3A4-mediated metabolism process, a Michaelis-Menten kinetic behavior was employed and described as follow:

$$\frac{dA_{CYP3A4}}{dt} = (V_{max\_CYP3A4} * C_{VLI})/(K_{m\_CYP3A4} + C_{VLI}) \qquad \text{Equation 19}$$

where V_{max_CYP3A4} is the maximum velocity of CYP3A4 (μmole/hr); K_{m_CYP3A4} is the Michaelis-Menten constant of CYP3A4 (μmole/L).

Model parameterizations

All parameters acquired in the developed PBPK model of mitragynine are shown in Table 12. In this model, the body weight for rats and humans were assumed to be 0.25 kg and 70 kg, respectively. The model parameterization was divided into 3 categories, i.e. physiological, physicochemical, and biochemical parameters. The physiological parameters including tissue volumes and blood flow rates both in rats and in humans were determined from the published study report by Brown, et al. (79). For physicochemical parameters, the partition coefficients of mitragynine in each tissue were calculated based on computational approach proposed by Poulin, et al. (2002) (41). This method was based on tissue compositions and specific chemical characteristics of the chemical. The biochemical parameters describing kinetic behaviors including the maximum velocity (V_{max}) and Michaelis-Menten constant (K_m) of protein-mediated transport and hepatic enzyme-mediated metabolism, fat diffusion permeation constant (PAFC), particularly absorption rate constant (k_a), and bioavailability (F) were obtained using the optimization process in Berkeley Madonna software.

Table 12 Parameters used in the developed PBPK model of mitragynine

Parameter (unit)	Symbol	Rat	Human
Reference body weight (kg)	BW	0.25	70
Tissue volume (L/kg)			
Lung	V_{LU}	0.005 [a]	0.08 [a]
Fat	V_F	0.07 [a]	0.214 [a]
Brain	V_{BR}	0.006 [a]	0.02 [a]
Slowly perfused tissues	V_{SP}	0.404 [a]	0.4 [a]
Liver	V_{LI}	0.007 [a]	0.004 [a]
Kidney	V_{KI}	0.034 [a]	0.026 [a]
Venous blood	V_V	0.0544 [a]	0.0514 [a]
Arterial blood	V_A	0.0272 [a]	0.0257 [a]
Tissue blood Flow (L/hr)			
Cardiac output	QC	5.30 [a]	363.01 [a]
Fat	Q_F	0.07 [a]	0.052 [a]
Brain	Q_{BR}	0.02 [a]	0.114 [a]
Slowly perfused tissues	Q_{SP}	0.278 [a]	0.191 [a]
Liver	Q_{LI}	0.141 [a]	0.175 [a]
Kidney	Q_{KI}	0.183 [a]	0.227 [a]
Fraction of blood in fat	FVBF	0.02 [b]	0.02 [b]
Molecular weight (g/mole)	MW	398.50	
Tissue partition coefficient			
Lung	P_{LU}	1.12 [c]	0.52 [c]
Fat	P_F	4.37 [c]	3.64 [c]
Brain	P_{BR}	0.86 [d]	2 [c]
Slowly perfused tissue	P_{SP}	0.74 [c]	0.98 [c]
Liver	P_{LI}	0.96 [c]	0.98 [c]
Kidney	P_{KI}	0.98 [c]	1.37 [c]
Binding affinity (μmole/L)			
Breast cancer resistance protein	K_{m_BCRP}	11 [g]	14 [e]
CytochromeP450 3A4	K_{m_CYP3A4}	85 [g]	103.3 [f]
Maximum velocity (μmole/hr)			
Breast cancer resistance protein	V_{max_BCRP}	1.7 [g]	*

Table 12 (cont.)

Parameter (unit)	Symbol	Rat	Human
CytochromeP450 3A4	V_{max_CYP3A4}	0.3 [g]	*
Fat diffusion rate constant (L/hr/kg of tissue)	PAFC	1.5 [g]	*
Absorption rate constant (1/hr)	k_a	0.5 [g]	*
Bioavailability	F	0.08 [g]	*

[a] Calculated from Brown, et al. (79)

[b] Adapted from Tornero-Velez, et al. (85)

[c] Calculated from Poulin, et al. (82)

[d] Adapted from Yusof, et al. (86)

[e] Adapted from Wagmann, et al. (2018) (60)

[f] Adapted from Hanapi, et al. (2013) (51)

[g] Optimized values from Berkeley Madonna software

Note: (*) Individual values of these parameter values are summarized in Table 13

Table 13 Individual optimized parameter values in the developed PBPK model of mitragynine in human subjects

Parameter (unit)	Symbol	Subject				
		1	2	3	4	5
Maximum velocity (μmole/hr)						
Breast cancer resistance protein	V_{max_BCRP}	325	75	149	312	115
CytochromeP450 3A4	V_{max_CYP3A4}	41	19	37	53	27
Fat diffusion rate constant (L/hr/kg of tissue)	PAFC	1	1.8	0.5	0.9	1.2
Absorption rate constant (1/hr)	k_a	2.2	0.7	1.7	2	1.5
Bioavailability	F	0.21	0.4	0.12	0.18	0.36

Computer software for model development

The PBPK model was constructed using Berkeley Madonna Software (developed by Robert Macey and George Oster of the University of California at Berkeley, version 8.3.18). This software was used to simulate, to analyze the sensitivity of the input parameters corresponding to the output, and to optimize the parameter values. The results of model simulation were compared with experimental dataset obtained from the selected pharmacokinetic studies. Plots of concentration versus time appeared in each experimental study were extracted using WebPlotDigitizer (version 4.1) which free online website.

Sensitivity analysis

In this model, sensitivity analysis was performed to prioritize the effect of each input parameter on certain output parameters (i.e. concentration-time course of mitragynine in the plasma). The sensitivity coefficient ($S_{p(t)}$) for parameter (p) at time (t) was calculated using the following formula:

$$S_{p(t)} = \frac{C_{2(t)} - C_{1(t)}}{\Delta} \qquad \text{Equation 20}$$

where $C_{1(t)}$ was the output parameter of mitragynine levels in the venous blood, arterial blood, lung, fat, brain, slowly perfused tissues, kidney, and liver using the initial parameter value at time (t), $C_{2(t)}$ was the output with a 1% increase of the parameter value at time (t), and Δ was equal to 0.001*P. The sensitivity coefficient was analyzed after the starting point. Each parameter was considered with the sensitivity coefficient of ≥ 10 or ≤ -10 during the analysis period of simulation and observation data were deemed as equivalent dose.

CHAPTER IV

RESULTS

This chapter represents the results of this study. The results were divided into 5 sections as follows: 1) PBPK model development of mitragynine; 2) PBPK model simulations of mitragynine in rats following a single dose intravenous administration; 3) PBPK model simulations of mitragynine in rats following a single dose oral administration; 4) PBPK model simulations of mitragynine in humans following orally repeated dose administration; and 5) Sensitivity analysis of the PBPK model simulation of mitragynine both in rats and in humans. The details for each section are described below.

Section I: PBPK model development of mitragynine

A conceptual PBPK model of mitragynine was illustrated in Figure 4. The model structure comprised of 6 tissue compartments including lung, fat, brain, slowly perfused tissues, kidney, and liver. All tissue compartments were described using a flow-limited assumption, except the fat compartment which was described as a diffusion-limited assumption. Initially, the fat tissue compartment followed as a flow-limited assumption like all other model compartments. The simulating results of mitragynine in fat compartment showed in Figure 5. However, the initial model failed to describe the available dataset such as plasma and brain, as presented in Figure 6 and Figure 7. As result, a diffusion-limited behavior of mitragynine transport within the fat compartment was introduced. The performance of the developed PBPK model under this newly introduced assumption was significantly improved, as shown in Figure 8.

After the model was modified, the PBPK model of mitragynine features 1) BCRP-mediated transport involved in the brain; 2) hepatic CYP3A4-mediated metabolism incorporated into our developed model; and 3) a diffusion-limited transport in the fat compartment. Model parameters acquired from published data as well as optimized parameter values for both rats and humans are summarized in Table 12 and Table 13.

The simulation results obtained from the developed PBPK model of mitragynine could describe the mitragynine concentration-time courses in plasma and in the brain of the experimental data acquired from selected pharmacokinetic studies conducted in rats following a single dose of intravenous administration (65). Then, PBPK model development of mitragynine could describe mitragynine concentration-time courses in plasma following a single dose oral administration in rats (64), and repeated oral dose administration in humans (68). Based on published pharmacokinetics of mitragynine, tissue disposition is not readily available except plasma and brain concentration-time courses of mitragynine in rats (65). Subsequently, this model could predict mitragynine concentration levels in other tissue compartments such as lung, fat, slowly perfused tissues, kidney, and liver both in rats and in humans but further experimental design on the tissue disposition of this compound should be conducted to be able to compare with those simulating results of the developed mitragynine PBPK model.

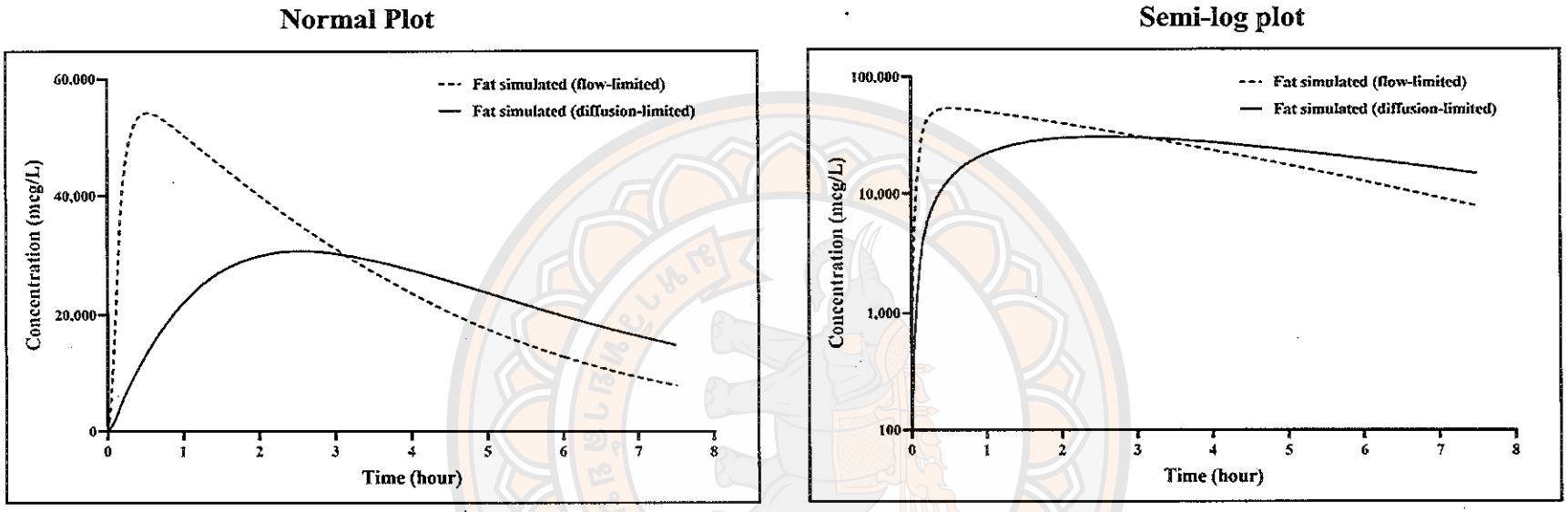

Figure 5 Model simulations of mitragynine in the fat compartment of rats following a single intravenous dose of mitragynine (10 mg/kg). Solid lines and dotted lines are mitragynine concentration levels in the fat compartment as a diffusion-limited and a flow-limited assumption, respectively

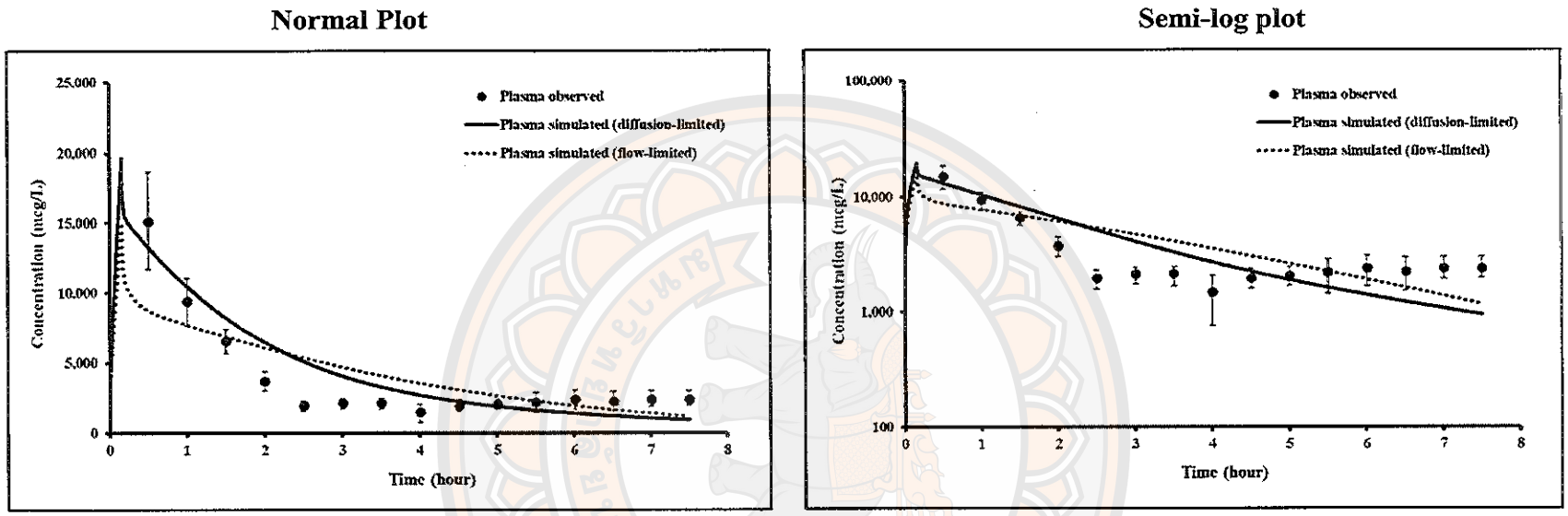

Figure 6 Comparison model simulations of mitragynine in plasma of rats using fat compartment as a diffusion-limited and a flow-limited assumption following a single intravenous dose of mitragynine (10 mg/kg). Close cycles with error bars (standard error) are plasma concentration levels of mitragynine in rats (n=6) taken from the study by Kong, et al. (65). Solid lines and dotted lines are model simulations of mitragynine in plasma of rats with fat compartment as a diffusion-limited and a flow-limited assumption, respectively

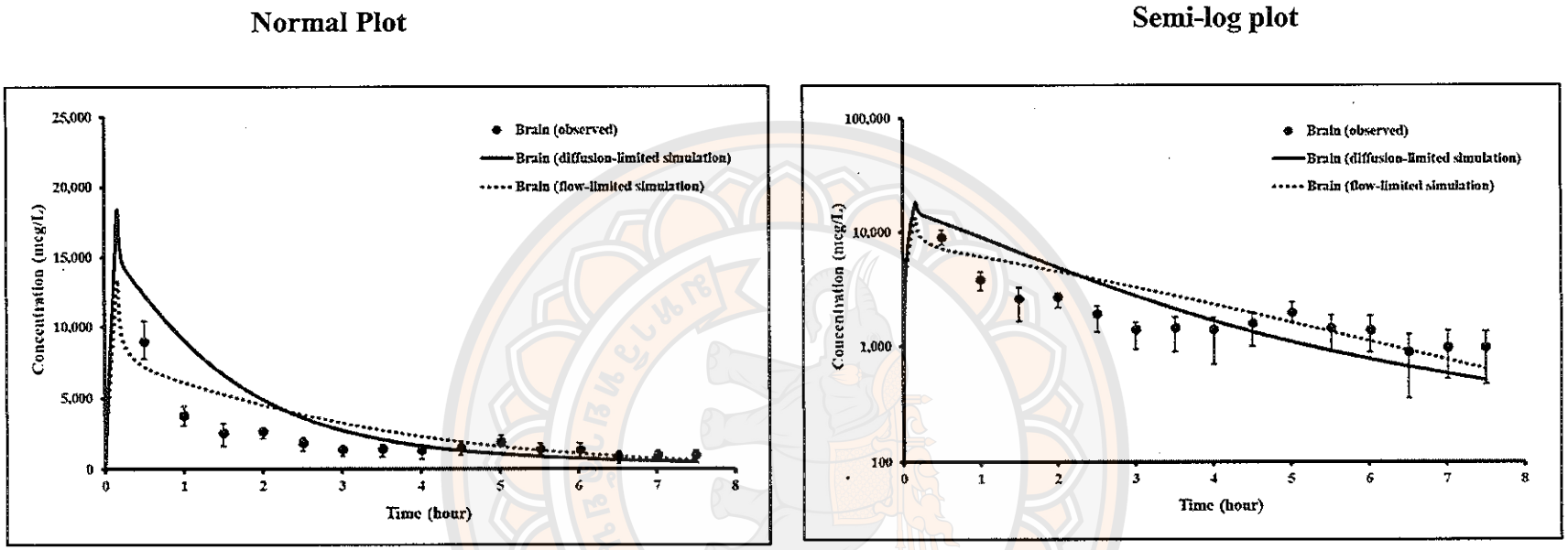

Figure 7 **Comparison model simulations of mitragynine in the brain of rats using fat compartment as a diffusion-limited and a flow-limited assumption following a single intravenous dose of mitragynine (10 mg/kg). Close cycles with error bars (standard error) are brain concentration levels of mitragynine in rats (n=6) taken from the study by Kong, et al. (65). Solid lines and dotted lines are model simulations of mitragynine in the brain of rats with fat compartment as a diffusion-limited and a flow-limited assumption, respectively**

Section II: PBPK model simulation of mitragynine in rats following a single dose of intravenous administration

This model successfully described the mitragynine concentration-time courses in plasma and in the brain of rats receiving 10 mg mitragynine per kg body weight through intravenous administration, as shown in Figure 8 and Figure 9. Model simulations of mitragynine concentration levels in plasma and in the brain can satisfactorily describe the experimental data acquired from the study by Kong, et al. (65). According to these simulating results, predicted C_{max} of mitragynine in plasma and in the brain are 19.67 and 18.41 μg/mL, respectively. While the observed datasets for assuming 90% protein binding, C_{max} of mitragynine in plasma and in the brain are 15.2 and 9.2 μg/mL, respectively (65). In addition, the observed and predicted AUC_{0-t} of mitragynine in plasma are 34.7 and 35.20 μg.hr/mL, respectively. While, the observed and predicted AUC_{0-t} of mitragynine in the brain are 22.4 and 27.34 μg.hr/mL, respectively.

The ratio of mitragynine concentration in the brain and in plasma (AUC_{brain}/AUC_{plasma}) from experimental study and simulating results are 0.65 and 0.77, respectively. These results suggested that mitrgynine can penetrate across the blood brain barrier into the brain. The average percentage difference between the observed data and simulating results of in plasma and in the brain are 1.82 and 8.52 %, respectively.

The developed PBPK model was employed to simulate the disposition of mitragynine in rat tissue compartments such as lungs, fat, slowly perfused tissues, kidney, and liver, as demonstrated in Figure 10. Those simulating results showed that concentration levels of mitragynine relatively decreased over time for all of those tissue compartments. However, mitragynine concentration levels in the fat compartment was higher with a substantially lowered rate elimination compared to those in other organ compartments.

Normal Plot

Semi-log plot

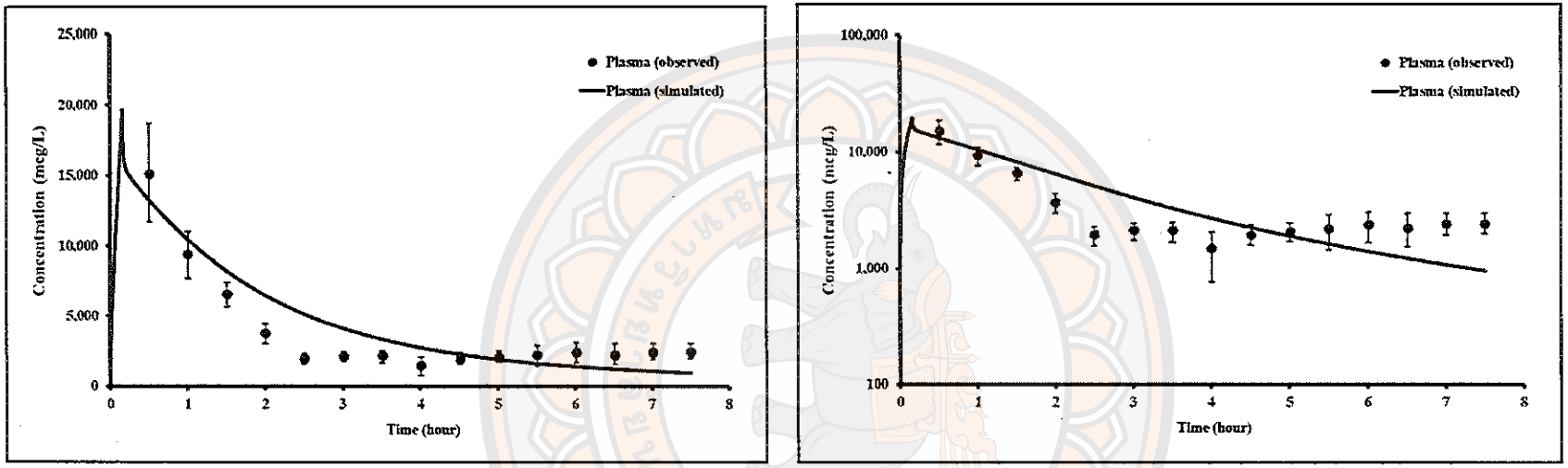

Figure 8 **Concentration-time profiles of mitragynine in plasma of rats following a single intravenous dose of mitragynine (10 mg/kg). Close cycles with error bars (standard error) are plasma concentration levels of mitragynine in rats (n=6) taken from the study by Kong, et al. (65). Solid lines are model simulations from the developed PBPK model of mitragynine**

Normal Plot **Semi-log plot**

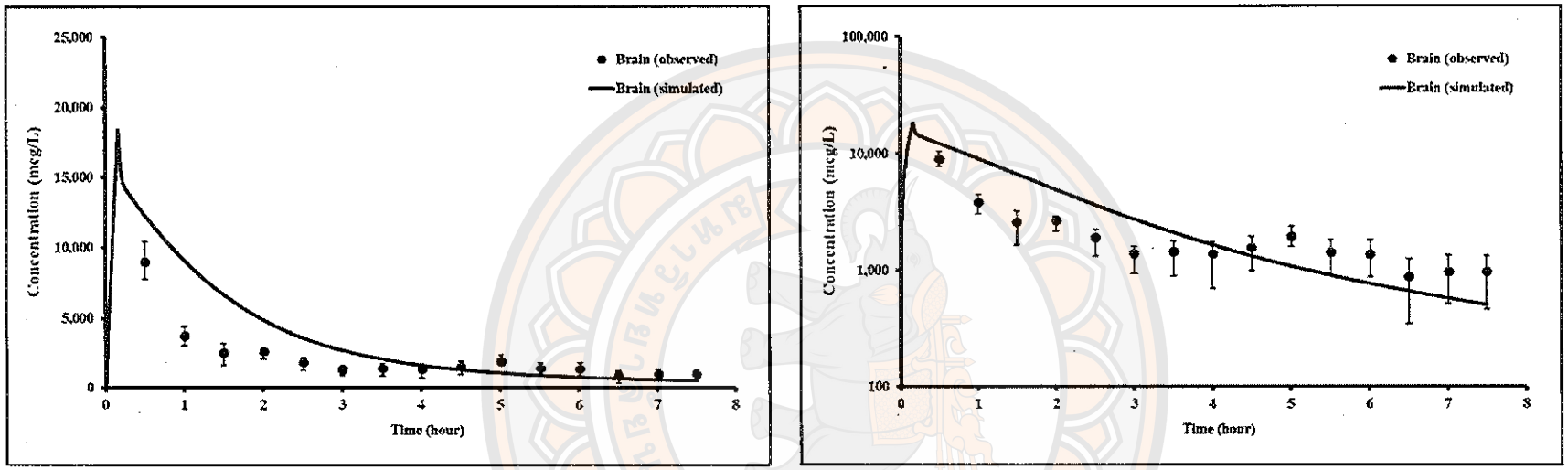

Figure 9 Concentration-time profiles of mitragynine in the brain of rats following a single intravenous dose of mitragynine (10 mg/kg). Close cycles with error bars (standard error) are brain concentration levels of mitragynine in rats (n=6) taken from the study by Kong, et al. (65). Solid lines are model simulations from the developed PBPK model of mitragynine

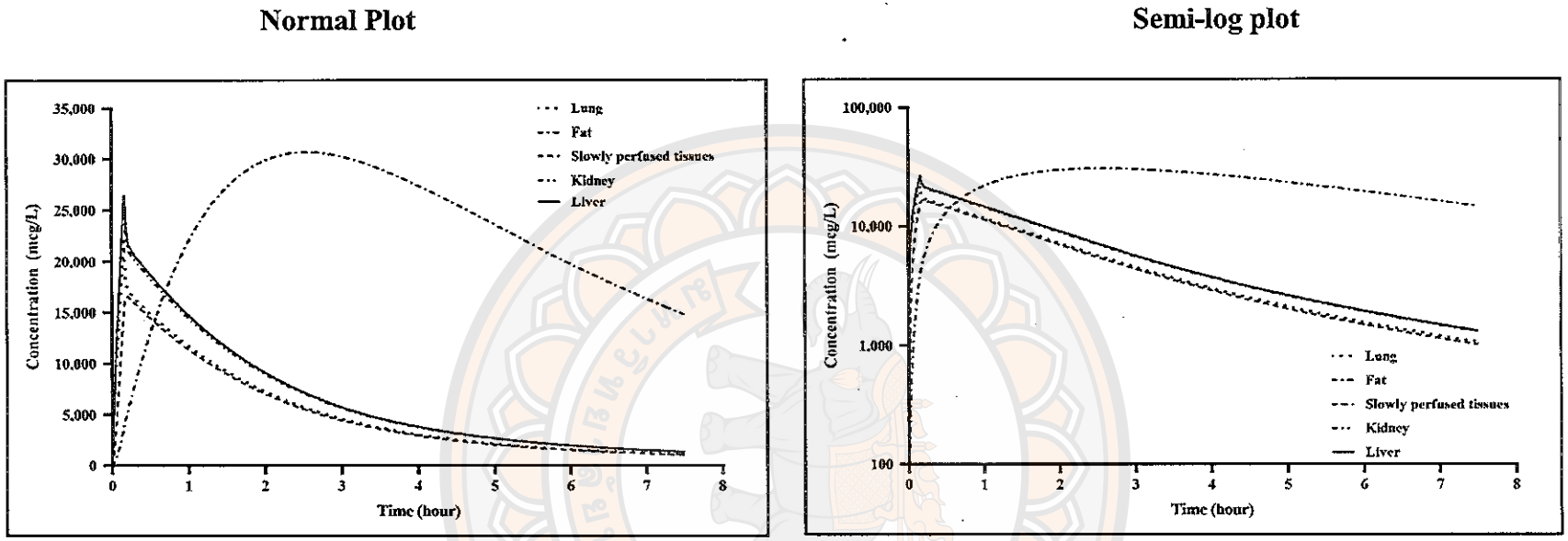

Figure 10 Model simulations of mitragynine concentration levels in rat tissue compartments following a single intravenous dose of mitragynine (10 mg/kg)

Section III: PBPK model simulation of mitragynine in rats following a single dose of oral administration

Our model outputs are compared to the observed plasma concentration-time courses in rats orally administered single dose 20 mg mitragynine per kg body weight, which acquired from the reported by Avery, et al. (64). Model simulation and observed plasma mitragynine concentration levels are presented in Figure 11. The observed and predicted C_{max} of mitragynine in plasma are 0.45 and 0.76 µg/mL, respectively. While the observed and predicted T_{max} of mitragynine in plasma are 1.5 and 1.62 hr, respectively. In addition, the observed and predicted AUC_{0-t} of mitragynine in plasma are 2.88 and 4.3 µg.hr/mL, respectively.

From model simulation of mitragynine in the brain of rats, predicted C_{max}, T_{max}, and AUC_{0-t} are 0.4 µg/mL, 1.63 hr, and 2.22 µg.hr/mL, respectively (Figure 12). According to simulating results of mitragynine in the brain and in plasma, ratio AUC_{brain}/AUC_{plasma} of mitragynine is about 0.5.

In addition, pharmacokinetic parameters of mitragynine are determined such as C_{max}, T_{max}, and AUC_{0-t} in all tissue compartments. Simulating results of mitragynine concentration levels in lung, fat, slowly perfused tissues, kidney, and liver with predicted C_{max} are 0.85, 2.7, 0.8, 1.04, and 1.15 µg/mL, respectively (Figure 13). The predicted T_{max} in those tissue compartments are 1.62, 4.27, 1.68, 1.62, and 1.5 hr, respectively. The predicted AUC_{0-t} of mitragynine in those tissue compartments are 4.82, 26.12, 4.53, 5.88, and 6.38 µg.hr/mL, respectively. Interestingly, mitragynine concentration level in the fat compartment are significantly higher and persist longer may be due to a much higher partition coefficient values of the fat.

Normal Plot **Semi-log plot**

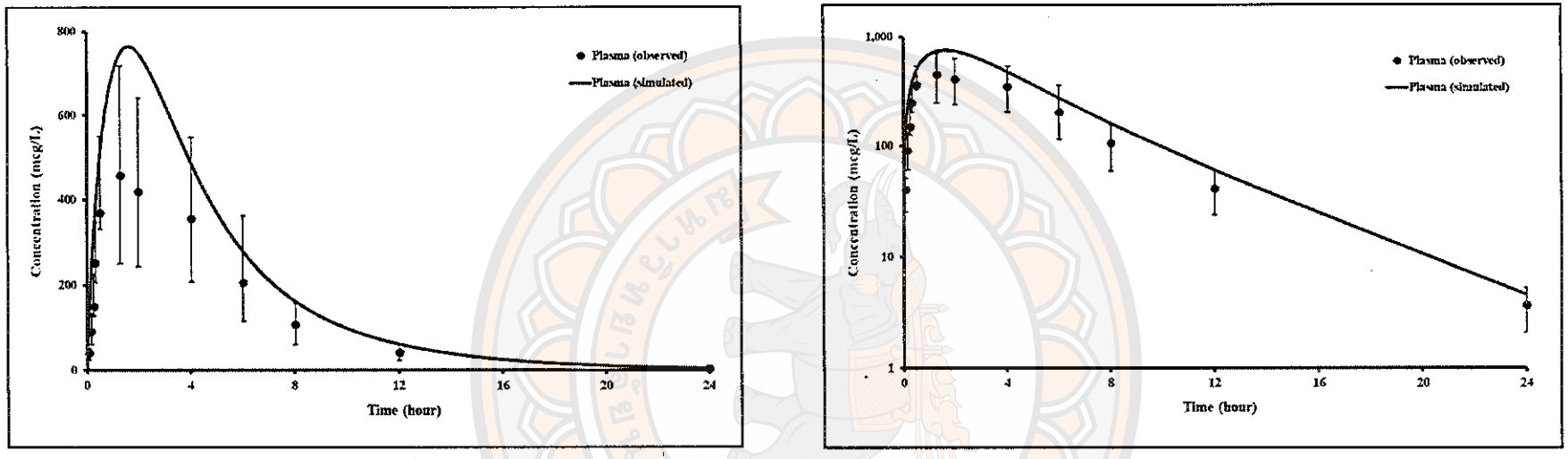

Figure 11 Concentration-time profiles of mitragynine in plasma of rats following a single oral dose of mitragynine (20 mg/kg). Close cycles with error bars (standard error) are plasma concentration levels of mitragynine in rats (n = 6) taken from the study by Avery, et al. (2019) (64). Solid lines are model simulations from the developed PBPK model of mitragynine

Normal Plot **Semi-log plot**

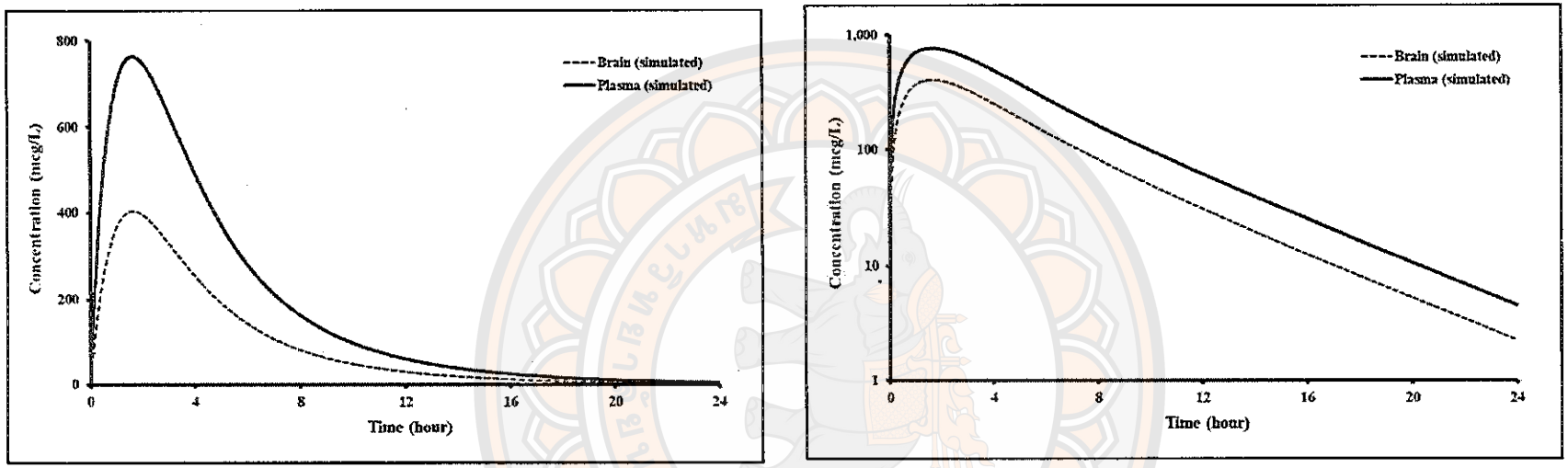

Figure 12 Model simulations of mitragynine concentration levels in plasma and in the brain of rats following a single oral dose of mitragynine (20 mg/kg)

Normal Plot **Semi-log plot**

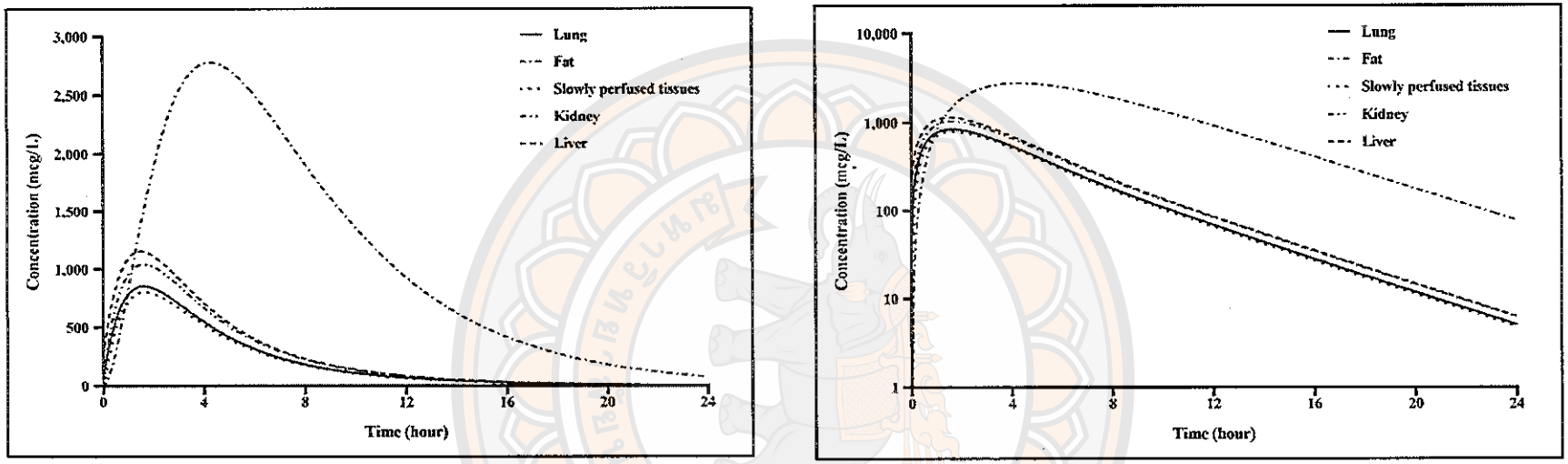

Figure 13 Model simulations of mitragynine concentration levels in rat tissue compartments following a single oral dose of mitragynine (20 mg/kg)

Section IV: PBPK model simulation of mitragynine in humans following orally repeated dose administration

Model simulations are compared to the observed datasets acquired from the study by Trakulsrichai, et al. (68). Five human subjects were orally administered 3 different dosing regimens of mitragynine in the form of kratom tea, as summarized in Table 11. Our model outputs can satisfactorily describe the individual plasma concentration-time profiles in five human subjects, as presented in Figure 14-18. From model outputs, predicted C_{max}, T_{max}, and $AUC_{0\text{-}t\ (D7\text{-}8)}$ of mitragynine in plasma and in the brain are determined to define rate and extent absorption, as presented in Table 14. For plasma concentration-time course in five human subjects, those simulating results compared to the individual observed data from the study by Trakulsrichai, et al. The average percentage difference between the observed datasets and simulating results is in the range of 1.9-54 %.

Providing that the developed model can adequately predict mitragynine concentration levels in the brain then determined C_{max}, T_{max}, and $AUC_{0\text{-}t\ (D7\text{-}8)}$, as presented in Table 14. These simulating results showed that predicted C_{max} and $AUC_{0\text{-}t\ (D7\text{-}8)}$ of mitragynine in the brain found to be 2 times higher than in plasma both observed datasets and model simulations in plasma. In addition, predicted ratio $AUC_{brain}/AUC_{plasma,\ (D7\text{-}8)}$ of mitragynine is in the range of 1.6-2.2, respectively.

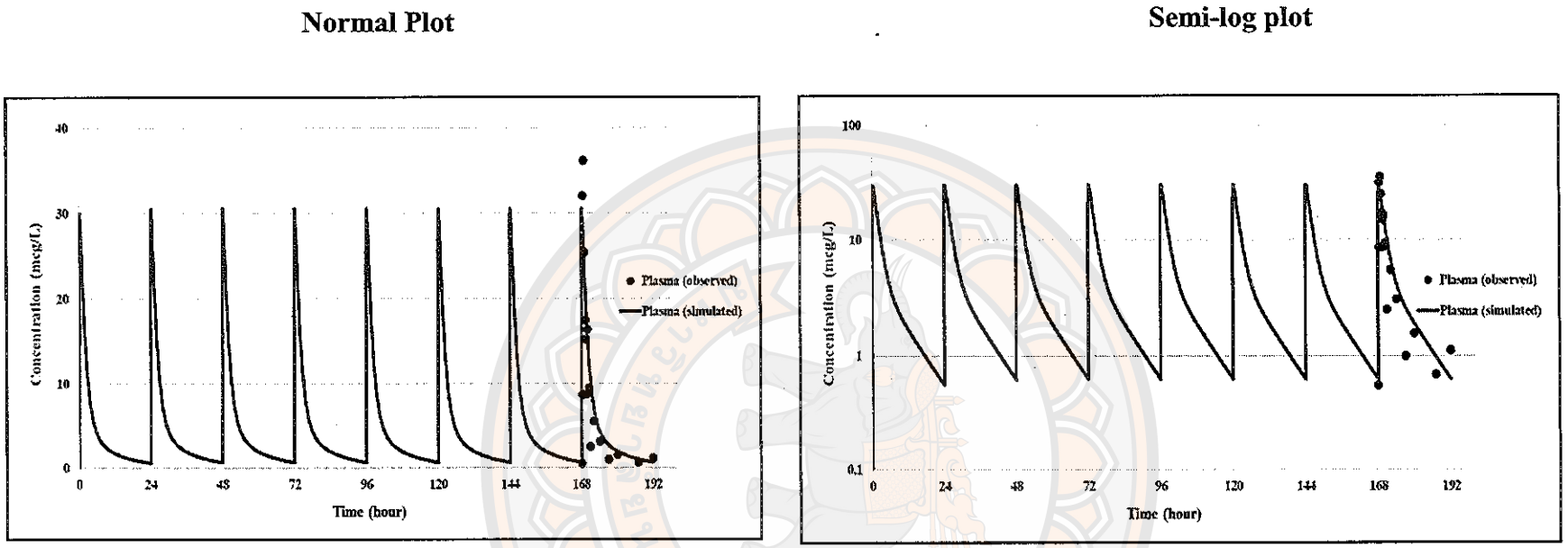

Figure 14 Concentration-time profiles of mitragynine in plasma of subject 1 receiving repeated oral dose of mitragynine in the form of kratom tea (dosing regimen I: 9.96 mg every day 7 days followed by 9.96 mg on day 8). Close cycles are plasma concentration levels of mitragynine taken from the study by Trakulsrichai, et al. (68). Solid lines are model simulations from the developed PBPK model of mitragynine

Normal Plot **Semi-log plot**

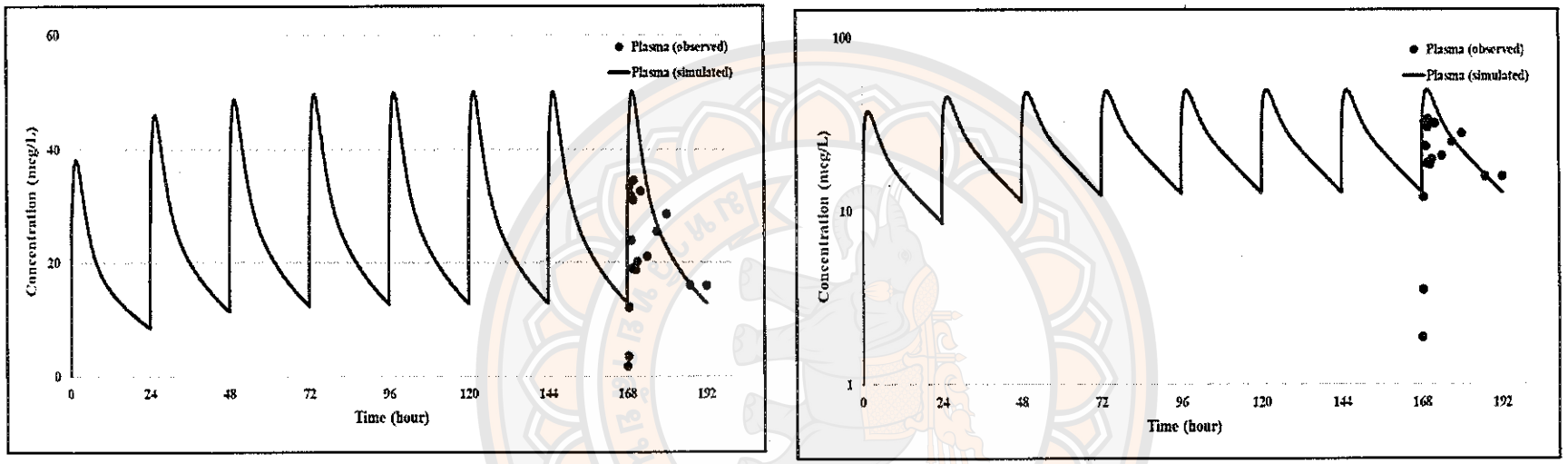

Figure 15 Concentration-time profiles of mitragynine in plasma of subject 2 receiving repeated oral dose of mitragynine in the form of kratom tea (dosing regimen I: 9.96 mg every day 7 days followed by 9.96 mg on day 8). Close cycles are plasma concentration levels of mitragynine taken from the study by Trakulsrichai, et al. (68). Solid lines are model simulations from the developed PBPK model of mitragynine

Normal Plot **Semi-log plot**

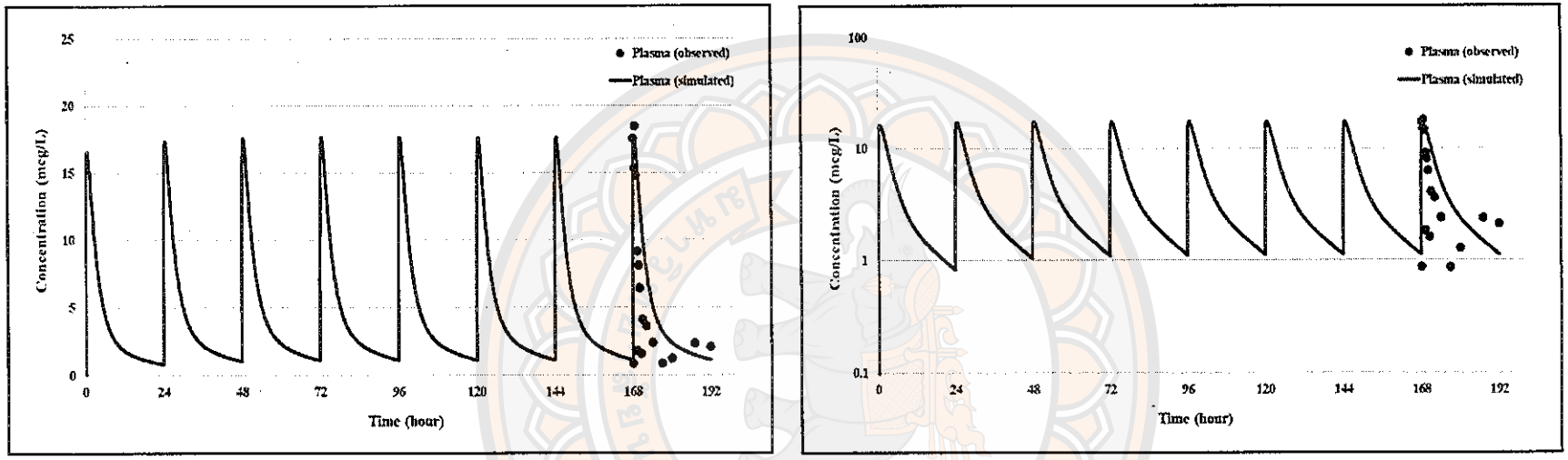

Figure 16 Concentration-time profiles of mitragynine in plasma of subject 3 receiving repeated oral dose of mitragynine in the form of kratom tea (dosing regimen I: 9.96 mg every day 7 days followed by 9.96 mg on day 8). Close cycles are concentration levels of mitragynine taken from the study by Trakulsrichai, et al. (68). Solid lines are model simulations from the developed PBPK model of mitragynine

Normal Plot **Semi-log plot**

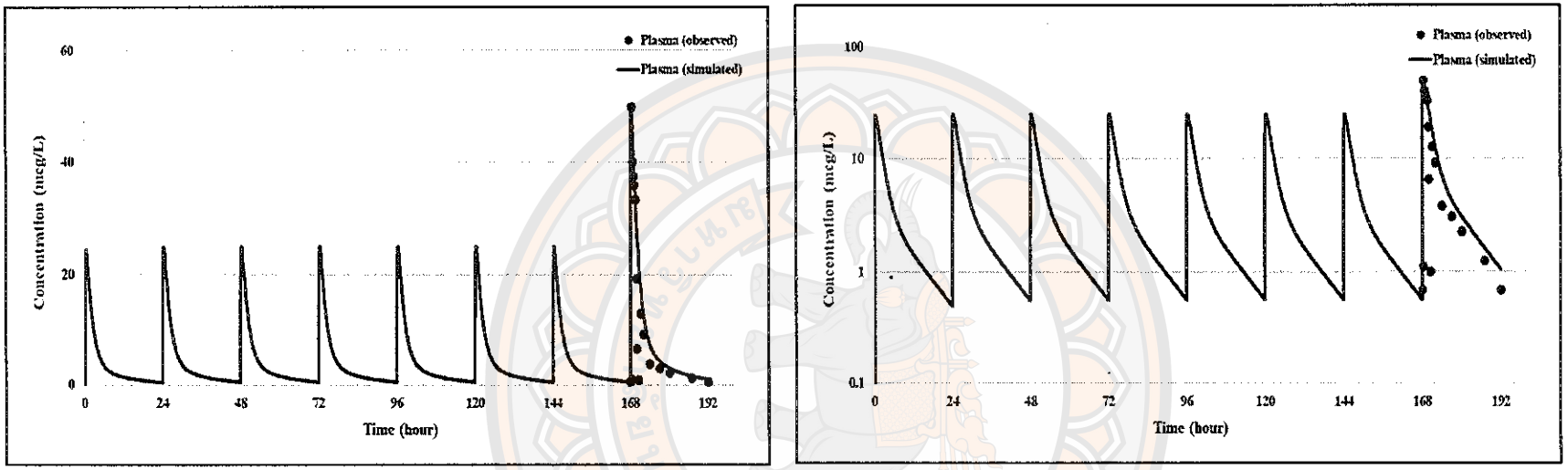

Figure 17 Concentration-time profiles of mitragynine in plasma of subject 4 receiving repeated oral dose of mitragynine in the form of kratom tea (dosing regimen II: 9.96 mg every day 7 days followed by 19.92 mg on day 8). Close cycles are concentration levels of mitragynine taken from the study by Trakulsrichai, et al. (68). Solid lines are model simulations from the developed PBPK model of mitragynine

Normal Plot **Semi-log plot**

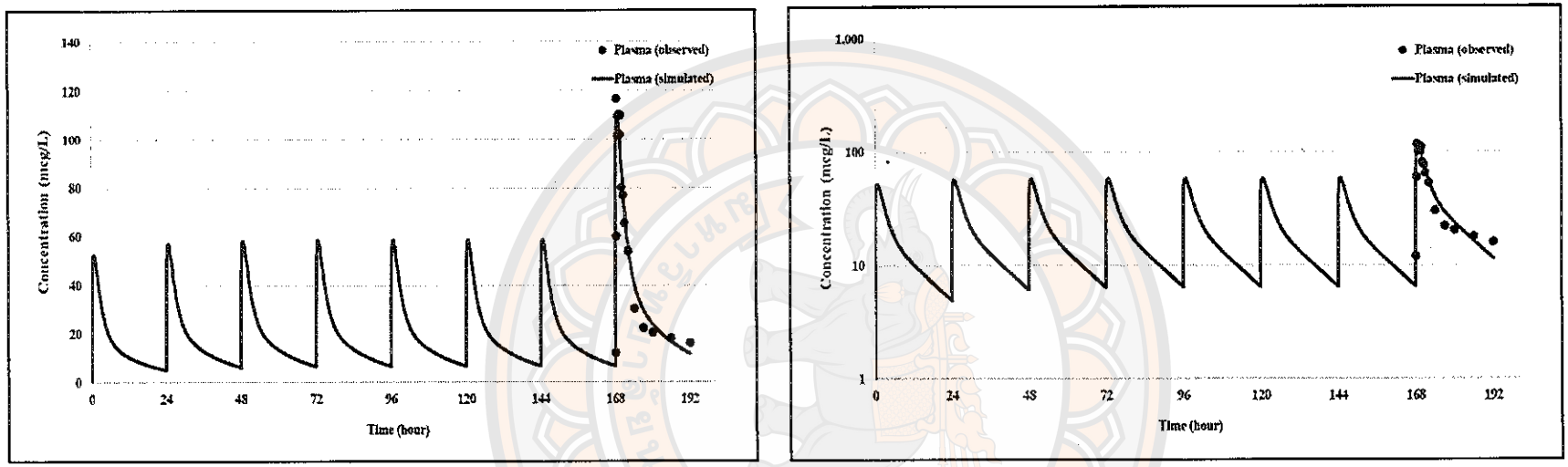

Figure 18 Concentration-time profiles of mitragynine in plasma of subject 5 receiving repeated oral dose of mitragynine in the form of kratom tea (dosing regimen III: 11.50 mg every day 7 days followed by 23 mg on day 8). Close cycles are concentration levels of mitragynine taken from the study by Trakulsrichai, et al. (68). Solid lines and are model simulations from the developed PBPK model of mitragynine

Table 14 Comparison pharmacokinetic parameters of five human subjects following multiple dosing regimens of mitragynine

Subject	C_{max} (µg/mL)		T_{max} (hr)		$AUC_{0\text{-}t\ (D7\text{-}8)}$ (µg.hr/mL)		$C_{max,\ brain}$ (µg/mL)	$T_{max,\ brain}$ (hr)	$AUC_{0\text{-}t\ (D7\text{-}8),}$ (µg.hr/mL)	Ratio $AUC_{0\text{-}t\ (D7\text{-}8),\ brain/plasma}$
	Observed	Predicted	Observed	Predicted	Observed	Predicted	Predicted	Predicted	Predicted	Predicted
1	0.036	0.03	0.75	0.35	0.082	0.109	0.048	0.41	0.175	1.6
2	0.034	0.05	2	1.71	0.533	0.626	0.114	1.78	1.437	2.2
3	0.018	0.017	0.75	0.64	0.067	0.105	0.035	0.71	0.214	2
4	0.049	0.049	0.5	0.4	0.12	0.184	0.08	0.45	0.3	1.6
5	0.116	0.111	0.5	0.74	0.769	0.825	0.238	0.8	1.773	2.14

Note: C_{max} = maximal concentration level; T_{max} = time to reach maximal concentration, AUC = area under the concentration-time curve

Section V: Sensitivity analysis of the PBPK model simulation of mitragynine both in rats and in humans

Sensitivity analysis was conducted both in rats and in humans. The sensitivity analysis of the input parameters values on mitragynine plasma concentration levels was determined at various time points in rats following a single intravenous dose (10 mg/kg), as shown in Figure 19. Whereas a single oral dose administration (20 mg/kg) is illustrated in Figure 20. Effects of the potential input parameters on plasma concentration levels of mitragynine are presented in Table 15.

In rats administered with a single-dose intravenous administration (10 mg/kg), at 15 min post-administration, the partition coefficient of mitragynine in the slowly perfused tissues (P_{SP}) had the strongest effect on the mitragynine plasma concentration levels, followed by the partition coefficient of mitragynine in the liver (P_{LI}) which had a moderate effect. At 2 hr post-mitragynine administration, parameters related to protein kinetics, the maximum velocity of BCRP-mediated transport (V_{max_BCRP}) had a stronger effect than the maximum velocity of hepatic CYP3A4-mediated metabolism (V_{max_CYP3A4}). The fat diffusion permeate constant (PAFC) had a moderate effect on the plasma concentration of mitragynine.

Following a single oral dose of mitragynine (20 mg/kg) in rats, at 1 hr post-administration, P_{SP} had the most prominent effect on mitragynine plasma concentration. For instance, at 4 hr post-mitragynine administration, V_{max_BCRP} and V_{max_CYP3A4} had moderate effect, while the PAFC had a minimal effect as compared to those input parameters.

In PBPK model of mitragynine in humans, the sensitivity analysis of the certain input parameter values on mitragynine plasma concentration levels in each human subject are presented on day 1 and day 8 at various time points followed by the multiple dosing of mitragynine, as summarized in Table 16. From sensitivity analysis results in five human subjects, the most sensitive input parameter on the rate of change of mitragynine plasma concentration levels is P_{SP}, while the partition coefficient of mitragynine in the brain (P_{BR}) and P_{LI} had moderate effects.

(A) (B)

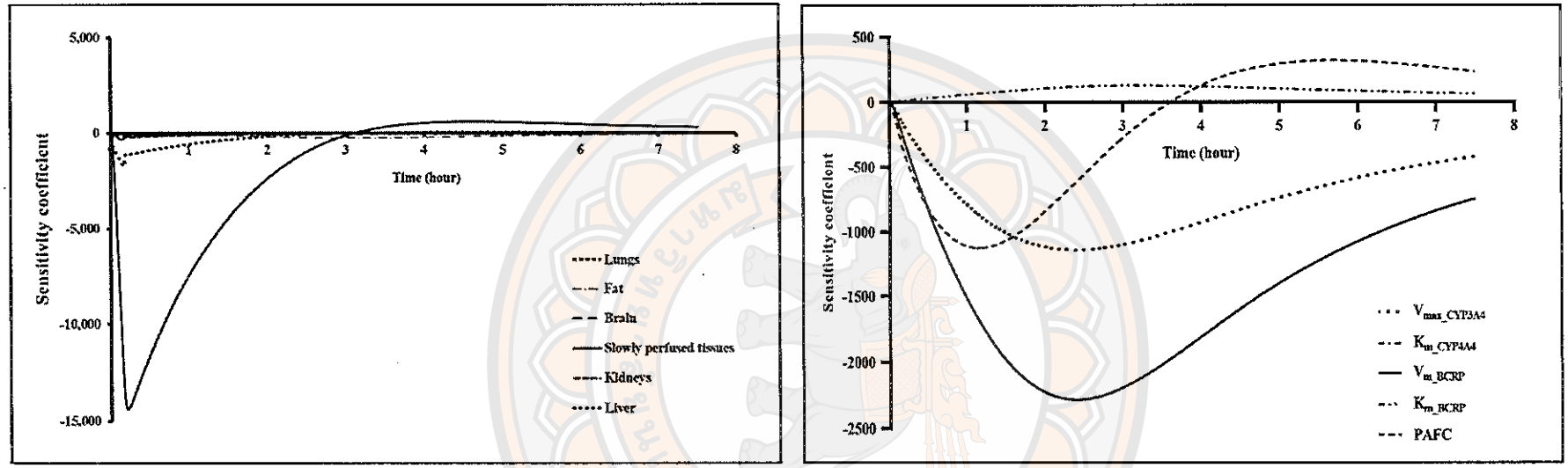

Figure 19 Sensitivity analysis of input parameters versus time in plasma of rats following a single intravenous administration of mitragynine (10 mg/kg). Figure 19 (A) and (B) represents the effect of partition coefficient of mitragynine in each tissue compartment and the effects of biochemical parameters, respectively

(A)

(B)

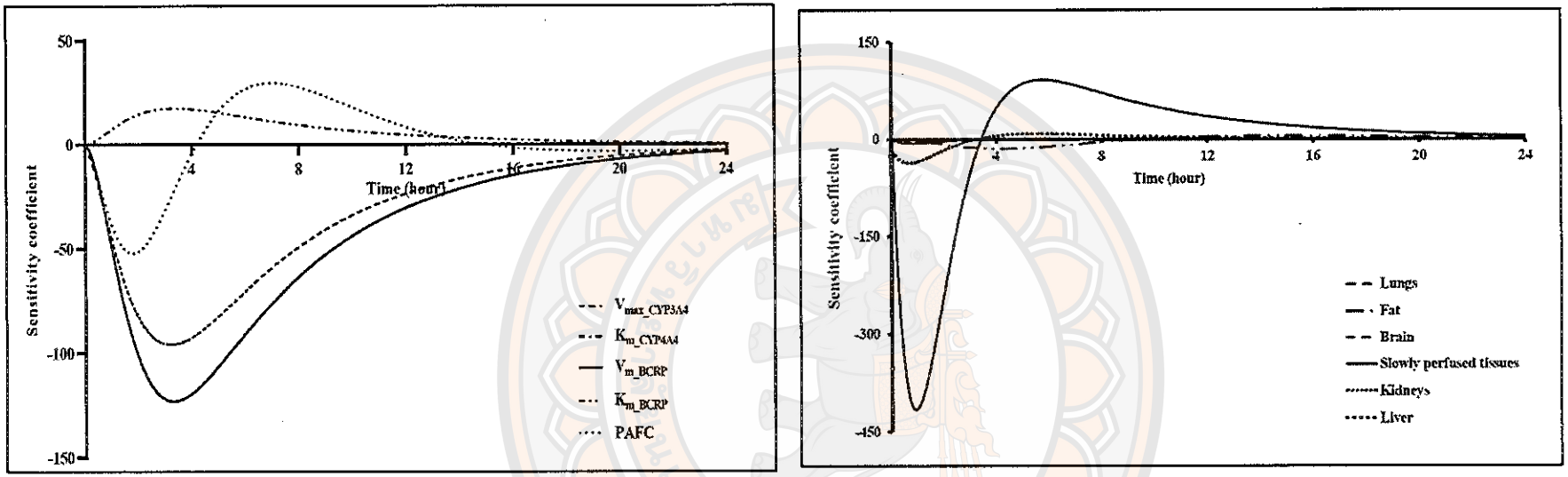

Figure 20 Sensitivity analysis of input parameters versus time in plasma of rats following a single oral dose of mitragynine (20 mg/kg). Figure 20 (A) and (B) represents the effect of partition coefficient of mitragynine in each tissue compartments and the effects of biochemical parameters, respectively

Table 15 Sensitivity analysis of the certain parameters in rats receiving a single intravenous dose of mitragynine (10 mg/kg) and a single oral dose of mitragynine (20 mg/kg)

Time (hour)	Partition coefficient		Protein kinetic characteristic		Fat diffusion
	P_{SP}	P_{LI}	V_{max_CYP3A4}	V_{max_BCRP}	PAFC
Intravenous administration of mitragynine					
0.25	-14127	-1086.73	-240.00	-411.77	-496.00
1	-7443.24	-574.49	-796.67	-1527.06	-1112.67
2	-2367.57	-176.53	-1118.33	-2229.71	-843.33
4	542.91	45.92	-926.67	-1805.44	126.00
7.5	307.35	24.94	-419.58	-745.96	233.33
Oral administration of mitragynine					
1	-413.01	-36.16	-45.83	-50.18	-38.88
4	47.59	5.61	-92.08	-118.99	-4.73
8	71.77	6.30	-49.01	-63.13	27.74
12	34.99	3.01	-23.82	-30.60	8.23
24	4.28	0.36	-2.75	-3.54	-2.78

Note: P_{SP} = partition coefficient in the slowly perfused tissues; P_{LI} = partition coefficient in the liver; PAFC = fat diffusion rate constant; V_{max_CYP3A4} = maximum velocity of cytochrome P450 3A4; V_{max_BCRP} = maximum velocity of breast cancer resistance protein

Table 16 Sensitivity analysis of the certain parameters in each human subject receiving an oral administration with multiple dosing regimens

Time (hour)	Subject 1						Time (hour)	Subject 2					
	P_{BR}	P_{SP}	P_{LI}	V_{max_3A4}	V_{max_BCRP}	PAFC		P_{BR}	P_{SP}	P_{LI}	V_{max_3A4}	V_{max_BCRP}	PAFC
	Day 1							Day 1					
1	-0.11	-11.29	-0.13	-0.01	-0.01	-2.14	1	-0.75	-14.95	-1.4	-0.01	-0.03	-1.5
4	0.05	1.94	0.2	-0.01	-0.01	-0.3	4	-0.21	-7.98	-0.25	-0.02	-0.1	-1.65
8	0.02	1.15	0.07	0	-0.01	0.73	8	-0.03	-0.98	-0.01	-0.02	-0.12	0.16
12	0.01	0.47	0.03	0	-0.01	0.55	12	-0.01	-0.23	0.01	-0.02	-0.12	0.66
24	0	0.17	0.01	0	0	0.02	24	0.03	0.79	0.06	-0.02	-0.12	0.34
	Day 8							Day 8					
1	-0.11	-11.1	-0.12	-0.01	-0.02	-2.18	1	-0.64	-12.17	-1.21	-0.05	-0.27	-1.26
4	0.05	2.1	0.21	-0.01	-0.02	-0.36	4	-0.11	-5.23	-0.06	-0.06	-0.32	-1.5
8	0.02	1.27	0.08	0	-0.01	0.66	8	0.08	1.69	0.17	-0.06	-0.32	0.22
12	0.01	0.56	0.04	0	-0.01	0.48	12	0.09	2.31	0.18	-0.06	-0.3	0.67
24	0	0.21	0.01	0	0	-0.02	24	0.11	2.79	0.19	-0.04	-0.24	0.26

Table 16 (cont.)

Time (hour)	Subject 3						Time (hour)	Subject 4						Time (hour)	Subject 5					
	P_{BR}	P_{SP}	P_{LI}	V_{max_3A4}	V_{max_BCRP}	PAFC		P_{BR}	P_{SP}	P_{LI}	V_{max_3A4}	V_{max_BCRP}	PAFC		P_{BR}	P_{SP}	P_{LI}	V_{max_3A4}	V_{max_BCRP}	PAFC
	Day 1							Day 1							Day 1					
1	-0.23	-7.96	-0.41	-0.01	-0.01	-2.66	1	-0.11	-9.65	-0.18	-0.01	-0.01	-2.03	1	-0.81	-24.35	-1.35	-0.02	-0.05	-3.85
4	0.02	-0.35	0.08	-0.01	-0.03	-2.36	4	0.04	1.61	0.18	-0.01	-0.01	-0.41	4	0	-2.68	0.13	-0.02	-0.09	-2.37
8	0.04	1.28	0.09	0	-0.02	0.25	8	0.02	1.07	0.06	0	-0.01	0.7	8	0.06	1.8	0.14	-0.02	-0.09	0.93
12	0.02	0.72	0.04	0	-0.01	1.11	12	0.01	0.43	0.03	0	0	0.57	12	0.04	1.22	0.09	-0.02	-0.08	1.42
24	0.01	0.2	0.01	0	-0.01	0.56	24	0	0.15	0.01	0	0	0.04	24	0.04	1.01	0.07	-0.01	-0.05	0.47
	Day 8							Day 8							Day 8					
1	-0.11	-11.1	-0.12	-0.01	-0.02	-2.18	1	-0.22	-19.16	-0.35	-0.01	-0.03	-4.08	1	-1.59	-47	-2.59	-0.05	-0.18	-7.49
4	0.05	2.1	0.21	-0.01	-0.02	-0.36	4	0.09	3.35	0.36	-0.01	-0.03	-0.88	4	0.06	-3.85	0.36	-0.06	-0.27	-4.71
8	0.02	1.27	0.08	0	-0.01	0.66	8	0.04	2.24	0.14	-0.01	-0.02	1.33	8	0.17	5.06	0.38	-0.05	-0.24	1.8
12	0.01	0.56	0.04	0	-0.01	0.48	12	0.02	0.93	0.06	0	-0.01	1.06	12	0.13	3.74	0.27	-0.04	-0.21	2.73
24	0	0.21	0.01	0	0	-0.02	24	0.01	0.33	0.02	0	0	0.03	24	0.1	2.88	0.2	-0.03	-0.14	0.77

Note: P_{BR} = partition coefficient in the brain; P_{SP} = partition coefficient in the slowly perfused tissues; P_{LI} = partition coefficient in the liver; V_{max_CYP3A4} = maximum velocity of cytochrome P450 3A4; V_{max_BCRP} = maximum velocity of breast cancer resistance protein; PAFC = fat diffusion rate constant

CHAPTER V

DISCUSSION AND CONCLUSION

Discussion

In this study, we conducted a PBPK model of mitragynine which is the first PBPK model of the potent psychoactive alkaloid in kratom leaves. A prominent feature of this PBPK model included 1) incorporating of the BCRP-mediated transport process in the brain, 2) involvement of hepatic CYP3A4-mediated metabolism in the liver, and 3) integrating of the diffusion-limited transport in the fat compartment.

The target tissue of the mitragynine pharmacological effect occurred in the central nervous system, which provided an analgesic effect (15). Our model could provide an accurate prediction of brain concentration levels; therefore, biologically relevant process (i.e. BCRP-mediated transport) in the brain was described. According to relativity affinity, BCRP-mediated transport is member of ATP binding cassette transporter and expressed at brain endothelial cells with considering as efflux transporter, which influence on the permeation of the compound in the brain (60). Biological relevant in the brain was assumed by incorporating of the BCRP-mediated transport process to describe the disposition of mitragynine in the brain.

Influence of mitragynine on other drug metabolizing enzymes was reported in published literature either inducer or inhibitor effect. Mitragynine is extensively metabolized in the liver which expressed major drug metabolizing enzymes. From one published study verified that fraction of mitragynine metabolized by CYP3A4 was found to be 67%, indicating that CYP3A4 plays a predominant role into the metabolism of mitragynine (53). Therefore, hepatic CYP3A4-mediated metabolism was incorporated into this model to describe the metabolism of mitragynine in the liver.

Previously, all tissue compartments were tested using a flow-limited assumption. The results showed that model simulations of mitragynine plasma concentration-time courses could not satisfactorily describe the observed data. Therefore, a diffusion-limited assumption was introduced to describe a different kinetic behavior of the compound in the fat. The PBPK model of mitragynine in rats was used as the principle for developing a PBPK model in human.

The capability of the PBPK model of mitragynine could describe several datasets from different studies such as 1) a study in rats following a single intravenous administration of mitragynine with plasma and brain concentration-time courses; 2) a study in rats following a single oral administration of mitragynine; and 3) a study in human subjects receiving multiple dosing regimens of mitragynine in the form of kratom tea. In addition, our PBPK model has the capacity to predict tissue kinetic behaviors of mitragynine relevant to its dispositions both in rats and in humans, which is not readily achieved by experimental approach.

After developed PBPK model of mitragynine, certain pharmacokinetic parameters are determined including C_{max}, T_{max}, and AUC_{0-t}. In addition, ratio of AUC_{brain}/AUC_{plasma} is one of indicator to measure the extent of the compound distribution equilibrium between brain and plasma (87). According to results from experimental study and model simulations following a single intravenous of mitragynine in rats showed that ratio AUC_{brain}/AUC_{plasma} values are equal to 0.65 and 0.77, respectively. Those results can describe instantaneously of the disposition of mitragynine into the brain but protein-mediated efflux transport activity at the blood brain barrier is involved. Following a single oral administration of mitragynine in rat, predicted ratio AUC_{brain}/AUC_{plasma} of mitragynine is equal to 0.55 that lower than intravenous administration, as described by slow dissolution rate of this compound at higher solvent related to its low bioavailability after oral administration.Fi

From simulating results of mitragynine following a single dose of intravenous and oral administration in rats, prediction mitragynine concentration-time course in the fat compartment found to be higher concentration levels with a much lower rate of elimination rate from the organ as compared to other tissue compartments (Figure 10 and Figure 13). These results can describe the disposition of mitragynine into fat compartment might not be instantaneously but still remained in this compartment, as indicated by its lipophilicity properties and low perfusion rate of the fat compartment leading to slowly released with involvement of a diffusion-limited transport in the fat organ compartment. Thus, it might be possible when receiving multiple dosing of mitragynine until reaching its steady state, the fat compartment functions as a storage depot of the alkaloid in the body.

In humans, our developed PBPK model of mitragynine could describe all concentration-time profiles from the observed data of five human subjects. According to simulating results in each individual subject, predicted C_{max} and $AUC_{0\text{-}t\ (D7\text{-}8)}$ of mitragynine in the brain found to be 2-times higher than in plasma both observed datasets and predicted values, as summarized in Table 14. These results obtained from experimental study and model simulation that performed a study on human subjects (kratom chronic user). Therefore, this PBPK model of mitragynine in humans predicted concentration levels of mitragynine in the brain for each individual receiving different dosage regimens of mitragynine in the form of kratom tea in order to reach at steady state. These levels may be able to reflect the concentration levels of this compound in the organ. Notably, prediction concentration levels of mitragynine both in rats and in humans are inconsistent, as described by model simulation was conducted with different dosing scenarios between rats and humans. Taken together, the developed PBPK model of mitragynine can be useful as a quantitative tool for predicting brain concentration levels of mitragynine both in rats and in humans.

The sensitivity analysis was performed to evaluate the relative of certain input parameter values on model output at various time points. After rats receiving with a single intravenous dose of mitragynine (10 mg/kg) and a single oral dose of mitragynine (20 mg/kg), the most sensitive input parameter is the partition coefficient of mitragynine in the slowly perfused tissues (P_{SP}), which had a high influence on the disposition of mitragynine in the plasma and also other tissue compartments. Then, the partition coefficient of mitragynine in the liver (P_{LI}) had a moderate effect on mitragynine plasma concentration-time profiles. For parameters related to protein kinetics, the maximum velocity of protein-mediated transport (V_{max_BCRP}) and hepatic enzyme-mediated metabolism (V_{max_CYP3A4}) also had a moderate effect on the mitragynine concentration levels in plasma, suggesting a significant role of the protein-mediated efflux transporter process in the brain and hepatic-mediated metabolism of mitragynine in the liver. Nonetheless, the fat diffusion rate constant (PAFC) showed a minimal effect on the model outputs, as suggested by integrating of diffusion-limited transport in the fat compartment. In addition, in the developed PBPK model in humans, P_{SP} also had the strongest effect on plasma mitragynine concentration levels, whereas P_{LI} and P_{BR} have a moderate effect. The results indicated that the sensitivity of the input model parameters

on model outputs might help to select the input parameters which require additional experiments in the future.

An optimization process in the Berkeley Madonna Software was conducted to determine individual oral bioavailability (F) values among five human subjects who are kratom chronic users. The optimized F values are in the range of 0.12-0.4, which is in agreement with those in animal studies. Those results both in rats and in human showed that optimized F values obtained low values, indicating that related to its physicochemical properties and then the extreme either first-pass metabolized or remains in the gut lumen unchanged. Therefore, to enhance oral bioavailability, specific formulation with an appropriate carrier should be used to avoid degradation in the stomach.

To our knowledge, the capability of the developed PBPK model primarily predict concentration-time profiles of the main psychoactive alkaloid in kratom leaves in plasma, in the brain, and other tissue dispositions, which mitragynine exerts its pharmacological and toxicological actions. This study's finding convenient as a quantitative tool on the estimation of mitragynine dosage regimens and can help minimize overdose problems of mitragynine.

Study limitations and future research directions

Some limitations of this study are noted. First, the PBPK model of mitragynine was conducted based on few available datasets both in rats and in humans. In particularly, tissue dispositions of mitragynine in some organs (i.e. fat, liver, kidney, slowly perfused tissues) are not readily available. Based on the systematical review, more pharmacokinetic studies of mitragynine with better design should be conducted particularly disposition of this compound in the other tissues. When additional information and data are available, the developed PBPK model of mitragynine could be modified and potentially be more predictive.

Second, biological relevance has an influence on the disposition of mitragynine leading to altered on pharmacokinetic behaviors of this compound. In this model, we can describe the involvement of the BCRP-meditated transport in the brain. Subsequently, mitragynine also exhibited as induction and inhibition of P-gp but it is still unclear whether or not mitragynine is a substrate of P-gp. Thus, additional experimental designs are required

to characterize biological properties of mitragynine particularly an involvement of the transporter activity not only in the brain but in other tissues.

Third, a PBPK model of mitragynine in humans was conducted with multiple dosing regimens on kratom chronic users based on only one published data in humans. Therefore, pharmacokinetics of mitragynine in humans should be investigated with better study designs following a single dose administration of this compound and/or various route of administration. In addition, kinetic behaviors of mitragynine with clearly quantify amount in other kratom formulations should be investigated.

Last, this study was conducted based on available published pharmacokinetic data, which performed by systematical review on electronic databases. This model can describe the kinetic behaviors of mitragynine, which is a major psychoactive alkaloid in the kratom leaves, related to its potential using and provided the therapeutic effect. Understanding concentration levels in both plasma and brain will enable identification with an appropriate dose metric of mitragynine and/or kratom; thus, the PBPK model incorporating with pharmacodynamics (PBPK/PD) should be conducted. Furthermore, this warrants further researches to investigate the minor alkaloid with more potent psychoactive alkaloid namely 7-hydroxymitragynine.

Conclusion

In conclusion, all available information relevant pharmacokinetic properties of mitragynine were described through a systemic review. Using the available published pharmacokinetic datasets, a PBPK model of mitragynine was successfully developed with various routes of administration following a single dose of intravenous and oral administration in rats, and repeated dosing of oral administration in humans. This model can be used to predict mitragynine concentration-time profiles in plasma and other tissue compartments related to its disposition, particularly mitragynine concentration levels in the brain both in rats and in humans. Model simulations can be informative for applying as a guide to define safer dosing regimen leading to achieving therapeutic effects. In addition, this modeling incorporating with biologically relevant features of the psychoactive alkaloid in the body also provided an important basis for further improvement in clinical applications including efficacy and safety assessment as necessitates additional studies.

REFERENCES

REFERENCES

1. Vicknasingam B, Narayanan S, Beng GT, Mansor SM. The informal use of ketum (Mitragyna speciosa) for opioid withdrawal in the northern states of peninsular Malaysia and implications for drug substitution therapy. The International journal on drug policy. 2010;21(4):283-8.

2. Hassan Z, Muzaimi M, Navaratnam V, Yusoff NHM, Suhaimi FW, Vadivelu R, et al. From Kratom to mitragynine and its derivatives: Physiological and behavioural effects related to use, abuse, and addiction. Neuroscience and Biobehavioral Reviews. 2013;37(2):138-51.

3. Warner ML, Kaufman NC, Grundmann O. The pharmacology and toxicology of kratom: from traditional herb to drug of abuse. International journal of legal medicine. 2016;130(1):127-38.

4. Tanguay P. Kratom in Thailand, decriminalisation and community control International Drug Policy Consortium (IDPC). 2011;Transnational Institute (Series on legislative reform of drug policies Nr.13).

5. Prozialeck WC, Jivan JK, Andurkar SV. Pharmacology of kratom: an emerging botanical agent with stimulant, analgesic and opioid-like effects. The Journal of the American Osteopathic Association. 2012;112(12):792-9.

6. Assanangkornchai S, Muekthong A, Sam-Angsri N, Pattanasattayawong U. The Use of Mitragynine speciosa ("Krathom"), an addictive plant, in Thailand. Substance use & misuse. 2007;42(14):2145-57.

7. Singh D, Narayanan S, Vicknasingam B. Traditional and non-traditional uses of Mitragynine (Kratom): A survey of the literature. Brain research bulletin. 2016;126(Pt 1):41-6.

8. Narcotics Act No.7 B.E. The Government Gazette 2019 (cited 2019 February 18). Available from: http://www.ratchakitcha.soc.go.th/DATA/PDF /2562/A/ 019/T_0001. PDF.

9. Boyer EW, Babu KM, Macalino GE, Compton W. Self-treatment of opioid withdrawal with a dietary supplement, Kratom. American Journal on Addictions. 2007;16(5):352-6.

10. Babu KM, McCurdy CR, Boyer EW. Opioid receptors and legal highs: Salvia divinorum and Kratom. Clinical toxicology (Philadelphia, Pa). 2008;46(2): 146-52.

11. Holler JM, Vorce SP, McDonough-Bender PC, Magluilo Jr J, Solomon CJ, Levine B. A drug toxicity death involving propylhexedrine and mitragynine. Journal of Analytical Toxicology. 2011;35(1):54-9.

12. Kronstrand R, Roman M, Thelander G, Eriksson A. Unintentional fatal intoxications with mitragynine and O-desmethyltramadol from the herbal blend Krypton. Journal of analytical toxicology. 2011;35(4):242-7.

13. Adkins JE, Boyer EW, McCurdy CR. Mitragyna speciosa, a psychoactive tree from Southeast Asia with opioid activity. Current topics in medicinal chemistry. 2011;11(9):1165-75.

14. Ponglux D, Wongseripipatana S, Takayama H, Kikuchi M, Kurihara M, Kitajima M, et al. A new indole alkaloid, 7α-hydroxy-7H-mitragynine, from Mitragyna speciosa in Thailand. Planta Medica. 1994;60(6):580-1.

15. Matsumoto K, Mizowaki M, Suchitra T, Takayama H, Sakai SI, Aimi N, et al. Antinociceptive action of mitragynine in mice: Evidence for the involvement of supraspinal opioid receptors. Life Sciences. 1996;59(14): 1149-55.

16. Matsumoto K, Mizowaki M, Suchitra T, Murakami Y, Takayama H, Sakai SI, et al. Central antinociceptive effects of mitragynine in mice: Contribution of descending noradrenergic and serotonergic systems. European Journal of Pharmacology. 1996; 317(1):75-81.

17. Thongpradichote S, Matsumoto K, Tohda M, Takayama H, Aimi N, Sakai SI, et al. Identification of opioid receptor subtypes in antinociceptive actions of supraspinally-administered mitragynine in mice. Life Sciences. 1998;62(16):1371-8.

18. Watanabe K, Yano S, Horie S, Yamamoto LT. Inhibitory effect of mitragynine, an alkaloid with analgesic effect from Thai medicinal plant Mitragyna speciosa, on electrically stimulated contraction of isolated guinea-pig ileum through the opioid receptor. Life sciences. 1997;60(12):933-42.

19. Tsuchiya S, Miyashita S, Yamamoto M, Horie S, Sakai SI, Aimi N, et al. Effect of mitragynine, derived from Thai folk medicine, on gastric acid secretion through opioid receptor in anesthetized rats. European Journal of Pharmacology. 2002;443(1-3):185-8.

20. Idayu NF, Hidayat MT, Moklas MAM, Sharida F, Raudzah ARN, Shamima AR, et al. Antidepressant-like effect of mitragynine isolated from Mitragyna speciosa Korth in mice model of depression. Phytomedicine. 2011;18(5): 402-7.

21. Utar Z, Majid MIA, Adenan MI, Jamil MFA, Lan TM. Mitragynine inhibits the COX-2 mRNA expression and prostaglandin E-2 production induced by lipopolysaccharide in RAW264.7 macrophage cells. Journal of Ethnopharmacology. 2011;136(1):75-82.

22. Kruegel AC, Gassaway MM, Kapoor A, Váradi A, Majumdar S, Filizola M, et al. Synthetic and Receptor Signaling Explorations of the Mitragyna Alkaloids: Mitragynine as an Atypical Molecular Framework for Opioid Receptor Modulators. Journal of the American Chemical Society. 2016;138(21): 6754-64.

23. Ramanathan S, Parthasarathy S, Murugaiyah V, Magosso E, Tan SC, Mansor SM. Understanding the physicochemical properties of mitragynine, a principal alkaloid of Mitragyna speciosa, for preclinical evaluation. Molecules. 2015;20(3):4915-27.

24. Manda VK, Avula B, Ali Z, Khan IA, Walker LA, Khan SI. Evaluation of in vitro absorption, distribution, metabolism, and excretion (ADME) properties of mitragynine, 7-hydroxymitragynine, and mitraphylline. Planta Med. 2014; 80(7):568-76.

25. Rowland M, Peck C, Tucker G. Physiologically-based pharmacokinetics in drug development and regulatory science. Annu Rev Pharmacol Toxicol. 2011; 51:45-73.

26. Boyer EW, Babu KM, Adkins JE, McCurdy CR, Halpern JH. Self-treatment of opioid withdrawal using kratom (Mitragynia speciosa korth). Addiction (Abingdon, England). 2008;103(6):1048-50.

27. Kupferschmidt H. Toxic hepatitis after kratom (Mitragyna SP.) consumption Clinical Toxicology. 2011;49(6):532-.

28. U.S. Food and Drug Administration (USFDA). Statement from FDA Commissioner Scott Gottlieb, M.D., on the agency's scientific evidence on the presence of opioid compounds in kratom, underscoring its potential for abuse 2018 (cited 2018 February 6). Available from: https://www.fda.gov/newsevents/newsroom/ pressannouncements/ucm 595622.htm.

29. Henningfield J, Gerlach K, Hufford M, Shiffman S. Kratom and its Mitragynines: A Path Away From Opioids? Neuropsychopharmacology. 2017;43:S619-S20.

30. Saingam D, Assanangkornchai S, Geater AF, Balthip Q. Pattern and consequences of krathom (Mitragyna speciosa Korth.) use among male villagers in southern Thailand: a qualitative study. The International journal on drug policy. 2013;24(4):351-8.

31. Singh D, Mulller CP, Vicknasingam BK. Kratom (Mitragyna speciosa) dependence, withdrawal symptoms and craving in regular users. Drug and Alcohol Dependence. 2014;139:132-7.

32. Singh D, Murugaiyah V, Hamid SBS, Kasinather V, Chan MSA, Ho ETW, et al. Assessment of gonadotropins and testosterone hormone levels in regular Mitragyna speciosa (Korth.) users. Journal of ethnopharmacology. 2018; 221:30-6.

33. Singh D, Narayanan S, Vicknasingam BK, Prozialeck WC, Ramanathan S, Zainal H, et al. Severity of Pain and Sleep Problems during Kratom (Mitragyna speciosa Korth.) Cessation among Regular Kratom Users. Journal of psychoactive drugs. 2018:1-9.

34. White CM. Pharmacologic and clinical assessment of kratom. American journal of health-system pharmacy: AJHP: official journal of the American Society of Health-System Pharmacists. 2018;75(5):261-7.

35. Arndt T, Claussen U, Güssregen B, Schröfel S, Stürzer B, Werle A, et al. Kratom alkaloids and O-desmethyltramadol in urine of a "Krypton" herbal mixture consumer. Forensic Science International. 2011;208(1-3):47-52.

36. Philipp AA, Meyer MR, Wissenbach DK, Weber AA, Zoerntlein SW, Zweipfenning PGM, et al. Monitoring of kratom or Krypton intake in urine using GC-MS in clinical and forensic toxicology. Analytical and Bioanalytical Chemistry. 2011;400(1):127-35.

37. Takayama H. Chemistry and pharmacology of analgesic indole alkaloids from the rubiaceous plant, Mitragyna speciosa. Chemical & pharmaceutical bulletin. 2004;52 (8):916-28.

38. Cinosi E, Martinotti G, Simonato P, Singh D, Demetrovics Z, Roman-Urrestarazu A, et al. Following "the Roots" of Kratom (Mitragyna speciosa): The Evolution of an Enhancer from a Traditional Use to Increase Work and Productivity in Southeast Asia to a Recreational Psychoactive Drug in Western Countries. BioMed Research International. 2015;2015.

39. Takayama H, Kurihara M, Kitajima M, Said IM, Aimi N. New indole alkaloids from the leaves of malaysian: Mitragyna speciosa. Tetrahedron. 1998;54 (29):8433-40.

40. Matsumoto K, Yamamoto LT, Watanabe K, Yano S, Shan J, Pang PKT, et al. Inhibitory effect of mitragynine, an analgesic alkaloid from Thai herbal medicine, on neurogenic contraction of the vas deferens. Life Sciences. 2005;78(2):187-94.

41. Purintrapiban J, Keawpradub N, Kansenalak S, Chittrakarn S, Janchawee B, Sawangjaroen K. Study on glucose transport in muscle cells by extracts from Mitragyna speciosa (Korth) and mitragynine. Natural product research. 2011;25(15):1379-87.

42. Sabetghadam A, Navaratnam V, Mansor SM. Dose-Response Relationship, Acute Toxicity, and Therapeutic Index between the Alkaloid Extract of Mitragyna speciosa and Its Main Active Compound Mitragynine in Mice. Drug Development Research. 2013;74(1):23-30.

43. Sabetghadam A, Ramanathan S, Sasidharan S, Mansor SM. Subchronic exposure to mitragynine, the principal alkaloid of Mitragyna speciosa, in rats. Journal of ethnopharmacology. 2013;146(3):815-23.

44. Zacharias DE, Rosenstein RD, Jeffrey GA. The structure of mitragynine hydroiodide. Acta Crystallographica. 1965;18(6):1039-43.

45. European Monitoring Centre for Drugs and Drug Addiction (EMCDDA). Kratom (Mitragyna speciosa) drug profile 2015 (cited 2015 January 8). Available from: http://www.emcdda.europa.eu/publications/drug-profiles/kratom.

46. Kong WM, Chik Z, Mohamed Z, Alshawsh MA. Physicochemical Characterization of Mitragyna speciosa Alkaloid Extract and Mitragynine using In Vitro High Throughput Assays. Combinatorial chemistry & high throughput screening. 2017;20(9):796-803.

47. (Bittermann K, Goss K-U. Predicting apparent passive permeability of Caco-2 and MDCK cell-monolayers: A mechanistic model. PLOS ONE. 2017;12(12): e0190319.

48. U.S. Department of Health and Human Services Food and Drug Administration Center for Drug Evaluation and Research (CDER). Waiver of In Vivo Bioavailability and Bioequivalence Studies for Immediate-Release Solid Oral Dosage Forms Based on a Biopharmaceutics Classification System Guidance for Industry 2017 (cited 2017 December). Available from: https://www.fda.gov/downloads/Drugs/Guidances/ucm 070246.pdf

49. Jagabalan JDY, Murugaiyah V, Zainal H, Mansor SM, Ramanathan S. Intestinal permeability of mitragynine in rats using in situ absorption model. Journal of Asian natural products research. 2018:1-13.

50. Lim EL, Seah TC, Koe XF, Wahab HA, Adenan MI, Jamil MFA, et al. In vitro evaluation of cytochrome P450 induction and the inhibition potential of mitragynine, a stimulant alkaloid. Toxicology in Vitro. 2013;27(2):812-24.

51. Hanapi NA, Ismail S, Mansor SM. Inhibitory effect of mitragynine on human cytochrome P450 enzyme activities. Pharmacognosy research. 2013;5(4): 241-6.

52. Manda VK, Avula B, Dale OR, Ali Z, Khan IA, Walker LA, et al. PXR mediated induction of CYP3A4, CYP1A2, and P-gp by Mitragyna speciosa and its alkaloids. Phytotherapy research : PTR. 2017;31(12):1935-45.

53. Kamble SH, Sharma A, King TI, León F, McCurdy CR, Avery BA. Metabolite profiling and identification of enzymes responsible for the metabolism of mitragynine, the major alkaloid of Mitragyna speciosa (kratom). Xenobiotica. 2018.

54. Anwar R, Ismail S, Mansor SM. In vitro effect of mitragynine on activity of drug metabolizing enzymes, n-demethylase and glutathione s-transferase in streptozotocin-induced diabetic rats. Pharmacologyonline. 2012;1:68-75.

55. Meyer MR, Schutz A, Maurer HH. Contribution of human esterases to the metabolism of selected drugs of abuse. Toxicology letters. 2015;232(1): 159-66.

56. Haron M, Ismail S. Effects of mitragynine and 7-hydroxymitragynine (the alkaloids of Mitragyna speciosa Korth) on 4-methylumbelliferone glucuronidation in rat and human liver microsomes and recombinant human uridine 5'-diphospho-glucuronosyltransferase isoforms. Pharmacognosy Research. 2015;7(4):341-9.

57. Huda Abdullah N, Ismail S. Inhibition of UGT2B7 Enzyme Activity in Human and Rat Liver Microsomes by Herbal Constituents2018. 2696 p.

58. Meyer MR, Wagmann L, Schneider-Daum N, Loretz B, Carvalho CD, Lehr CM, et al. P-glycoprotein interactions of novel psychoactive substances - Stimulation of ATP consumption and transport across Caco-2 monolayers. Biochemical Pharmacology. 2015;94(3):220-6.

59. (Rusli N, Amanah A, Kaur G, Adenan MI, Sulaiman SF, Wahab HA, et al. The inhibitory effects of mitragynine on P-glycoprotein in vitro. Naunyn-Schmiedeberg's archives of pharmacology. 2019.

60. Wagmann L, Maurer HH, Meyer MR. Inhibition and stimulation of the human breast cancer resistance protein as in vitro predictor of drug–drug interactions of drugs of abuse. Archives of Toxicology. 2018;92(9):2875-84.

61. Philipp AA, Wissenbach DK, Zoerntlein SW, Klein ON, Kanogsunthornrat J, Maurer HH. Studies on the metabolism of mitragynine, the main alkaloid of the herbal drug Kratom, in rat and human urine using liquid chromatography -linear ion trap mass spectrometry. Journal of mass spectrometry: JMS. 2009;44(8):1249-61.

62. Parthasarathy S, Ramanathan S, Ismail S, Adenan MI, Mansor SM, Murugaiyah V. Determination of mitragynine in plasma with solid-phase extraction and rapid HPLC-UV analysis, and its application to a pharmacokinetic study in rat. Analytical and bioanalytical chemistry. 2010;397(5):2023-30.

63. Vuppala PK, Boddu SP, Furr EB, McCurdy CR, Avery BA. Simple, sensitive, high-throughput method for the quantification of mitragynine in rat plasma using UPLC-MS and its application to an intravenous pharmacokinetic study. Chromatographia. 2011;74(9-10):703-10.

64. Avery BA, Boddu SP, Sharma A, Furr EB, Leon F, Cutler SJ, et al. Comparative Pharmacokinetics of Mitragynine after Oral Administration of Mitragyna speciosa (Kratom) Leaf Extracts in Rats. Planta Med. 2019;85(4):340-6.

65. Kong WM, Mohamed Z, Alshawsh MA, Chik Z. Evaluation of pharmacokinetics and blood-brain barrier permeability of mitragynine using in vivo microdialysis technique. Journal of pharmaceutical and biomedical analysis. 2017;143:43-7.

66. Janchawee B, Keawpradub N, Chittrakarn S, Prasettho S, Wararatananurak P, Sawangjareon K. A high-performance liquid chromatographic method for determination of mitragynine in serum and its application to a pharmacokinetic study in rats. Biomedical chromatography: BMC. 2007;21 (2):176-83.

67. (de Moraes NV, Moretti RAC, Furr Iii EB, McCurdy CR, Lanchote VL. Determination of mitragynine in rat plasma by LC-MS/MS: Application to pharmacokinetics. Journal of Chromatography B: Analytical Technologies in the Biomedical and Life Sciences. 2009;877(24):2593-7.

68. Trakulsrichai S, Sathirakul K, Auparakkitanon S, Krongvorakul J, Sueajai J, Noumjad N, et al. Pharmacokinetics of mitragynine in man. Drug design, development and therapy. 2015;9:2421-9.

69. B M, Clewell Iii HJ, Lave T, E M. Physiologically Based Pharmacokinetic Modeling: A Tool for Understanding ADMET Properties and Extrapolating to Human. 2013.

70. Gerlowski LE, Jain RK. Physiologically based pharmacokinetic modeling: principles and applications. Journal of pharmaceutical sciences. 1983;72 (10):1103-27.

71. Jones H, Rowland-Yeo K. Basic concepts in physiologically based pharmacokinetic modeling in drug discovery and development. CPT Pharmacometrics Syst Pharmacol. 2013;2:e63.

72. Kuepfer L, Niederalt C, Wendl T, Schlender JF, Willmann S, Lippert J, et al. Applied Concepts in PBPK Modeling: How to Build a PBPK/PD Model. CPT: pharmacometrics & systems pharmacology. 2016;5(10):516-31.

73. Khalil F, Laer S. Physiologically based pharmacokinetic modeling: methodology, applications, and limitations with a focus on its role in pediatric drug development. J Biomed Biotechnol. 2011;2011:907461.

74. Espié P, Tytgat D, Sargentini-Maier M-L, Poggesi I, Watelet J-B. Physiologically based pharmacokinetics (PBPK). Drug Metabolism Reviews. 2009;41(3):391-407.

75. Zhuang X, Lu C. PBPK modeling and simulation in drug research and development. Acta pharmaceutica Sinica B. 2016;6(5):430-40.

76. Albanese RA, Banks HT, Evans MV, Potter LK. Physiologically based pharmacokinetic models for the transport of trichloroethylene in adipose tissue. Bulletin of Mathematical Biology. 2002;64(1):97.

77. Thompson MD, Beard DA. Development of appropriate equations for physiologically based pharmacokinetic modeling of permeability-limited and flow-limited transport. Journal of pharmacokinetics and pharmacodynamics. 2011;38(4):405-21.

78. Hu Z-Y, Lu J, Zhao Y. A physiologically based pharmacokinetic model of alvespimycin in mice and extrapolation to rats and humans. British journal of pharmacology. 2014;171(11):2778-89.

79. Brown RP, Delp MD, Lindstedt SL, Rhomberg LR, Beliles RP. Physiological parameter values for physiologically based pharmacokinetic models. Toxicology and industrial health. 1997;13(4):407-84.

80. Reitz RH, McDougal JN, Himmelstein MW, Nolan RJ, Schumann AM. Physiologically based pharmacokinetic modeling with methylchloroform: implications for interspecies, high dose/low dose, and dose route extrapolations. Toxicology and Applied Pharmacology. 1988;95(2):185-99.

81. Kenyon EM. Interspecies Extrapolation. In: Reisfeld B, Mayeno AN, editors. Computational Toxicology: Volume I. Totowa, NJ: Humana Press; 2012. pp. 501-20.

82. Poulin P, Theil FP. Prediction of pharmacokinetics prior to in vivo studies. 1. Mechanism-based prediction of volume of distribution. Journal of pharmaceutical sciences. 2002;91(1):129-56.

83. Krishnan K, Loizou G, Spendiff M, Lipscomb JC, Andersen M. PBPK modeling: A primer2010. 19-58 p.

84. Lipscomb JC, Haddad S, Poet T, Krishnan K. Physiologically-Based Pharmacokinetic (PBPK) Models in Toxicity Testing and Risk Assessment. In: Balls M, Combes RD, Bhogal N, editors. New Technologies for Toxicity Testing. New York, NY: Springer US; 2012. p. 76-95.

85. Tornero-Velez R, Davis J, Scollon EJ, Starr JM, Setzer RW, Goldsmith M-R, et al. A Pharmacokinetic Model of cis- and trans-Permethrin Disposition in Rats and Humans With Aggregate Exposure Application. Toxicological Sciences. 2012;130(1) :33-47.

86. Yusof SR, Mohd Uzid M, Teh EH, Hanapi NA, Mohideen M, Mohamad Arshad AS, et al. Rate and extent of mitragynine and 7-hydroxymitragynine blood–brain barrier transport and their intra-brain distribution: the missing link in pharmacodynamic studies. Addiction Biology. 2018.

87. Hammarlund-Udenaes M, Fridén M, Syvänen S, Gupta A. On The Rate and Extent of Drug Delivery to the Brain. Pharmaceutical research. 2008;25: 1737-50.

APPENDIX

APPENDIX A A SYSTEMATIC REVIEW OF PHARMACOKINETIC PROPERTIES OF MITRAGYNINE

In this part, systematic search was performed through 3 databases: PubMed, Scopus, and Web of Science from their inception to January 2019. The search terms were used as follows: kratom OR ketum OR "biak-biak" OR kakuam OR ithang OR thom OR krathom OR kraton OR mitragynine OR "Mitragyna speciosa". The inclusion and exclusion criteria were described in Table 17. The results of the study selection were shown in the PRISMA flow diagram in Figure 21, as well as the characteristic of the studies were detailed in Table 18.

Table 17 Inclusion and exclusion criteria for this systematic review

Inclusion criteria	Exclusion criteria
• Studies investigating pharmacokinetics of mitragynine through *in vitro*, *in situ*, *in vivo* either animals or humans • Studies providing sufficient information on the pharmacokinetics of mitragynine (i.e. methodology, routes of administration)	• Not written in English • Not related to pharmacokinetics of mitragynine as follows: review articles, surveys, case reports, policies, pharmacological effects and toxicities, pharmacokinetics of other alkaloids in the kratom leaves

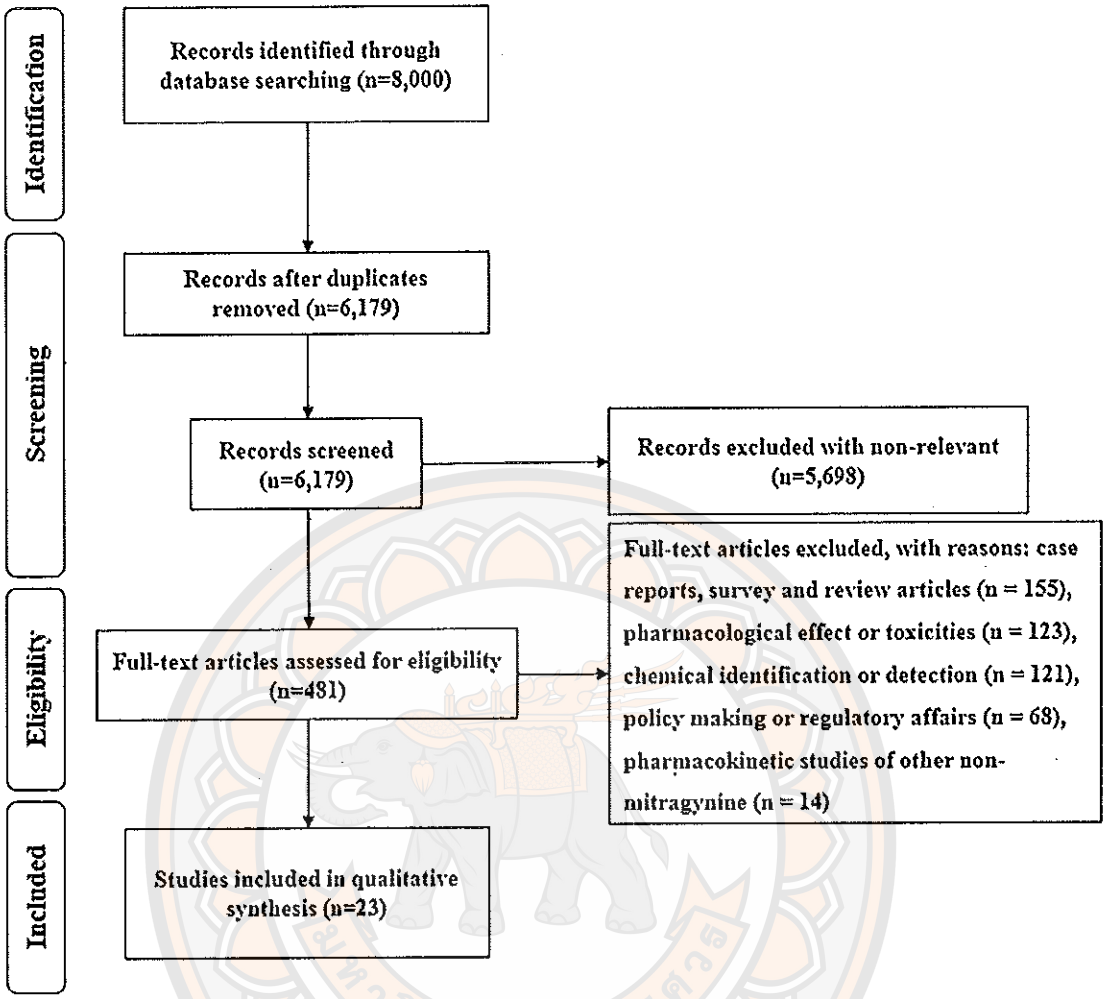

Figure 21 PRISMA flow diagram for systematic review of pharmacokinetics of mitragynine

Table 18 Study characteristic of pharmacokinetic studies of mitragynine

Author (Year)	Studies	Description
Ramanathan, et al. (2015) (23); Manda, et al. (2014) (24); Kong, et al. (2017) (46)	3	Determination on the solubility, permeability, plasma protein binding, and metabolic stability
Jagabalan, et al. (2018) (49)	1	Permeability of mitragynine intact rat's intestinal wall (*in situ*)
Lim, et al. (2013) (50); Hanapi, et al. (2010) (51); Manda, et al. (2017) (52); Kamble, et al. (2018) (53); Anwar, et al. (2012) (54); Meyer, et al. (2015) (55); Haron, et al. (2015) (56); Huda Abdullah, et al. (2018) (57); Meyer, et al. (2015) (58); Rusli, et al. (2015) (59); Wagmann, et al. (2018) (60);	11	Contribution of various drug metabolizing enzymes and protein-mediated transporters
Phillip, et al. (2009) (61)	1	Metabolites of mitragynine in rats and humans urine
Parthasarathy, et al. (62); Vuppala, et al. (2011) (63); Avery, et al. (2019) (64); Kong, et al. (2017) (65); Janchawee, et al. (2006) (66); de Moraes, et al. (2009) (67)	6	Oral and intravenous administration into rats
Trakulsrichai, et al. (2015) (68)	1	Pharmacokinetics of mitragynine in human volunteers

APPENDIX B PUBLICATION OF A SYSTEMATIC REVIEW OF PHARMACOKINETICS OF MITRAGYNINE

Asian Journal of Psychiatry 43 (2019) 73–82

Contents lists available at ScienceDirect

Asian Journal of Psychiatry

Journal homepage: www.elsevier.com/locate/ajp

Pharmacokinetics of mitragynine, a major analgesic alkaloid in kratom (*Mitragyna speciosa*): A systematic review

Kimheang Ya[a,b,c], Wimonchat Tangamornsuksan[d], C. Norman Scholfield[a,c], Janthima Methaneethorn[a,b], Manupat Lohitnavy[a,b,c,*]

[a] Center of Excellence for Environmental Health & Toxicology, Faculty of Pharmaceutical Sciences, Naresuan University, Phitsanulok, Thailand
[b] Pharmacokinetic Research Unit, Faculty of Pharmaceutical Sciences, Naresuan University, Phitsanulok, Thailand
[c] Department of Pharmacy Practice, Faculty of Pharmaceutical Sciences, Naresuan University, Phitsanulok, Thailand
[d] Faculty of Medicine and Public Health, HRH Princess Chulabhorn College of Medical Science, Chulabhorn Royal Academy, Bangkok, Thailand

ARTICLE INFO

Keywords:
Mitragyna speciosa
Kratom
Mitragynine
Pharmacokinetic
Systematic review

ABSTRACT

Background and objective: Kratom (*Mitragyna speciosa*) is a tropical tree found in southern Thailand and northern states of the Malay Peninsula. Kratom is commercially available and used as an alternative to treat opioid withdrawal. Mitragynine is the major indole alkaloid found in kratom leaves. This review aimed to summarize available pharmacokinetic information about mitragynine.

Methods: PubMed, Scopus, and Web of Science were systematically searched from their inceptions to June 2018. All types of pharmacokinetic studies of mitragynine were included for further systematic review.

Results: Seventeen articles were reviewed. Mitragynine is a lipophilic weak base passively transported across the intestinal wall and blood brain barrier. 85–95% is bound to plasma protein and extensively metabolized by phase I and particularly phase II enzymes. Actions on CYP enzymes are unlikely to impact drug metabolism at concentrations likely to exist in kratom-consuming humans. In rats and humans, mitragynine is rapidly absorbed after orally administration (T_{max} 1.5 h, C_{max} 0.3 – 1.8 μM). V_d was 37–90 L/kg; $t_{1/2}$ was 3–9 hr; mostly excreted as metabolites in urine. Bioavailability was estimated as 21%. It also rapidly penetrated and redistributed in brain. A quality assessment tool tailored for pharmacokinetic studies was also created which rated some studies of lower value.

Conclusion: Rudimentary pharmacokinetics of mitragynine was described in this systematic review. However, the discovered studies provided scant information on the role of metabolism and redistribution into tissues nor the rate of excretion.

1. Introduction

Mitragyna speciosa (Rubiaceae) is a tropical tree common in southern Thailand and the adjoining northern Malaysia. In Thailand, it is variously known as kratom, thom, ithang, kakuam, kraton, krathom, and as biak-biak, ketum in Malaysia (Hassan et al., 2013; Tanguay, 2011; Warner et al., 2016). Traditionally, kratom is consumed by chewing the fresh leaves, smoking dried leaves, or as tea from dried leaves (Tanguay, 2011). In Southeast Asia, laborers eat its fresh leaves to promote physical endurance, to increase energy, to relief fatigue, and to improve their heat tolerance. Kratom also has appeared in folk remedy to treat some illnesses including coughing, diarrhea, diabetes, and hypertension (Assanangkornchai et al., 2007). Kratom leaves showed opioid-like effect in dose-dependent (Prozialeck et al., 2012). Kratom has many adverse effects including anorexia, dehydration, weight loss, hyperpigmentation (green/dark colored skin), constipation, and psychosis (Saingam et al., 2013; Vicknasingam et al., 2010). However, kratom is rapidly becoming a substance of abuse in southern Thailand; it is consumed as homemade ice-cocktails called a "4 × 100 Cocktail" where kratom leaves are suspended "Coca-Cola" with codeine or diphenhydramine syrup (Tanguay, 2011; White, 2018). Kratom is also consumed as a herbal blend called "krypton" which is a mixture of

Abbreviations: Caco-2, human colonic adenocarcinoma; MDR-MDCK, Multidrug Resistance Protein in Madin-Darby Canine Kidney; CYP, cytochrome P450; P-gp, P-glycoprotein; C_{max}, maximum serum/plasma concentration; T_{max}, time to reach maximum concentration; $t_{1/2}$, half-life; AUC, area under the curve; F, oral bioavailability; V_d, volume distribution; CL_s, clearance

* Corresponding author at: Center of Excellence for Environmental Health & Toxicology, Faculty of Pharmaceutical Sciences, Naresuan University, Phitsanulok, 65000, Thailand.
E-mail address: manupatl@gmail.com (M. Lohitnavy).

https://doi.org/10.1016/j.ajp.2019.05.016
Received 8 March 2019; Received in revised form 5 May 2019; Accepted 8 May 2019

kratom leaves with O-desmethyltramadol and sold widely on the internet (Arndt et al., 2011). Regarding to uncertainly on safety and efficacy, kratom is monitored as controlled substance in some countries. Kratom is classified as a narcotic and illegal in some countries including Malaysia, Myanmar, and Australia (Singh et al., 2016) but currently Thai National Legislation Assembly permits kratom for medical use only (Narcotics Act No.7 B.E. (2562) (2019)). Currently, it is not controlled but under surveillance in the UK and Germany and the US where stocks are confiscated by the US Food and Drug Administration (Hassan et al., 2013; Prozialeck et al., 2012; Schmidt et al., 2011). It is commercially available as a dietary supplement for chronic pain (Boyer et al., 2007), and as an alternative treatment for opioid withdrawal (Boyer et al., 2008). Although, kratom is considered as not an illegal substance in most states in the US. However, an increasingly trend of kratom use as well as its adverse events was observed (Galbis-Reig, 2016). Kratom toxicity and the potential associated fatalities have been reported when kratom is used concurrently with other substances, i.e. propylhexedrine (Holler et al., 2011), O-desmethyltramadol (Kronstrand et al., 2011). Kratom also has a psychoactive effect as opioid substance lead to physically dependent or addiction. Thus, kratom is increasingly emerged as an abuse potential in the western countries (Singh et al., 2014). Nonetheless, with its effects to the central nervous system, mitragynine can have additive effects. Therefore, its use of this psychoactive alkaloid should be controlled.

More than 40 alkaloids have been isolated from kratom (Adkins et al., 2011). Among these, mitragynine is the principle indole alkaloid in Thai kratom (66% of total alkaloids) when extracted by organic solvents (Adkins et al., 2011; Ponglux et al., 1994). Mitragynine shares many kratom effects including its opioid action (Prozialeck et al., 2012; Warner et al., 2016). In addition, mitragynine has antinociceptive/analgesic, ileal relaxing and gastric relaxing effects (Suhaimi et al., 2016). It also appears to be an antidepressant (Idayu et al., 2011), and an anti-inflammatory (Utar et al., 2011). The molecular targets of mitragynine are μ opioid receptors acting as a partial agonist while being a competitive antagonist at κ and δ opioid receptors. Full agonists such as morphine, recruit β-arrestin of the μ receptor which mediates much of the opiate toxicity, particularly respiratory depression. β-arrestin also inhibits the G-protein signaling which is normally responsible for analgesia but leads to opiate tolerance (Camilleri, 2018). In contrast, mitragynine is a G-protein-biased agonist at μ opioid receptors but without recruiting β-arrestin, thus causing less respiratory depression while maintaining analgesia (Kruegel et al., 2016). There is increasing interest in partial agonist of μ opioid receptors including mitragynine as alternatives to opiates. In addition, mitragynine also bind to alpha-2 adrenergic receptor, adenosine, dopamine D2 receptors and serotonin receptors but the affinity between mitragynine and these receptors has not well-described.

In some countries, over-prescribing of opiate analgesic can lead to addiction. Kratom has been used as an alternative for opiate addiction (Boyer et al., 2009). Thus, the legalization of kratom in Thailand paves the way to the development of safer analgesic medications. A necessary prelude to this is having the ability to predict mitragynine disposition on overall efficacy. Mitragynine has the potential as a replacement for opiate analgesics but its therapeutic window or controlled clinical trials on the safety and efficacy needs better defining which needs clear understanding its pharmacokinetics. To this end, we aimed to systematically review the pharmacokinetics and relevant properties of mitragynine from the available scientific literature.

2. Methods

2.1. Data sources and search strategy

Studies related to pharmacokinetics of mitragynine were systematically searched from three databases: PubMed, Scopus, and Web of Science from their inception to June 2018. The search terms were kratom OR ketum OR "biak-biak" OR kakuam OR ithang OR thom OR krathom OR kraton OR mitragynine OR "Mitragyna speciosa".

2.2. Study selection

Two reviewers (KY and WT) independently appraised titles and abstracts retrieved from the searches. Any disputes were resolved by a third reviewer (ML). Studies were included if they met all of the following criteria: (1) studies investigating pharmacokinetics of mitragynine or pharmacokinetic-related properties of mitragynine (i.e. solubility, permeability) through *in vitro*, *in situ*, *in vivo* either with experimental animals or human participants; and (2) studies providing sufficient information on the pharmacokinetics of mitragynine including methodology and routes of administration. The exclusion criteria were the following: (1) not written in English; (2) review articles, surveys, case reports, policies; (3) pharmacological effects and toxicities; and (4) pharmacokinetic studies on non-mitragynine alkaloids. Bibliographies of the included articles were examined to identify additional studies. If sufficient details were provided, abstracts and non-journal publications were included. All procedures of the study selection were performed using the PRISMA statement (Moher et al., 2009).

2.3. Data extraction

Data extraction from all the selected articles were performed by two reviewers (KY and WT) and discrepancies were resolved through discussion with a third reviewer (ML). The following data were extracted from studies: (1) physicochemical properties, solubility, and permeability; (2) plasma protein binding; (3) metabolism and membrane transport; and (4) pharmacokinetic parameters in animals and humans.

2.4. Quality assessment

An essential part of a PRISMA systematic review is a quality assessment of extracted studies but often confined to clinical studies focusing on risk of bias tools. Increasingly, tools reflecting CONSORT and ARRIVE are being used to provide more comprehensive quality assessment in animal and clinical studies (Gagnier et al., 2006; Kilkenny et al., 2010). The CONSORT (consolidated standards of reporting trials) statement for randomized controlled clinical trials is applied to control for bias in clinical intervention including herbal products (Gagnier et al., 2006). The ARRIVE (animals in research: reporting *in vivo* experiments) is a guideline that help to improve reporting of research using animals (Kilkenny et al., 2010). Therefore, we adapted CONSORT and ARRIVE checklist items into a quality assessment tool equally applicable for animal and human pharmacokinetic studies (Table 4). The guidance notes for users is given in supplement S1. Only 6 pharmacokinetic studies underwent this assessment (de Moraes et al., 2009; Janchawee et al., 2007; Kong et al., 2017b; Parthasarathy et al., 2010; Trakulsrichai et al., 2015; Vuppala et al., 2011).

3. Results

3.1. Study selection

Of the 7348 articles identified from the databases, title and abstract screening left 419 studies that fitted the eligibility criteria. Exclusion criteria removed 402 of these leaving 17 studies for this systematical review as shown in the PRISMA flow diagram (Fig. 1).

3.2. Study characteristic

Among these 17 selected articles, 9 studies were performed *in vitro* to test mitragynine solubility, permeability to lipid bilayers or cell monolayers, plasma protein binding, metabolic stability, and disposition of mitragynine (metabolism and/or transport) (Anwar et al., 2012;

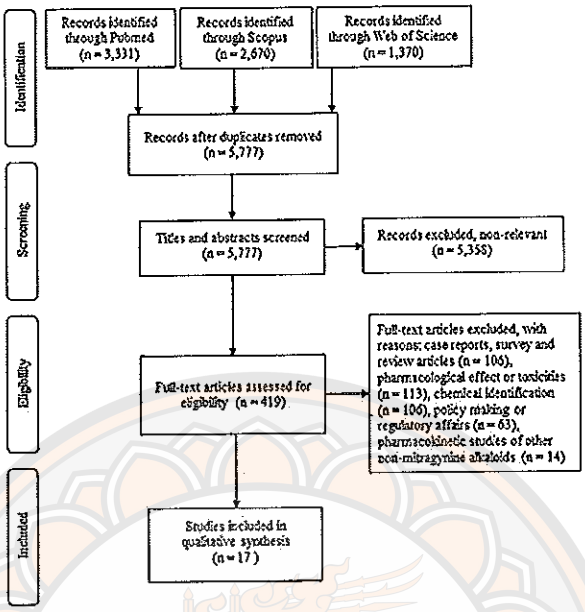

Fig. 1. PRISMA flow diagram of this study 21.

Hanapi et al., 2013; Haron and Ismail, 2015; Kong et al., 2017a; Lim et al., 2013; Manda et al., 2014, 2017; Meyer et al., 2015; Ramanathan et al., 2015). One study used intestine *in situ* to measure mitragynine permeability to the intact intestinal wall (Jagaballan et al., 2018). There were 6 *in vivo* studies: 1 study identified mitragynine metabolites in rats and in humans urine; 5 studies administered mitragynine intravenously or orally to rats and blood sampled for pharmacokinetic studies (de Moraes et al., 2009; Janchawee et al., 2007; Kong et al., 2017b; Parthasarathy et al., 2010; Philipp et al., 2009; Vuppala et al., 2011). One study determined mitragynine pharmacokinetics in humans (Trakulsrichai et al., 2015)

3.3. Physicochemical properties of mitragynine

Mitragynine is an indole alkaloid (Fig. 2) comprising 66% of total alkaloids in extracts of *Mitragyna speciosa* leaves (Adkins et al., 2011; Ponglux et al., 1994). Mitragynine is a weak base (pKa = 8.1) and lipophilic (Log P = 1.73) (Ramanathan et al., 2015). In an aqueous media at pH 4 and 7, mitragynine would be dissolved with concentration levels of 130 μM and 83 μM, respectively (Kong et al., 2017a). This compound at 37 °C was moderately stable at neural pH (~3.5% degradation after 3 h) but degraded at pH 1.2 (by 26% degradation after 1–2 hr) (Manda et al., 2014; Ramanathan et al., 2015), Table 1(a).

3.4. Pharmacokinetics of mitragynine

3.4.1. Absorption

Absorption in vitro: mitragynine fluxes through the phospholipid bilayer at pH 4 and 7.4 were 0.23×10^{-6} and 11×10^{-6} cm/s, respectively (Kong et al., 2017a); these values suggested that mitragynine permeated as the unionized form. In coherent Caco-2 cell monolayers

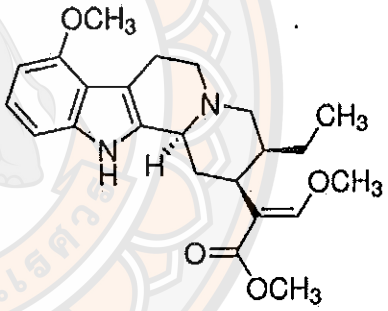

Fig. 2. Chemical structure of mitragynine 21.

(imitating the intestinal barrier), forward and reverse fluxes were 25×10^{-6} and 27×10^{-6} cm/s, which were independent of concentration (Manda et al., 2014). Flux ratios of mitragynine were approximately equated 1, as indicated passively diffusion through membranes. Those results suggested that mitragynine is not a substrate for P-glycoprotein (P-gp). Interestingly, mitraphylline, a minor kratom constituent, was strongly extruded by P-gp. Likewise, mitragynine fluxes across MDR-MDCK cell monlayers (model of the blood brain barrier) were symetrical 15×10^{-6} and 17×10^{-6} cm/s, respectively (Manda et al., 2014). Mitragynine was rated as diffusible using atenolol, propranolol, caffeine, carbamazepine, furosemide, and metoprolol as comparators, as summarized in Table 1(b).

Absorption across the gut epithelium: another study measured mitragynine permeability to intact intestine *in situ* as 1.11×10^{-4} cm/s in

Table 1
In vitro experiment responsible on solubility and permeability of mitragynine.

(a): solubility determinations

Media (incubation period)	pH	Solubility (μM) (% RD)	Reference
SGF (120 min)	1.2	8.03 ± 0.5 (26%)	(Manda et al., 2014)
SIF (180 min)	6.8	10.79 ± 0.25 (3.6%)	
SGF (60 min)	1.2	35.13 ± 0.5 (26%)	(Kamkaen et al., 2015)
SIF (180 min)	6.8	17.57 ± 2.01 (3.5%)	
Water	4	130.0 ± 0.1[a]	(Kong et al., 2017a)
	7	82.7 ± 1.9[b]	

(b): apparent permeability (P_{app} = 10^{-6} cm/s) through cell layers Caco-2 colonic epithelial, brain vascular endothelial cell, and artificial membranes

Model	Compound (tested concentration)	P_{app} (10^{-6} cm/sec)		Reference
		Absorptive flux	Secretory flux	
Gut wall Caco-2 cell monolayers	Mitragynine (5 μM)	24.2 ± 2.6	26.3 ± 2.7	(Manda et al., 2014)
	Mitragynine (10μM)	25.3 ± 2.2	29.1 ± 2.0	
	Atenolol (200μM)	2.0 ± 0.6	2.1 ± 0.4	
	Propranolol (200μM)	34.2 ± 2.6	35.4 ± 1.9	
Brain endothelial MDR-MDCK cells monolayer	Mitragynine (5 μM)	15.3 ± 1.7	17.2 ± 1.6	
	Mitragynine (10μM)	16.2 ± 1.8	18.1 ± 1.7	
	Atenolol (200μM)	1.1 ± 0.2	1.2 ± 0.1	
	Caffeine (100μM)	23.2 ± 2.8	24.3 ± 1.5	
PAMPA	Mitragynine	0.23 ± 0.0005	11.14 ± 0.06	(Kong et al., 2017a)
	Carbamazepine	0.21 ± 0.005	0.13 ± 0.002	
	Furosemide	0.72 ± 0.008	0.75 ± 0.003	
	Metoprolol	4.55 ± 0.002	4.49 ± 0.007	

Abbreviations:SGF = simulated gastric fluid; SIF = simulated intestinal fluid; RD = relative deviation; DES = diethylstilbestrol; Caco-2 cells = human colonic adenocarcinoma cells; MDR-MDCK = multi drug resistance in Madin-Darby Canine Kidney; PAMPA = parallel artificial membrane permeability assay; P_{app} = apparent permeability.
DES (24.1 ± 4.2 μM), estriol (89.8 ± 8.17 μM), and furosemide (187.8 ± 1.0 μM), respectively.
DES (19.3 ± 0.5 μM), estriol (86.5 ± 3.0 μM), and furosemide (197.5 ± 3.1μM), respectively.
[a]At pH 4, this value was compared to low, medium, and high solubility references as followed.
[b]At pH 7, this value was compared to low, medium, and high solubility references as followed.

the absorption direction (Jagaballan et al., 2018), which compared favourably with permeant propranolol (1.12×10^{-4} cm/s) and atenolol (0.41×10^{-4} cm/s). The inhibitors of P-gp (azithromycin) or CYP3A4 (ciprofloxacin) had no influence on mitragynine fluxes (1.13×10^{-4} cm/s and 1.17×10^{-4} cm/s), again suggesting that mitragynine absorption is passive and rapid.

3.4.2. Binding to plasma protein

By equilibrium dialysis, about 95% of mitragynine at tested concentration range of 5–15 μM bound to plasma protein after 24 h at 37 °C in human plasma (Manda et al., 2014). About 85% of mitragynine at a tested concentration of 10 μM binds to plasma proteins after 1 h at 37 °C in human plasma, determined by ultrafiltration (Kong et al., 2017a).

3.4.3. Metabolism and excretion

For metabolism of mitragynine, most of its metabolism occurs in the liver. Both phase I and phase II metabolism involved in the metabolism of this psychoactive alkaloid. There were several studies investigating roles of phase I and phase II using a system with liver microsomes or liver S9 fraticitons (Kong et al., 2017a; Manda et al., 2014), as summarized in Table 2(a). Interestingly, Philipp et al. (2009) measured urinary metabolites by LC–MS/MS after oral dosing of 40 mg/kg mitragynine to rats and urine samples were collected after 24 h. Seven phase I mitragynine metabolites were identified and a further 5 conjugates as one sulphonate and 4 glucuronides presumed to be phase II metabolites. In human urine, 3 sulphonates and 4 glucuronidates were found (Philipp et al., 2009). Mitragynine metabolites were summarized in Table 2(b). Numerous other metabolites were found in urine samples referred for toxicology assessment but had no accompanying history. Samples also contained 10–30 % mitragynine (our estimate from published chromatograms) (Philipp et al., 2011). Trakulsrichai et al. (2015) measured urinary mitragynine and reported levels "as low as 0.14% of mitragynine in an unchanged form" (Trakulsrichai et al., 2015). Lee et al. (2012) measured mitragynine in urine samples provided by the judiciary without any donor history (presumed to be kratom overdose victims) and found urinary mitragynine to vary between 0.004–150 μM and small amounts of 7-hydroxymitragynine. Two phase I metabolites were also detected in small and variable amounts. These studies show that mitragynine is extensively metabolized and an uncertain amount of mitragynine is directly excreted (Le et al., 2012).

For effect of mitragynine on metabolic enzymes, mitragynine enhanced expression of CYP1A2, CYP3A4, CYP2D6, and CYP2C9 (Hanapi et al., 2013; Lim et al., 2013; Manda et al., 2017), Table 2(c). Mitragynine induced CYP1A2 and weakly induced CYP3A4, as measured protein and mRNA expression (Lim et al., 2013). Substantially, identification on pregnane X receptor, which the transcription factor for P-gp and some CYPs, was also upregulated. However, a common enzyme inducer (aryl hydrocarbon receptor) was unaffected but mitragynine can induced CYP1A2 only (Manda et al., 2017). For instance, mitragynine can inhibited CYP2D6 and weakly inhibited some other CYP enzymes (Hanapi et al., 2013). However, the tested concentration employed unlikely to arise in plasma at doses used by human (see below). Other drug metabolizing enzymes, aminopyrine N-demethylase and glutathione S-transferase (Anwar et al., 2012), and uridine 5′-diphospho-glucuronosyltransferase (Haron and Ismail, 2015) showed weak effects and needed high concentrations Table 2(c). Regarding, the activity of mitragynine on P-gp was investigated by three studies (Manda et al., 2014, 2017; Meyer et al., 2015), Table 2(c). Those studies concluded that mitragynine can induced and inhibited P-gp; thus, co-administraiton of mitragynine with drugs which are P-gp substrated may possibly lead to occur drug-herbal interaction. Notably, when protein binding is considered, free mitragynine concentration and by extension

Table 2
In vitro metabolism and excretion of mitragynine.

(a): metabolic stability of mitragynine in rat or human liver microsomes or liver S9 fraction.

Model	Compound	Metabolic stability	Results	Reference
HLM	Mitragynine	% metabolized	30 %	(Manda et al., 2014)
Liver S9 fraction			55 %	
RLM	Mitragynine	% remained	84.5 ± 1.8 %	(Kong et al., 2017a)
	Propranolol[a]		21.4 ± 0.6 %	
	Verapamil[a]		69.0 ± 1.6 %	

(b): phase I and phase II metabolites of mitragynine, adapted from (Philipp et al., 2099)

Metabolites of mitragynine	Abbreviation
Phase I metabolites	
9-O-demethyl mitragynine	9-O-DM-MG, 2
16-carboxy mitragynine	16-COOH-MG, 3
9-O-demethyl-16-carboxy mitragynine	9-O-DM-16-COOH-MG, 4
17-O-demethyl-16,17-dihydro mitragynine	17-O-DM-DH-MG, 5
9,17-O-bisdemethyl-16,17-dihyro mitragynine	9,17-O-BDM-DH-MG, 6
17-carboxy-16,17-dihydro mitragynine	17-COOH-DH-MG, 7
9-O-demethyl-17-carboxy-16,17-dihydro mitragynine	9-O-DM-17-COOH-DH-MG, 8
Phase II metabolites	
9-O-demethyl mitragynine glucuronide	9-O-DM-G-MG, 2G [a, b]
9-O-demethyl mitragynine sulfate	9-O-DM-S-MG, 2S [b]
16-carboxy mitragynine glucuronide	16-COOH-G-MG, 3G [a, b]
9-O-demethyl-16-carboxy mitragynine glucuronide	9-O-DM-16-COOH-G-MG, 4G [a]
9-O-demethyl-16-carboxy mitragynine sulfate	9-O-DM-16-COOH-S-MG, 4S [a, b]
17-O-demethyl-16,17-dihydro mitragynine glucuronide	17-O-DM-DH-G-MG, 5G [b]
9,17-O-bisdemethyl-16,17-dihyro mitragynine glucuronide	9,17-O-BDM-DH-G-MG, 6G [a]
9,17-O-bisdemethyl-16,17-dihyro mitragynine sulfate	9,17-O-BDM-DH-S-MG, 6S [b]

(c): effect of mitragynine on metabolic enzymes

Enzyme	Tested concentration of mitragynine	Results	Reference
Cytochrome P450-mediated metabolism of mitragynine			
CYP1A2	25 μM	Induction	(Lee et al., 2013)
CYP2D6		No induction	
CYP3A4		Weak induction	
CYP2D6	0.02 – 200 μM	Potent inhibitory (noncompetitive)	(Hanapi et al., 2013)
		IC_{50} = 0.4 ± 0.3 μM (K_i = 12.9 μM)	
CYP3A4		Moderate inhibitory (competitive)	
		IC_{50} = 41.3 ± 6.7 μM (K_i = 379.2 μM)	
CYP2C9		Moderate inhibitory (noncompetitive)	
		IC_{50} = 9.7 ± 4.8 μM (K_i = 155.8 μM)	
CYP1A2	1 – 10 μM	Induction	(Manda et al., 2017)
CYP3A4		No induction	
Effect of mitragynine on the other drug metabolizing enzymes			
N-demethylase	0.25 – 250 μM	Induction	(Anwar et al., 2012)
glutathione S-transferase		Inhibition (IC_{50} = 11.8-24.4 μM)	
UGT	100 μM	Inhibition 4-methylumbelliferone glucuronidation in RLM, HLM, UGT1A1 and UGT2B7 (IC_{50} > 100 μM)	(Haron and Ismail, 2015)
Protein-mediated efflux transporters of mitragynine			
P-glycoprotein	5 – 10 μM	Inhibition	(Manda et al., 2014)
	5 μM	Inhibition	(Meyer et al., 2015)
	1 – 10 μM	Induction	(Manda et al., 2017)

Abbreviations: HLM = human liver microsomes; RLM = rat liver microsomes; CYP450 = cytochrome P450; UGT = uridine 5′-diphospho-glucuronosyltransferase; IC_{50} = half maximal inhibitory concentration; EC_{50} = half maximal effective concentration; K_i = inhibitory constant.
[a]Standard reference compounds of low and high metabolic stability.
[b]Metabolites of mitragynine could identified in urinary rats.
[c]Metabolites of mitragynine could identified in urinary humans.

the extracellular levels fall below the micromolar ranges and clearly well below those in Table 2(c). Thus, these actions on drug metabolism are mostly irrelevant to therapeutic or even toxic doses of mitragynine.

3.5. Pharmacokinetic studies of mitragynine in animals and humans

From our systematic reviewing process, five pharmacokinetic studies on mitragynine in rats were retrieved (de Moraes et al., 2009; Janchawee et al., 2007; Kong et al., 2017b; Parthasarathy et al., 2010; Vuppala et al., 2011). Among these studies, one rat study used a two compartment pharmacokinetic model (Kong et al., 2017b) while the others assumed a single compartment (de Moraes et al., 2009; Janchawee et al., 2007; Parthasarathy et al., 2010; Vuppala et al., 2011). Furthermore, one study determined about pharmacokinetics of mitragynine in human subjects (Trakulsrichai et al., 2015).

3.5.1. Intravenous administration of mitragynine to rats

Two studies reported on pharmacokinetics of intravenously administered mitragynine (1.5 and 5 mg/kg) into rats, presumably as a bolus (Parthasarathy et al., 2010; Vuppala et al., 2011), Table 3. The

Table 3
Pharmacokinetics of mitragynine in animals and humans.

Reference	Species	BW (g)	Sample	Dose (mg/kg)	Route (sampling)	Analytical method	LOD	LOQ	C_{max}	T_{max}	k_a	$AUC_{0-\infty}$	V_d, V_d/F	CL, CL/F	k_e	$t_{1/2}$
							μM**	μM**	μM**	hr	1/hr	μM/h**	L/kg	L/hr kg	1/hr	hr
Intravenous administration of mitragynine to rats (1.5–10 mg/kg)																
(Parthasarathy et al., 2016)	male SD rats	280-315	Plasma	1.5	i.v. (tail vein)	HPLC-UV	0.063	0.125	5.77 ± 3.01	1.2 ± 1.1	–	23.09 ± 16.31	0.79 ± 0.42	0.29 ± 0.27	–	2.9 ± 2.1
(Vergote et al., 2011)	male SD rats	150-250	Plasma	5	i.v. (jugular vein cannula)	UPLC-MS	0.0005	0.0025	9.79 ± 1.76	1 min	–	8.53 ± 2.26	8.2 ± 2.2	1.2 ± 0.2	–	2.6 ± 0.4
(Kong et al., 2017b)	female SD rats	250-300	Dialysed plasma	10	i.v. (jugular vein)	UPLC-MS	–	0.025	[3.81 ± 0.38]	[0.5]	–	11.62 ± 1.10	9.84 ± 0.62	2.26 ± 0.21	0.24 ± 0.03	13.14 ± 1.42
			Brain						[2.31 ± 0.13]	[0.5]	–	6.73 ± 0.35	16.94 ± 1.11	3.78 ± 0.18	0.23 ± 0.01	13.22 ± 2.55
			ECF													
Oral administration of mitragynine to rats (20-50 mg/kg)																
(Limchaveer et al., 2007)	male Wistar rats	220-290	Serum	40	p.o. (orbital sinus)	HPLC-UV	0.075	0.251	1.58 ± 0.45	1.83 ± 1.25	1.43 ± 0.90	17.54 ± 7.35	89.50 ± 30.30	7.3[a]	0.07 ± 0.01	9.43 ± 1.74
(de Moraes et al., 2009)	male Wistar rats	200-250	Plasma	20	p.o. (decapitation)	LC-MS/MS	–	0.0005	1.06	1.26	2.4	7.9	37.90	6.35	0.18	3.85
(Parthasarathy et al., 2016)	male SD rats	280-315	Plasma	50	p.o. (tail vein)	HPLC-UV	0.063	0.125	1.76 ± 0.53	4.5 ± 3.9	–	20.58 ± 7.53	64 ± 23	7.0 ± 3.0	0.105[b]	6.6 ± 1.3
Human subjects																
(Trakulsrichai et al., 2015)	Healthy volunteers	–	Plasma and urine	kratom tea***	p.o	LC-MS/MS	–	–	0.26[c]	0.83 ± 0.35	–	1.68[c]	38.04 ± 24.32	98.1 ± 51.34	–	~3 hr

** All values reported values in ng/mL have been converted to μM.
*** Kratom tea 60 mL (containing various concentration of mitragynine 6.25–11.5 mg) for 7 days and loading doses (6.25–23 mg) on days 8.
[x] These values are for unbound mitragynine, presumably excluding protein bound and each sample taken over 30 min.
[a] value convert unit from L/h to L/h kg.
[b] value has been calculated from formulation ($k_e = 0.693/t_{1/2}$).
[c] value has been found at highest loading dose (23 mg).
V_d/F and CL/F were apparent volume distribution and apparent total clearance that were calculated for oral administration.
Abbreviations:SD = Sprague-Dawley; BW = body weight; p.o. = per oral; i.v. = intravenous; ECF = extracellular fluid; HPLC-UV = high performance liquid chromatography coupled to ultra-violet; LC-MS/MS = high performance liquid chromatography coupled to tandem mass spectrometry; UPLC-MS = ultra-performance liquid chromatography coupled with a mass spectrometer; UFLC-MS = ultra-fast liquid chromatography equipped with a mass spectrometer; LOD = limit of detection; LOQ = limit of quantification; C_{max} = maximum serum/plasma concentration; T_{max} = time to reach maximum concentration; k_a = absorption rate constant; $AUC_{0-\infty}$ = area under the curve from time equals zero to infinity; V_d = volume distribution; CL = clearance; k_e = elimination rate constant; $t_{1/2}$ = half-life.

Table 4
Quality assessment of pharmacokinetic studies of mitragynine.

No.	Main domain	Sub-domains	(Janchawee et al., 2007)	(de Moraes et al., 2009)	(Parthasarathy et al., 2010	(Yuppadu et al., 2011)	(Kong et al., 2017b)	(Trakulsrichai et al., 2015)
1	Title and abstract	Title identified the compound, species, administration route. Abstract includes all key information of domains 2-12 and key numerical data.	Y/N	Y	Y/N	Y/N	Y	Y
2	Background, objectives	Scientific background and explanation of the rationale, clear objectives, hypotheses, and usefulness.	Y	Y	Y/N	Y/N	Y	Y
Methods								
3	Participants, subjects	Appropriate selection criteria, sample size, and recruitment.	Y	Y	Y/N	Y	Y	Y/N
4	Approvals	Full complied with ethical and safety standards and approvals.	Y/N	Y/N	Y/N	Y/N	Y/N	Y/N
5	Design and protocols	Adequately spaced sampling of blood, and includes urine and fecal samples. Appropriate design. Appropriate dose.	Y/N	Y/N	Y/N	Y	Y	Y/N
6	Procedures	Subject depositions and sampling methods, enough detail to permit study replication.	Y/N	Y	Y	Y	Y	Y/N
7	Chemical assays	Suitable standards and extraction controls including 'spiking', sensitivity, reproducibility, and selectivity.	Y	Y	Y	Y	Y	Y
Results								
8	Flow	Flow experienced by each participant/animal.	N	N	N	N	N	N
9	Data reporting	Reporting adequate; availability of raw data.	N	N	N	N	N	N
10	Baseline data	Baseline demographics that might influence pharmacokinetics.	NA	NA	NA	NA	NA	Y/N
11	Analysis	Data and analysis adequately extracted key pharmacokinetic parameters and statistic where appropriate. Described data pooling.	Y	Y	Y/N	Y	Y	Y/N
Discussion and conclusions								
12	Interpretation	Relating the key biological factors to pharmacokinetics and predictable clinical outcomes. Generalizability of results. Validation on conclusion.	Y/N	Y/N	N	Y/N	Y/N	Y/N
	Mean overall score, %		59%	68%	45%	64%	73%	54%

Abbreviation: NA = Not appropriate. Scoring: complete domains attracted a "Y" score = 1; some missing formulation was "Y/N" score 0.5; missing information prevented the reader from drawing conclusion was given "N" score = 0.

maximal plasma concentration (C_{max}) was 10 μM at time to reach maximum concentration (T_{max}) of 1 min (Yuppala et al., 2011) but Parthasarathy et al. (2010) either missed T_{max} by late sampling or it was very delayed (C_{max}~6 μM at T_{max}~70 min) (Parthasarathy et al., 2010). Parthasarathy et al. (2010) used a robust cross-over design but measurements may have been compromised by using the tail vein for sampling.

Kong et al., (2017) used the same injection protocol but sampled by dialysis tubing from blood and brain but temporal resolution was slow because of 30 min sampling periods (Kong et al., 2017b). The C_{max} in blood was 3.8 μM which equates to ~38 μM for whole plasma assuming 90% protein binding. Volume distribution (V_d) was 9.8 L/kg and half-life ($t_{1/2}$~13 h) was much longer than the other intravenous studies. For brain, C_{max} was lower (2.3 μM) and V_d was higher (17 L/kg) than blood. AUC_{brain}/AUC_{plasma} was 0.66, indicating substantial penetration of the blood-brain barrier and tissue loading.

3.5.2. Oral administration of mitragynine to rats

Three studies reported on pharmacokinetics of orally administered mitragynine (20–50 mg/kg) in rats (de Moraes et al., 2009; Janchawee et al., 2007; Parthasarathy et al., 2010) (Table 3). The pharmacokinetic studies serially sampled with time from each animal, except de Maoraes et al., (2009) who used 8 animals, a protocol suited to tissue collection. Here, there was less variation than between intravenous studies and C_{max} (1–1.8 μM) appeared linearly related to dose. Mitragynine was rapidly absorbed with T_{max}~1.5 h; although Parthasarathy et al. (2010) had no characteristic well-defined peak in the reported pooled data. The oral bioavailability of mitragynine was calculated by (Parthasarathy et al., 2010), indicating as low oral bioavailability (F~3%). However, the area under the curve (AUC) values and intravenous dosing from the study (Yuppala et al., 2011) and oral dosing from the study (de Moraes et al., 2009) both who had reliable sampling blood methods, sampling times, and assay procedures that allowed us to calculate F as ~21%.

3.5.3. Oral administration to humans

Mitragynine pharmacokinetics were studied in ten men having a history of kratom abuse (Trakulsrichai et al., 2015). They were randomly divided into five unequal groups and given daily conditioning doses of kratom tea containing 6.25–11.5 mg of mitragynine for 7 days. On day 8, participants were given a single oral dose of kratom tea standardized for mitragynine contents (6.25–23 mg), then blood and urine sampled over 24 h. For plasma mitragynine, C_{max} and AUC values (Table 3) suggested dose dependency but the data were too scattered and underpowered for a definitive conclusion. The declines were mostly bi-exponential so a two-compartment pharmacokinetic model was assumed. The average apparent V_d was 38.0 ± 24.3 L/kg and clearance (CL) was 98.1 ± 51.3 L/hr/kg. Time-plots were shown for each participant and for 6 records, the baseline plasma mitragynine concentrations were similar to those after 24 h. Graph crowding made it difficult distinguish other records. Two participants displayed a maintained plateaued plasma concentration. Reader is not informed of the test and conditioning doses used for each participant.

3.6. Quality assessment of pharmacokinetic studies

Six pharmacokinetic studies were assessed for their quality (Table 4). The protocols were fundamentally similar but without adequate reporting the causes of differences in pharmacokinetic variables were unclear.

For intravenous administration, only Yuppala et al. (2011) began sampling quickly after injection (1 min) while other studies of Parthasarathy et al. (2010) sampled too late to capture C_{max}. Kong, Mohamed, et al., (2017) were restricted to 30 min periods of slow sampling of dialysate. Particularly, crucial details about drug administration and specially sampling were scant; except in study of Yuppala et al. (2011) which stands out as the most reliable study by injecting and sampling from a large venous cannula that a method suited for small animal pharmacokinetic studies with many sampling times.

For oral administration, animals deprived of food and dosed with a variety of mitragynine formulations (100% propylene glycol; pH 4.7 acetate; 20% Tween 80) that are likely to impact on absorption especially the dispersing agents. Animals were anaesthetized or free-ranging or unreported. Different activity levels and particular high blood flow to active tissues probably promotes re-distribution. de Moraes et al. (2009) sampled blood by decapitation thus ideally able to follow tissue levels of mitragynine also having ample blood to measure at least key metabolites by LC/MS but did not do so. Only Trakulsrichai et al. (2015) provided data for each participant but could be related to dose (see above) and no study provided raw data. Raw data shows the sources of variability and allows verification of data-analysis. Raw data for the Parthasarathy et al., (2009) study may have explained the apparently flat concentration time curve after oral administration and for the delayed C_{max} with both routes of mitragynine administration. Had urinary pH and creatinine been measured by Le et al., (2011) and Trakulsrichai et al. (2015) disparate urinary mitragynine concentrations might have been explained. Only study by Trakulsrichai et al. (2015) focused on pharmacokinetics while other studies used pharmacokinetics as an adjunct to describing assay methods which in some cases occupied nearly all abstracts, a common strategy in herbal medicinal chemistry. Notwithstanding the above, most deficiencies arose from adhering to laxed reporting standards prevailing at the time of execution.

In vitro studies were not systematically screened for quality but the concentrations used exceeded high concentration levels of mitragynine up to 200 μM, a problem that is rife in herbal medicine research. Thus, although many drug metabolism enzymes were modified by mitragynine only a few effects are translatable to its therapeutic application.

4. Discussion

A substantial amount of data relevant to the pharmacokinetics of mitragynine has been published. Being a weak base, mitragynine absorption is moderately rapid at physiological pH in the distal small intestine and appears to be passive. Like most weak bases, it diffuses as the unionized form into the cytosol. The drug then becomes ion-trapped by the lower cytosolic pH, leading typically to a 6-fold concentration compared to the extracellular levels (Brown and Garthwaite, 1979). The uncharged form can also partition into fat stores but tendency is reduced in the more acidic cytosol surrounding most lipid deposits. This explains the high V_d of weakly basic drugs including mitragynine. Thus, filling this large sink can account for much of the initial decline. This justifies at least a two-compartment pharmacokinetic model. The 85–95 % plasma protein binding introduces two complications: (i) the effective mitragynine concentration in extracellular space is approximately 10% of the measured plasma concentration lowering activation of membrane receptors and concentration dependent diffusion; and (ii) the calculated V_d value can be lowered.

Mitragynine metabolism also influences $t_{1/2}$ predominantly by conjugation but also phase I modifications that contributed to excreted mitragynine. No discovered study could delineate contributions of metabolism, excretion, and redistribution to $t_{1/2}$ making it difficult to predict drug clearance for any particular person. An important variable is urinary pH, that normally varies between 4.6 and 8.0, could account for up to a 100-fold range of mitragynine excretion as a weak base. Thus measuring urine volume, pH, creatinine provides all the data to assess drug excretion but no study performed these. To date, contribution of phase I and phase II drug metabolizing enzyme on mitragyine has been established. Consequently, when co-administered mitragynine with other drugs, which extensively metabolized by these enzymes as described above, intreaction herbal-drug might be possible.

No study assessed tissue levels of mitragynine over time as a guide to redistribution. While perfusion rates are fairly constant for brain, kidney, liver, other tissues (gut and muscle) have highly variable perfusion rates; hence, the rate and size of the redistribution pool may be highly variable and impact on $t_{1/2}$. Therefore, the pharmacokinetics are complex and the studies so far have provided incomplete data. The pharmacokinetic studies in rat were similar to those in the human study except for lower C_{max} in humans (range 45–300 nM, cf 1500 nM in rats). The fast T_{max} of 0.8 h in human compared with ~1.5 h in rat suggests that simple dissolution in the aqueous media fed to humans without dispersing agents is enough for fast absorption. The different C_{max} reflects higher oral doses (20-50 mg/kg) given to rats (body weight: 0.22 – 0.32 kg). These equate to 220–550 mg in human (70 kg) using allometric scaling from rats (Sharma and McNeill, 2009), doses regarded as toxic in humans. Thus studies on human cell lines *in vitro* or human proteins should aim for actions evoked at submicromolar concentrations.

Pharmacokinetic parameters of mitragynine in rats show some variability between studies. For intravenous delivery, only Vuppala et al. (2011) began early enough to obtain a near true C_{max} while Kong, Mohamed et al. (2017) started sampling at 30 min and Parthasarathy et al. (2010) started at 20 min. The latter authors using tail vein also obtained a delayed C_{max}, suggesting either slow drug infusion or poor mixing. Their volume distribution was atypically low for a diffusable weak base and far lower than the two other intravenous studies. These questions about the Parthasarathy et al. (2010) data and their low 3% bioavailability determination is also worrisome. Due to its lipophilicity and poor water solubility at physiological pH, mitragynine can be classified as Class II Drug according to the Biopharmaceutical Classification System (BCS) (Sachan et al., 2009). Dissolution is one of the major factors influencing mitragynine oral bioavailability. A slow dissolution rate may play an important role in its low bioavailability (Barthe et al., 1999). Therefore, a development of an appropriate salt form of mitragynine may be able to increase its bioavailability oral. Our determination of 21% using data deemed as the most reliable accords with other diffusible weak bases including codeine which has a similar single pKa to mitragynine, undergoes extensive metabolism, additional polar (–OH) group, high V_d, and high bioavailability of > 50%. The remaining 80% of ingested mitragynine is either first-pass metabolized, remains in the gut unchanged, or degraded by the microbiota which is common with herbal medicines. Feces determination could help resolve this question. This is important because heterogeneity of the human microbiota can influence potency enormously.

We also designed a quality assessment which arose from a careful in-depth analysis of the discovered papers which lead to the guidance notes listed in supplement S1. Such detailed assessment tools should be mandatory for all systematic reviews if their conclusions are to be reliable. The PRISMA statement should be updated to account for this increased assessment rigor and extended to animal studies.

These studies leave many questions unanswered. Our quality assessment tool found some studies had poor design, execution, and laxed reporting creates confusion. Production of metabolites that are also biologically active or toxic were not considered. Nevertheless, one well-designed robust animals and human study could provide all the missing data, except concentration-time courses of mitragynine in organ tissues (i.e. brain, fat, muscle, kidneys, liver) would need an animal study as well as studies involving roles of protein transporter in mitragynine disposition. These new results from the studies are possibly explain more about pharmacokinetic behaviors of mitragynine.

5. Conclusion

This systematic review found several pharmacokinetic studies on mitragynine which varied in reporting, reliability, and completeness. While crude changes in blood levels after oral mitragynine can be modelled. The data on metabolism and excretion cannot be applied to humans. Future studies on mitragynine and other medicine should fully report methods, data, adhere to ethics, and maximise data collection. This includes a full 48 h blood time course including major metabolites, urinalysis of the agent and metabolites, fecal samples and a bioavailability determination. Nonetheless, the available information regarding the pharmacokinetics of mitragynine is not complete. For example, metabolism of the compound, bioavailability problem, disposition of this compound in the other tissues, mode of protein transporter into the brain, and potential interactions with other drugs or chemicals. There gaps of knowledge need further research.

Financial disclosure

None.

Contributions

Study concept and design: Ms. YA, Dr. Methaneethorn, and Dr. Lohitnavy

Drafting of the manuscript: Ms. YA, Dr. Methaneethorn, and Dr. Lohitnavy

Processing of the methodology and result: Ms. YA and Dr. Tangamornsuksan

Writing of the manuscript: Ms. YA

Quality assessment performing: Ms. YA, Dr. Methaneethorn, and Dr. Scholfield

Critical revision of the manuscript: Dr. Scholfield, Dr. Methaneethorn, and Dr. Lohitnavy

Conflict of interest

No conflict declared

Author disclosures

All authors approved for submission this manuscript. The authors have no relevant financial source to disclose and no conflicts of interest.

Acknowledgements

Ms. Kimheang YA was supported by Royal Scholarship under Her Royal Highness Princess Maha Chakri Sirindhorn Education Project, Faculty of Pharmaceutical Sciences, Naresuan University.

Appendix A. Supplementary data

Supplementary material related to this article can be found, in the online version, at doi:https://doi.org/10.1016/j.ajp.2019.05.016.

References

Adkins, J.E., Boyer, E.W., McCurdy, C.R., 2011. Mitragyna speciosa, a psychoactive tree from Southeast Asia with opioid activity. Curr. Top. Med. Chem. 11, 1165-1175.
Azizi, R., Ismail, S., Mansor, S.M., 2012. In Vitro Effect of Mitragynine on Activity of Drug Metabolizing Enzymes, N-Demethylase and Glutathione S-Transferase in Streptozotocin-Induced Diabetic Rats.
Arndt, T., Claussen, U., Güssregen, B., Schröfel, S., Stürzer, B., Werle, A., Wolf, G., 2011. Kratom alkaloids and O-desmethyltramadol in urine of a "Krypton" herbal mixture consumer. Forensic Sci. Int. 208, 47–52.
Assanangkornchai, S., Muekthong, A., Sam-Angsri, N., Pattanasattayawong, U., 2007. The Use of Mitragynine speciosa ("Krathom"), an addictive plant, in Thailand. Subst. Use Misuse 42, 2145–2157.
Barthe, L., Woodley, J., Houin, G., 1999. Gastrointestinal absorption of drugs: methods and studies. Fundam. Clin. Pharmacol. 13, 154-168.
Boyer, E.W., Babu, K.M., Macalino, G.E., 2007. Self-treatment of opioid withdrawal with a dietary supplement, Kratom. Am J Addict 16, 352-356.
Boyer, E.W., Babu, K.M., Adkins, J.E., McCurdy, C.R., Halpern, J.H., 2008. Self-treatment of opioid withdrawal using kratom (Mitragynia speciosa korth). Addiction 103, 1048-1050.
Brown, D.A., Garthwaite, J., 1979. Intracellular pH and the distribution of weak acids and

bases in isolated rat superior cervical ganglia. J. Physiol. 297, 597–620.
Camilleri, M., 2018. Toward an effective peripheral visceral analgesic: responding to the national opioid crisis. Am. J. Physiol. Gastrointest. Liver Physiol. 314, g637–g646.
de Moraes, N.V., Moretti, R.A., Furr 3rd, E.B., McCurdy, C.R., Lanchote, V.L., 2009. Determination of mitragynine in rat plasma by LC-MS/MS: application to pharmacokinetics. J. Chromatogr. B Analyt. Technol. Biomed. Life Sci. 877, 2593–2597.
Gagnier, J.J., Boon, H., Rochon, P., Moher, D., Barnes, J., Bombardier, C., 2006. Recommendations for reporting randomized controlled trials of herbal interventions: explanation and elaboration. J. Clin. Epidemiol. 59, 1134–1149.
Galbis-Reig, D., 2016. A case report of kratom addiction and withdrawal. Wmj 115, 49–52 quiz 53.
Hanapi, N.A., Ismail, S., Mansor, S.M., 2013. Inhibitory effect of mitragynine on human cytochrome P450 enzyme activities. Pharmacognosy Res. 5, 241–246.
Haron, M., Ismail, S., 2015. Effects of mitragynine and 7-hydroxymitragynine (the alkaloids of Mitragyna speciosa Korth) on 4-methylumbelliferone glucuronidation in rat and human liver microsomes and recombinant human uridine 5'-diphospho-glucuronosyltransferase isoforms. Pharmacognosy Res. 7, 341–349.
Hassan, Z., Muzaimi, M., Navaratnam, V., Yusoff, N.H., Suhaimi, F.W., Vadivelu, R., Vicknasingam, B.K., Amato, D., von Horsten, S., Ismail, N.I., Jayabalan, N., Hazim, A.I., Mansor, S.M., Muller, C.P., 2013. From Kratom to mitragynine and its derivatives: physiological and behavioural effects related to use, abuse, and addiction. Neurosci. Biobehav. Rev. 37, 138–151.
Holler, J.M., Vorce, S.P., McDonough-Bender, P.C., Magluilo Jr., J., Solomon, C.J., Levine, B., 2011. A drug toxicity death involving propylhexedrine and mitragynine. J. Anal. Toxicol. 35, 54–59.
Idayu, N.F., Hidayat, M.T., Moklas, M.A., Sharida, F., Raudzah, A.R., Shamima, A.R., Apryani, E., 2011. Antidepressant-like effect of mitragynine isolated from Mitragyna speciosa Korth in mice model of depression. Phytomedicine 18, 402–407.
Jagabalan, J.D.Y., Murugaiyah, V., Zainal, H., Mansor, S.M., Ramanathan, S., 2019. Intestinal permeability of mitragynine in rats using in situ absorption model. J. Asian Nat. Prod. Res. 1–13.
Janchawee, B., Keawpradub, N., Chittrakarn, S., Prasettho, S., Wararatananurak, P., Sawangjareon, K., 2007. A high-performance liquid chromatographic method for determination of mitragynine in serum and its application to a pharmacokinetic study in rats. Biomed. Chromatogr. 21, 176–183.
Kilkenny, C., Browne, W.J., Cuthill, I.C., Emerson, M., Altman, D.G., 2010. Improving bioscience research reporting: the ARRIVE guidelines for reporting animal research. PLoS Biol. 8, e1000412.
Kong, W.M., Chik, Z., Mohamed, Z., Alshawsh, M.A., 2017a. Physicochemical characterization of Mitragyna speciosa alkaloid extract and Mitragynine using in vitro high throughput assays. Comb. Chem. High Throughput Screen. 20, 796–803.
Kong, W.M., Mohamed, Z., Alshawsh, M.A., Chik, Z., 2017b. Evaluation of pharmacokinetics and blood-brain barrier permeability of mitragynine using in vivo microdialysis technique. J. Pharm. Biomed. Anal. 143, 43–47.
Kronstrand, R., Roman, M., Thelander, G., Eriksson, A., 2011. Unintentional fatal intoxications with mitragynine and O-desmethyltramadol from the herbal blend Krypton. J. Anal. Toxicol. 35, 242–247.
Kruegel, A.C., Gassaway, M.M., Kapoor, A., Varadi, A., Majumdar, S., Filizola, M., Javitch, J.A., Sames, D., 2016. Synthetic and receptor signaling explorations of the mitragyna alkaloids: mitragynine as an atypical molecular framework for opioid receptor modulators. J. Am. Chem. Soc. 138, 6754–6764.
Le, D., Goggin, M.M., Janis, G.C., 2012. Analysis of Mitragynine and metabolites in human urine for detecting the use of the psychoactive plant kratom. J. Anal. Toxicol. 36, 616–625.
Lim, E.L., Seah, T.C., Koe, X.F., Wahab, H.A., Adenan, M.I., Jamil, M.F., Majid, M.I., Tan, M.L., 2013. In vitro evaluation of cytochrome P450 induction and the inhibition potential of mitragynine, a stimulant alkaloid. Toxicol. In Vitro 27, 812–824.
Manda, V.K., Avula, B., Ali, Z., Khan, I.A., Walker, L.A., Khan, S.I., 2014. Evaluation of in vitro absorption, distribution, metabolism, and excretion (ADME) properties of mitragynine, 7-hydroxymitragynine, and mitraphylline. Planta Med. 80, 568–576.
Manda, V.K., Avula, B., Dale, O.R., Ali, Z., Khan, I.A., Walker, L.A., Khan, S.I., 2017. PXR mediated induction of CYP3A4, CYP1A2, and P-gp by Mitragyna speciosa and its alkaloids. Phytother. Res. 31, 1935–1945.
Meyer, M.R., Wagmann, L., Schneider-Daum, N., Loretz, B., Carvalho, C.D., Lehr, C.M., Maurer, H.H., 2015. P-glycoprotein interactions of novel psychoactive substances - Stimulation of ATP consumption and transport across Caco-2 monolayers. Biochem. Pharmacol. 94, 220–226.
Moher, D., Liberati, A., Tetzlaff, J., Altman, D.G., 2009. Preferred reporting items for systematic reviews and meta-analyses: the PRISMA statement. PLoS Med. 6, e1000097.
Narcotics Act No.7 B.E., 2562, 2019. The Government Gazette.
Parthasarathy, S., Ramanathan, S., Ismail, S., Adenan, M.I., Mansor, S.M., Murugaiyah, V., 2010. Determination of mitragynine in plasma with solid-phase extraction and rapid HPLC-UV analysis, and its application to a pharmacokinetic study in rat. Anal. Bioanal. Chem. 397, 2023–2030.
Philipp, A.A., Wissenbach, D.K., Zoerntlein, S.W., Klein, O.N., Kanogsunthornrat, J., Maurer, H.H., 2009. Studies on the metabolism of mitragynine, the main alkaloid of the herbal drug Kratom, in rat and human urine using liquid chromatography-linear ion trap mass spectrometry. J. Mass Spectrom. 44, 1249–1261.
Philipp, A.A., Meyer, M.R., Wissenbach, D.K., Weber, A.A., Zoerntlein, S.W., Zweipfenning, P.G., Maurer, H.H., 2011. Monitoring of kratom or Krypton intake in urine using GC-MS in clinical and forensic toxicology. Anal. Bioanal. Chem. 400, 127–135.
Ponglux, D., Wongseripipatana, S., Takayama, H., Kikuchi, M., Kurihara, M., Kitajima, M., Aimi, N., Sakai, S., 1994. A new indole alkaloid, 7 alpha-Hydroxy-7H-mitragynine, from Mitragyna speciosa in Thailand. Planta Med. 60, 580–581.
Prozialeck, W.C., Jivan, J.K., Andurkar, S.V., 2012. Pharmacology of kratom: an emerging botanical agent with stimulant, analgesic and opioid-like effects. J. Am. Osteopath. Assoc. 112, 792–799.
Ramanathan, S., Parthasarathy, S., Murugaiyah, V., Magosso, E., Tan, S.C., Mansor, S.M., 2015. Understanding the physicochemical properties of mitragynine, a principal alkaloid of Mitragyna speciosa, for preclinical evaluation. Molecules 20, 4915–4927.
Sachan, N., Bhattacharya, A., Pushkar, S., Mishra, A., 2009. Biopharmaceutical classification system: A strategic tool for oral drug delivery technology. Asian J. Pharm.
Saingam, D., Assanangkornchai, S., Geater, A.F., Balthip, Q., 2013. Pattern and consequences of krathom (Mitragyna speciosa Korth.) use among male villagers in southern Thailand: a qualitative study. Int. J. Drug Policy 24, 351–358.
Schmidt, M.M., Sharma, A., Schifano, F., Feinmann, C., 2011. "Legal highs" on the net-Evaluation of UK-based Websites, products and product information. Forensic Sci. Int. 206, 92–97.
Sharma, V., McNeill, J.H., 2009. To scale or not to scale: the principles of dose extrapolation. Br. J. Pharmacol. 157, 907–921.
Singh, D., Muller, C.P., Vicknasingam, B.K., 2014. Kratom (Mitragyna speciosa) dependence, withdrawal symptoms and craving in regular users. Drug Alcohol Depend. 139, 132–137.
Singh, D., Narayanan, S., Vicknasingam, B., 2016. Traditional and non-traditional uses of Mitragynine (Kratom): a survey of the literature. Brain Res. Bull. 126, 41–46.
Suhaimi, F.W., Yusoff, N.H., Hassan, R., Mansor, S.M., Navaratnam, V., Muller, C.P., Hassan, Z., 2016. Neurobiology of Kratom and its main alkaloid mitragynine. Brain Res. Bull. 126, 29–40.
Tanguay, P., 2011. Kratom in Thailand. Decriminalisation and Community Control. International Drug Policy Consortium (IDPC) Transnational Institute.
Trakulsrichai, S., Sathirakul, K., Auparakkitanon, S., Krongvorakul, J., Sueajai, J., Noumjad, N., Sukasem, C., Wananukul, W., 2015. Pharmacokinetics of mitragynine in man. Drug Des. Devel. Ther. 9, 2421–2429.
Utar, Z., Majid, M.I.A., Adenan, M.I., Jamil, M.F.A., Lan, T.M., 2011. Mitragynine inhibits the COX-2 mRNA expression and prostaglandin E2 production induced by lipopolysaccharide in RAW264.7 macrophage cells. J. Ethnopharmacol. 136, 75–82.
Vicknasingam, B., Narayanan, S., Beng, G.T., Mansor, S.M., 2010. The informal use of ketum (Mitragyna speciosa) for opioid withdrawal in the northern states of peninsular Malaysia and implications for drug substitution therapy. Int. J. Drug Policy 21, 283–288.
Vuppala, P.K., Boddu, S.P., Furr, E.B., McCurdy, C.R., Avery, B.A., 2011. Simple, sensitive, high-throughput method for the quantification of Mitragynine in rat plasma using UPLC-MS and its application to an intravenous pharmacokinetic study. Chromatographia 74, 703.
Warner, M.L., Kaufman, N.C., Grundmann, O., 2016. The pharmacology and toxicology of kratom: from traditional herb to drug of abuse. Int. J. Legal Med. 130, 127–138.
White, C.M., 2018. Pharmacologic and clinical assessment of kratom. Am. J. Health. Syst. Pharm. 75, 261–267.

APPENDIX C COMPUTER CODE OF THE PBPK MODEL FOR MITRAGYNINE IN RATS (INTRAVENOUS DOSING)

```
METHOD RK4
STARTTIME       = 0                     ; hr
STOPTIME        = 7.5                   ; hr
DT              = 0.0005        ; hr
Dose            = 2.5           ; mg
Duration        = 0.16                  ; hr

{Rat physiological parameter}
BW              = 0.25                  ; Reference body weight (kg)
QCC             = 15                    ; Blood flow fraction (L/hr)
VLUC            = 0.005                 ; Vol fraction of lung (L/kg)
VFC             = 0.07                  ; Vol fraction of fat
VBRC            = 0.006                 ; Vol fraction of brain
VSPC            = 0.404                 ; Vol fraction of slowly perfused
VKIC            = 0.007                 ; Vol fraction of kidney
VLIC            = 0.034                 ; Vol fraction of liver
VVC             = 0.0544                ; Vol fraction of vein
VAC             = 0.0272                ; Vol fraction of artery
QC              = QCC*BW^0.75           ; Blood flow (L/hr)
QFC             = 0.07                  ; BF fraction of fat
QBRC            = 0.02                  ; BF fraction of brain
QSPC            = 0.278                 ; BF fraction of slowly perfused
QKIC            = 0.141                 ; BF fraction of kidney
QLIC            = 0.183                 ; BF fraction of liver
```

{Chemical specific parameter for HCN}

MW = 398.50 ; Molecular weight (g/mole)

PCLU = 1.12 ; Partition coefficient of lung/blood

PCF = 4.37 ; Partition coefficient of fat/blood

PCBR = 0.86 ; Partition coefficient of brain/blood

PCSP = 0.74 ; Partition coefficient of slowly perfused/blood

PCKI = 0.96 ; Partition coefficient of kidney/plasma

PCLI = 0.98 ; Partition coefficient of liver/blood

Vmax_BR = 1.7 ; mcmole/hr (BCRP)

Km_BR = 11 ; mcmolar

Vmax_LI = 0.3 ; mcmole/hr (CYP3A4)

Km_LI = 85 ; mcmolar

FVBF = 0.02 ; Blood volume fraction of fat (%)

PAFC = 1.5 ; Fat tissue permeability (L/hr/kg tissue)

{Calculated parameters}

VLU = VLUC*BW ; L

VF = VFC*BW

VBR = VBRC*BW

VSP = VSPC*BW

VKI = VKIC*BW

VLI = VLIC*BW

VV = VVC*BW

VA = VAC*BW

PAF = PAFC*VF ; Fat:blood permeability (L/hr)

VFb = FVBF*VF ; Fat compartment blood volume

VFt = VF-VFb ; Fat compartment tissue volume

```
{Blood flow of organs}
QF          = QFC*QC                ; L/hr
QBR         = QBRC*QC
QSP         = QSPC*QC
QKI         = QKIC*QC
QLI         = QLIC*QC

{Mass balance in Vein}
Rate_in = Dose*(1000/MW)/Duration*(1-step(1, duration))
AV'         = (QF*CVF+QBR*CVBR+QSP*CVSP+QKI*CVKI+QLI*CVLI)
              -(QC*CV)+BR_ET+Rate_in
INIT AV     = 0.0                   ; mcmole
CV          = AV/VV                 ; mcmole/L
CV_mcg      = CV*MW                 ; mcg/L

{Mass balance in Artery}
AA'         = (QC*CLUA)-CA*(QF+QBR+QSP+QKI+QLI)-BR_ET
INIT AA     = 0.0                   ; mcmole
CA          = AA/VA                 ; mcmole/L
CA_mcg      = CA*MW                 ; mcg/L

{Mass balance in Lung}
ALU'        = QC*(CV-CLUA)
INIT ALU    = 0.0                   ; mcmole
CLU         = ALU/VLU               ; mcmole
CLUA        = ALU/(VLU*PCLU)        ; mcmole/L
CLU_mcg     = CLU*MW                ; mcg/L
```

```
{Mass balance in Fat}
AFb'        = QF*(CA-CVF)+PAF*(CFt/PCF-CVF)
INIT AFb    = 0.0                    ; mcmole
CVF         = AFb/VFb                ; mcmole/L

AFt'        = PAF*(CVF-CFt/PCF)
INIT AFt    = 0.0                    ; mcmole
CFt         = AFt/VFt                ; mcmole/L

AFtotal     = AFb+AFt                ; mcmole
CF          = AFtotal/VF             ; mcmole/L
CF_mcg      = CF*MW                  ; mcg/L

{Mass balance in Brain}
ABR'        = QBR*(CA-CVBR)-BR_ET
INIT ABR    = 0.0                    ; mcmole
CBR         = ABR/VBR                ; mcmole/L
CVBR        = ABR/(VBR*PCBR)         ; mcmole/L
CBR_mcg     = CBR*MW                 ; mcg/L

BR_ET       = (Vmax_BR*CVBR)/(Km_BR+CVBR)
ABR_ET'     = BR_ET
INIT ABR_ET = 0.0

{Mass balance in Slowly perfused tissues}
ASP'        = QSP*(CA-CVSP)
INIT ASP    = 0.0                    ; mcmole
CSP         = ASP/VSP                ; mcmole/L
CVSP        = ASP/(VSP*PCSP)         ; mcmole/L
CSP_mcg     = CSP*MW                 ; mcg/L
```

```
{Mass balance in Kidney}
AKI'      = QKI*(CA-CVKI)
INIT AKI  = 0.0                  ; mcmole
CKI       = AKI/VKI              ; mcmole/L
CVKI      = AKI/(VKI*PCKI)       ; mcmole/L
CKI_mcg   = CKI*MW               ; mcg/L

{Mass balance in Liver}
ALI'      = QLI*(CA-CVLI)-LI_Met
INIT ALI  = 0.0                  ; mcmole
CLI       = ALI/VLI              ; mcmole/L
CVLI      = ALI/(VLI*PCLI)       ; mcmole/L
CLI_mcg   = CLI*MW               ; mcg/L

LI_Met  = (Vmax_LI*CVLI)/(Km_LI+CVLI)
ALI_Met'  = LI_Met
INIT ALI_Met= 0.0

{Total mass}
MB      = AV+AA+ALU+ABR+AFTotal+ASP+AKI+ALI+ABR_ET+ALI_Met
; mcmole

MB_mg = MB*MW/1000               ; mg

display PCLU, PCBR, PCF, PCSP, PCKI, PCLI, Dose, Duration, Vmax_LI, Km_LI,
Vmax_BR, Km_BR, PAFC, FVBF

display MB_mg, CV_mcg, CA_mcg, CLU_mcg, CF_mcg, CBR_mcg, CSP_mcg,
CKI_mcg, CLI_mcg
```

APPENDIX D COMPUTER CODE OF THE PBPK MODEL FOR MITRAGYNINE IN RATS (ORAL DOSING)

```
METHOD RK4
STARTTIME       = 0             ; hr
STOPTIME        = 24            ; hr
DT              = 0.0005        ; hr
Dose            = 5                     ; mg

Oral_in         = Ka*AGU
AGU'            = -Oral_in
INIT AGU        = Dose*(1000/MW)*F

{Rat physiological parameter}
BW              = 0.25          ; Reference body weight (kg)
QCC             = 15            ; Blood flow fraction (L/hr)
VLUC            = 0.005         ; Vol fraction of lung (L/kg)
VFC             = 0.07          ; Vol fraction of fat
VBRC            = 0.006         ; Vol fraction of brain
VSPC            = 0.404         ; Vol fraction of slowly perfused
VKIC            = 0.007         ; Vol fraction of kidney
VLIC            = 0.034         ; Vol fraction of liver
VVC             = 0.0544        ; Vol fraction of vein
VAC             = 0.0272        ; Vol fraction of artery
QC              = QCC*BW^0.75   ; Blood flow (L/hr)
QFC             = 0.07          ; BF fraction of fat
QBRC            = 0.02          ; BF fraction of brain
QSPC            = 0.278         ; BF fraction of slowly perfused
QKIC            = 0.141         ; BF fraction of kidney
QLIC            = 0.183         ; BF fraction of liver
```

{Chemical specific parameter for HCN}

MW = 398.50 ; Molecular weight (g/mole)
PCLU = 1.12 ; Partition coefficient of lung/blood
PCF = 4.37 ; Partition coefficient of fat/blood
PCBR = 0.86 ; Partition coefficient of brain/blood
PCSP = 0.74 ; Partition coefficient of slowly perfused/blood
PCKI = 0.96 ; Partition coefficient of kidney/plasma
PCLI = 0.98 ; Partition coefficient of liver/blood
Vmax_BR = 1.7 ; mcmole/hr (BCRP)
Km_BR = 11 ; mcmolar
Vmax_LI = 0.3 ; mcmole/hr (CYP3A4)
Km_LI = 85 ; mcmolar
FVBF = 0.02 ; Blood volume fraction of fat (%)
PAFC = 1.5 ; Fat tissue permeability (L/hr/kg tissue)
Ka = 0.5 ; Absorption rate constant (1/hr)
F = 0.08 ; Bioavailability

{Calculated parameters}

VLU = VLUC*BW ; L
VF = VFC*BW
VBR = VBRC*BW
VSP = VSPC*BW
VKI = VKIC*BW
VLI = VLIC*BW
VV = VVC*BW
VA = VAC*BW
PAF = PAFC*VF ; Fat:blood permeability (L/hr)
VFb = FVBF*VF ; Fat compartment blood volume
VFt = VF-VFb ; Fat compartment tissue volume

```
{Blood flow of organs}
QF          = QFC*QC                ; L/hr
QBR         = QBRC*QC
QSP         = QSPC*QC
QKI         = QKIC*QC
QLI         = QLIC*QC

{Mass balance in Vein}
AV'         = (QF*CVF+QBR*CVBR+QSP*CVSP+QKI*CVKI+QLI*CVLI)
              -(QC*CV)+BR_ET
INIT AV     = 0.0                   ; mcmole
CV          = AV/VV                 ; mcmole/L
CV_mcg      = CV*MW                 ; mcg/L

{Mass balance in Artery}
AA'         = (QC*CLUA)-CA*(QF+QBR+QSP+QKI+QLI)-BR_ET
INIT AA     = 0.0                   ; mcmole
CA          = AA/VA                 ; mcmole/L
CA_mcg      = CA*MW                 ; mcg/L

{Mass balance in Lung}
ALU'        = QC*(CV-CLUA)
INIT ALU    = 0.0                   ; mcmole
CLU         = ALU/VLU               ; mcmole
CLUA        = ALU/(VLU*PCLU)        ; mcmole/L
CLU_mcg     = CLU*MW                ; mcg/L
```

```
{Mass balance in Fat}
AFb'        = QF*(CA-CVF)+PAF*(CFt/PCF-CVF)
INIT AFb    = 0.0
CVF         = AFb/VFb

AFt'        = PAF*(CVF-CFt/PCF)
INIT AFt    = 0.0
CFt         = AFt/VFt

AFtotal  = AFb+AFt          ; mcmole
CF       = AFtotal/VF       ; mcmole/L
CF_mcg= CF*MW               ; mcg/L

{Mass balance in Brain}
ABR'        = QBR*(CA-CVBR)-BR_ET
INIT ABR = 0.0                      ; mcmole
CBR      = ABR/VBR                  ; mcmole/L
CVBR     = ABR/(VBR*PCBR)           ; mcmole/L
CBR_mcg  = CBR*MW                   ; mcg/L

BR_ET  = (Vmax_BR*CVBR)/(Km_BR+CVBR)
ABR_ET'  = BR_ET
INIT ABR_ET= 0.0

{Mass balance in Slowly perfused tissues}
ASP'        = QSP*(CA-CVSP)
INIT ASP  = 0.0                     ; mcmole
CSP       = ASP/VSP                 ; mcmole/L
CVSP      = ASP/(VSP*PCSP)          ; mcmole/L
CSP_mcg   = CSP*MW                  ; mcg/L
```

```
{Mass balance in Kidney}
AKI'       = QKI*(CA-CVKI)
INIT AKI   = 0.0                    ; mcmole
CKI        = AKI/VKI                ; mcmole/L
CVKI       = AKI/(VKI*PCKI)         ; mcmole/L
CKI_mcg    = CKI*MW                 ; mcg/L

{Mass balance in Liver}
ALI'       = QLI*(CA-CVLI)-LI_Met+Oral_in
INIT ALI   = 0.0                    ; mcmole
CLI        = ALI/VLI                ; mcmole/L
CVLI       = ALI/(VLI*PCLI)         ; mcmole/L
CLI_mcg    = CLI*MW                 ; mcg/L

LI_Met  = (Vmax_LI*CVLI)/(Km_LI+CVLI)
ALI_Met'  = LI_Met
INIT ALI_Met= 0.0

{Total mass}
MB =    AV+AA+ALU+ABR+AFTotal+ASP+AKI+ALI+ABR_ET+ALI_Met+AGU
; mcmole

MB_mg = (MB*MW)/(F*1000)       ; mg

display PCLU, PCBR, PCF, PCSP, PCKI, PCLI, Dose, Vmax_LI, Km_LI, Vmax_BR,
Km_BR, PAFC, FVBF, F, Ka

display MB_mg, CV_mcg, CA_mcg, CLU_mcg, CF_mcg, CBR_mcg, CSP_mcg,
CKI_mcg, CLI_mcg
```

APPENDIX E COMPUTER CODE OF THE PBPK MODEL FOR MITRAGYNINE IN HUMANS (REPEATED DOSING)

```
METHOD RK4
STARTTIME       = 0         ; hr
STOPTIME        = 192       ; hr
DT              = 0.0005    ; hr
Dose1           = 9.96      ; mg
Dose2           = 9.96      ; mg
Dose3           = 9.96      ; mg
Dose4           = 9.96      ; mg
Dose5           = 9.96      ; mg
Dose6           = 9.96      ; mg
Dose7           = 9.96      ; mg
Dose8           = 9.96      ; mg

Dosing_1        = if time <= 24 then 1 else 0
Input_1         = pulse (Dose1,0,24)*Dosing_1
Dosing_2        = if time >= 24 AND time <= 48 then 1 else 0
Input_2         = pulse (Dose2,24,48)*Dosing_2
Dosing_3        = if time >= 48 AND time <= 72 then 1 else 0
Input_3         = pulse (Dose3,48,72)*Dosing_3
Dosing_4        = if time >= 72 AND time <= 96 then 1 else 0
Input_4         = pulse (Dose4,72,96)*Dosing_4
Dosing_5        = if time >= 96 AND time <= 120 then 1 else 0
Input_5         = pulse (Dose5,96,120)*Dosing_5
Dosing_6        = if time >= 120 AND time <= 144 then 1 else 0
Input_6         = pulse (Dose6,120,144)*Dosing_6
Dosing_7        = if time >= 144 AND time <= 168 then 1 else 0
Input_7         = pulse (Dose7,144,168)*Dosing_7
Dosing_8        = if time >= 168 AND time <= 192 then 1 else 0
Input_8         = pulse (Dose8,168,192)*Dosing_8
```

```
Oral_in        = Ka*AGU
AGU'           = -Oral_in+(input_1+input_2+input_3+input_4+input_5+input_6
                +input_7+input_8)*F*(1000/MW)
INIT AGU = 0.0

{Human physiological parameter}
BW      = 70            ; Reference body weight (kg)
QCC     = 15            ; Blood flow fraction (L/hr)
VLUC    = 0.008         ; Vol fraction of lung (L/kg)
VFC     = 0.214         ; Vol fraction of fat
VBRC    = 0.02          ; Vol fraction of brain
VSPC    = 0.4           ; Vol fraction of slowly perfused
VKIC    = 0.004         ; Vol fraction of kidney
VLIC    = 0.026         ; Vol fraction of liver
VVC     = 0.0514        ; Vol fraction of vein
VAC     = 0.0257        ; Vol fraction of artery
QC      = QCC*BW^0.75   ; Blood flow (L/hr)
QFC     = 0.052         ; BF fraction of fat
QBRC    = 0.114         ; BF fraction of brain
QSPC    = 0.191         ; BF fraction of slowly perfused
QKIC    = 0.175         ; BF fraction of kidney
QLIC    = 0.227         ; BF fraction of liver

{Chemical specific parameter for HCN}
MW      = 398.50  ; Molecular weight (g/mole)
PCLU    = 0.52          ; Partition coefficient of lung/blood
PCF     = 3.64          ; Partition coefficient of fat/blood
PCBR    = 2             ; Partition coefficient of brain/blood
PCSP    = 0.98          ; Partition coefficient of slowly perfused/blood
PCKI    = 0.98          ; Partition coefficient of kidney/plasma
PCLI    = 1.37          ; Partition coefficient of liver/blood
Vmax_BR = 325           ; mcmole/L (BCRP)
```

```
Km_BR = 14          ; mcmole
Vmax_LI  = 41       ; mcmole/hr (CYP3A4)
Km_LI    = 103.3    ; mcmolar
FVBF     = 0.02     ; Blood volume fraction of fat (%)
PAFC     = 1        ; Fat tissue permeability (L/hr/kg tissue)
Ka       = 2.2      ; Absorption rate constant (1/hr)
F        = 0.21     ; Bioavailability

{Calculated parameters}
VLU      = VLUC*BW                ; L
VF       = VFC*BW
VBR      = VBRC*BW
VSP      = VSPC*BW
VKI      = VKIC*BW
VLI      = VLIC*BW
VV       = VVC*BW
VA       = VAC*BW
PAF      = PAFC*VF                ; Fat:blood permeability (L/hr)
VFb      = FVBF*VF                ; Fat compartment blood volume
VFt      = VF-VFb                 ; Fat compartment tissue volume

{Blood flow of organs}
QF       = QFC*QC                 ; L/hr
QBR      = QBRC*QC
QSP      = QSPC*QC
QKI      = QKIC*QC
QLI      = QLIC*QC
```

```
{Mass balance in Vein}
AV'       = (QF*CVF+QBR*CVBR+QSP*CVSP+QKI*CVKI+QLI*CVLI)
              -(QC*CV)+BR_ET
INIT AV   = 0.0              ; mcmole
CV        = AV/VV            ; mcmole/L
CV_mcg    = CV*MW            ; mcg/L

{Mass balance in Artery}
AA'       = (QC*CLUA)-CA*(QF+QBR+QSP+QKI+QLI)-BR_ET
INIT AA   = 0.0              ; mcmole
CA        = AA/VA            ; mcmole/L
CA_mcg    = CA*MW            ; mcg/L

{Mass balance in Lung}
ALU'      = QC*(CV-CLUA)
INIT ALU  = 0.0                    ; mcmole
CLU       = ALU/VLU                ; mcmole
CLUA      = ALU/(VLU*PCLU)         ; mcmole/L
CLU_mcg   = CLU*MW                 ; mcg/L

{Mass balance in Fat}
AFb'      = QF*(CA-CVF)+PAF*(CFt/PCF-CVF)
INIT AFb  = 0.0
CVF       = AFb/VFb

AFt'      = PAF*(CVF-CFt/PCF)
INIT AFt  = 0.0
CFt       = AFt/VFt

AFtotal   = AFb+AFt          ; mcmole
CF        = AFtotal/VF       ; mcmole
CF_mcg= CF*MW                ; mcg/L
```

```
{Mass balance in Brain}
ABR'      = QBR*(CA-CVBR)-BR_ET
INIT ABR  = 0.0                    ; mcmole
CBR       = ABR/VBR                ; mcmole/L
CVBR      = ABR/(VBR*PCBR)         ; mcmole/L
CBR_mcg   = CBR*MW                 ; mcg/L

BR_ET  = (Vmax_BR*CVBR)/(Km_BR+CVBR)
ABR_ET'  = BR_ET
INIT ABR_ET= 0.0

{Mass balance in Slowly perfused}
ASP'      = QSP*(CA-CVSP)
INIT ASP  = 0.0                    ; mcmole
CSP       = ASP/VSP                ; mcmole/L
CVSP      = ASP/(VSP*PCSP)         ; mcmole/L
CSP_mcg   = CSP*MW                 ; mcg/L

{Mass balance in Kidney}
AKI'      = QKI*(CA-CVKI)
INIT AKI  = 0.0                    ; mcmole
CKI       = AKI/VKI                ; mcmole/L
CVKI      = AKI/(VKI*PCKI)         ; mcmole/L
CKI_mcg   = CKI*MW                 ; mcg/L

{Mass balance in Liver}
ALI'      = QLI*(CA-CVLI)-LI_Met+Oral_in
INIT ALI  = 0.0                    ; mcmole
CLI       = ALI/VLI                ; mcmole/L
CVLI      = ALI/(VLI*PCLI)         ; mcmole/L
CLI_mcg   = CLI*MW                 ; mcg/L
```

```
LI_Met  = (Vmax_LI*CVLI)/(Km_LI+CVLI)
ALI_Met'  = LI_Met
INIT ALI_Met= 0.0

{Total mass}
MB     = AV+AA+ALU+ABR+AFtotal+ASP+AKI+ALI+ALI_Met+ABR_ET+AGU
; mcmole

MB_mg = (MB*MW)/(F*1000)                ; mg

display PCLU, PCBR, PCF, PCSP, PCKI, PCLI,  Vmax_BR, Km_BR, Vmax_LI,
Km_LI, FVBF, PAFC, F, Ka

display MB_mg, CV_mcg, CA_mcg, CLU_mcg, CF_mcg, CBR_mcg, CSP_mcg,
CKI_mcg, CLI_mcg
```